Diss. ETH No. 20801

Quantification of oxygen turnover in groundwater by continuous on-site gas concentration measurements

A dissertation submitted to
ETH ZURICH

for the degree of
DOCTOR OF SCIENCES

presented by
LARS MÄCHLER
Dipl. Phys. ETH
born 30 July 1982
citizen of Vorderthal (SZ)

accepted on the recommendation of
Prof. Dr. Rolf Kipfer, examiner
Dr. Matthias S. Brennwald, co-examiner
Prof. Dr. Bernhard Wehrli, co-examiner

2012

Chapter 3 has been published as:
Mächler, L., Brennwald, M. S. and Kipfer, R. (2012). Membrane inlet mass spectrometer for the quasi-continuous on-site analysis of dissolved gases in groundwater. *Environ. Sci. Technol.* **46**, 8288–8296.

Chapter 4 has been submitted for publication in Environmental Science and Technology:
Mächler, L., Brennwald, M. S. and Kipfer, R. (2012). Argon concentration time-series as a tool to study gas dynamics in the hyporheic zone.

Chapter 5 has been submitted for publication in Water Resources Research:
Mächler, L., Peter, S., Brennwald, M. S. and Kipfer, R. (2012). Excess air formation as a mechanism for delivering oxygen to groundwater.

Acknowledgements

I would like to thank the referees of my dissertation Rolf Kipfer, Matthias Brennwald and Bernhard Wehrli. In particular, I am grateful for all the support from Matthias and RoKi which helped to improved this work considerably.
I would like to express my thanks to all the present and former members of the Enviromental Isotopes group at EAWAG: Christian Holzner, David Livingstone (who corrected the english of my first paper), Eduard Hoehn, Helena Amaral, Lina Tyroller, Markus Hofer, Nadja Vogel, Ola Kwiece, Ryan North (who corrected some of my drafts), Simon Figura, Stephan Huxol, Yama Tomonaga (with whom I also shared the office and his coffee machine) and Yvonne Scheidegger. Thanks for the great company and the good working atmosphere.
Furthermore I am very grateful for all the people in and associated to the RECORD project. In particular Samuel Diem, Sebastian Huntscha, Simone Peter (and her office mates: Roland, Nuttakan, Jasmin, who gave me asylum every now and then) and Tobias Vogt. Thanks for the great company and all the support in the field. Thank is also due to all the other Colleagues from W+T department, specially to mention Mario Schirmer's group and Annette Johnson's group, in particular Anja Bretzler (who corrected the english of my drafts).
Special thanks goes to the the members of the noble gas laboratory at ETHZ Zürich. In particular I thank Heiri Baur, Urs Menet, Donat Niederer and Andreas Süsli (who built the "Spectromobil") for their indispensable technical support. Further I thank Heinz Surbeck for the very helpful and interesting technical discussions and Masaki Hayashi for the interesting scientific collaboration. I would also like to thank all the other colleges of EAWAG, my colleagues teaching at the lab course in physics, and in particular also the football team Eawag-EMPA. Finally, I want to thank for all the support and encouragement of my family and friends.

Contents

1 Introduction **1**
- 1.1 Motivation . . . 1
- 1.2 Outline . . . 2

2 Scientific background **7**
- 2.1 Dissolved gases in water . . . 7
  - 2.1.1 Henry and diffusion coefficient . . . 7
  - 2.1.2 Excess air . . . 9
  - 2.1.3 O_2 and excess air . . . 9
  - 2.1.4 Excess air models . . . 10
  - 2.1.5 Gases related to redox processes . . . 14
- 2.2 Study site: Niederneunforn at river Thur . . . 15
- 2.3 Membrane inlet mass spectrometry . . . 16
  - 2.3.1 Ion source, separator and detector . . . 16
  - 2.3.2 Membrane inlets . . . 17

3 Membrane inlet mass spectrometer for the quasi continuous on-site analysis of dissolved gases in groundwater **21**
- 3.1 Introduction . . . 21
- 3.2 Method . . . 23
- 3.3 Measurement procedure . . . 25
- 3.4 Laboratory-based measurements . . . 27
  - 3.4.1 Dependence of the nondimensional deviation function F_i^f on the water flow rate Q_{w} . . . 27
  - 3.4.2 Dependence of the nondimensional deviation function F_i^f on water temperature T_{w} . . . 28
- 3.5 Field measurements: Oxygen dynamics in the hyporheic zone of a stream . . . 32
- 3.6 Discussion . . . 34
- 3.7 Appendix . . . 35
  - 3.7.1 Gas flux calculation . . . 35
  - 3.7.2 Part list . . . 36

4 Argon concentration time-series as a tool to study gas dynamics in the hyporheic zone **39**
- 4.1 Introduction . . . 39
- 4.2 Methods . . . 41
  - 4.2.1 Study site . . . 41
  - 4.2.2 Dissolved gas measurement system . . . 42
- 4.3 Results and Discussion . . . 42

4.3.1 Temporal evolution of temperature and Ar concentration 42
4.3.2 Temporal evolution of O_2 and CO_2 concentrations 45
4.3.3 Oxygen turnover 46
4.3.4 Discussion 47
4.4 Appendix 48
4.4.1 Diel evolution of the dissolved Ar concentration in a river 48

5 Excess air formation as a mechanism for delivering oxygen to groundwater 51
5.1 Introduction 51
5.2 Methods 53
5.2.1 Study site 53
5.2.2 Measurements 54
5.2.3 Gas exchange in porous media 55
5.3 Results and calculations 56
5.3.1 Changes in dissolved gas concentrations in response to the flood . 56
5.3.2 Calculations of O_2 input due to excess air formation 60
5.3.3 Accuracy and reliability of the used CE-model 63
5.4 Conclusion 64

6 Conclusion and outlook 69
6.1 Noble gas concentration time series 69
6.2 Oxygen dynamics at the field site 70
6.3 Outlook 72

Bibliography 75

Appendix 85

Summary

This work focuses on the combined measurement of (stable) noble gas and oxygen concentrations in riparian groundwaters. The aim of this work is to study the oxygen dynamics in such groundwaters in terms of separating biogeochemical mediated concentration changes from physical exchange and transport mechanisms, in order to both quantify oxygen input into and oxygen turnover of riparian groundwaters.
Noble gases are generally not affected by biogeochemical reactions, hence their dissolved concentrations depend on physical processes only. One significant characteristic of such a process is the temperature dependence of atmospheric solubility, i.e. the equilibrium of gas exchange between an open water body and the atmosphere, which is used in reconstructing past temperatures that prevailed during last air/water partitioning. However, noble gases in groundwater are often found to be super saturated with respect to atmospheric solubility. Due to the air-like composition and the actual atmospheric origin of this concentration surplus, the term "excess air" is commonly used to denote it. In the last decade the mechanism of excess air formation, i.e. the complete or partial dissolution of entrapped air into the groundwater body, was thoroughly studied. The thereby developed models are widely used to improve quantitative interpretation of measured noble gas concentrations in terms of temperature reconstruction and groundwater age determination.
The entrapped air also contains oxygen and therefore excess air formation is a potential driver of oxygen availability in groundwater. Thus, excess air formation needs to be considered to quantify oxygen turnover. In conclusion, studies with combined measurements of both noble gas and oxygen concentrations are necessary to understand the lateral dynamics of oxygen in the aquatic environment of a porous medium.
However, to study the formation of excess air in the field, an instrument to quantify dissolved noble gases with a time resolution sufficient to resolve the noble gas and oxygen concentration changes occurring in riparian groundwaters and which is able to operate over several days autonomously, had to be developed first. The developed instrument which fulfilled this task is based on membrane inlet mass spectrometry. However, in contrast to the "classical" membrane inlet mass spectrometer (MIMS) where the membrane separates the water from the high vacuum environment of the mass spectrometer directly, the developed MIMS uses an intermediate pressure reduction step after the membrane inlet. Hence, the gas concentrations after the membrane are in a steady state near solubility equilibrium with the water to be analyzed. This design enables the in-field calibration with ambient air and therefore enables the instrument to autonomous in-field operation.
In the following field study of a riparian groundwater of a peri-alpine river (Thur, Switzerland), it was documented that noble gas concentration time series, acquired by the instrument developed for this work, enable the gas dynamics in groundwater to be studied in real time and in-situ. The oxygen and argon concentration time series that were acquired revealed information on the temperature dependence of oxygen consumption, and hence on microbial activity. Furthermore, in a study at the same location during a small flood,

excess air formation was documented to enhance oxygen concentrations in the groundwater considerably. The results show that excess air formation is a non-negligible factor in the biochemical system of groundwaters and hence for drinking water quality as such.
In conclusion, the quasi-continuous measurements of noble gas concentrations in combination with oxygen, and even nitrogen and carbon dioxide, will improve current knowledge on the physical and biochemical gas dynamics in groundwaters. This work is a first step in introducing noble gas concentration time series as a new and valuable analytical tool in hydrogeology.

Zusammenfassung

Diese Arbeit befasst sich mit der Beschreibung und Entwicklung einer Messmethode, welche erlaubt gleichzeitig Sauerstoff- und Edelgaskonzentrationen in Grundwasser zu quantifizieren. Ziel dieser Arbeit ist es, die Sauerstoffdynamik im flussnahen Grundwasser zu untersuchen, wobei physikalische und biogeochemische Prozesse, welche die Sauerstoffkonzentration ändern, gesondert quantifiziert werden müssen, um den Sauerstoffeintrag und den mikrobiellen Sauerstoffumsatz zu bestimmen.
Edelgase sind chemisch inert. Folglich werden Konzentrationsänderungen von in Wasser gelöster Edelgase ausschliesslich durch physikalische Prozesse verursacht. Der Bekannteste dieser Prozesse ist der Gasaustausch eines Wasserkörpers mit der Atmosphäre. Die Löslichkeit der Gase, d.h. die im Gleichgewicht des Gasaustausches eingestellte Konzentration, ist abhängig von der Wassertemperatur. Im Grundwasser sind die meisten Edelgaskonzentrationen bezüglich dieser Löslichkeit allerdings übersättigt, wobei die elementare Zusammensetzung dieses Überschusses oft ähnlich derjenigen der Atmosphäre ist. Deswegen wird dieser Überschuss als "Excess Air" bezeichnet, was dem deutschen Begriff "Luftüberschuss" entspricht. Modelle, welche die Bildung von "Excess Air", durch das Einschliessen und (partielle) Auflösen von Luftblasen beschreiben, wurden mehrheitlich im letzten Jahrzehnt entwickelt. Methoden, zur Datierung von Grundwässern, sowie zur Rekonstruktion von Temperaturen des Wassers in der Vergangenheit, welche auf der Bestimmung der Edelgaskonzentrationen basieren, vertrauen auf diese Modelle.
"Excess Air" ist aber keinesfalls nur auf Edelgase beschränkt, sondern betrifft alle atmosphärischen Gase, insbesondere auch Sauerstoff. Darum kann "Excess Air" für die Grundwasserbiota eine wichtige Sauerstoffquelle darstellen. Um die Menge des durch die Grundwasserbiota verbrauchten Sauerstoffes präzis zu bestimmen, muss folglich auch der Anteil des durch "Excess Air" eingetragenen Sauerstoffes abgeschätzt werden. Der Sauerstoffumsatz in einem Grundwasser kann deshalb nur bestimmt werden, wenn zusätzlich zur Sauerstoffkonzentration auch Edelgaskonzentrationen quantifiziert werden.
Durch Flusswasser gespeiste Grundwasser zeichnen sich oft durch dynamische Änderungen in Temperatur und den Konzentrationen gelöster Gase aus. Um diese Konzentrationsänderungen zu erfassen, wurde zu Beginn dieses Doktorats eine Messmethode entwickelt, welche autonom und kontinuierlich die Konzentrationen von Edelgasen, Sauerstoff, Stickstoff und Kohlendioxid in Wasser quantifizieren kann. Die entwickelte Methode nutzt eine Membrane, um die gelösten Gase aus dem Wasser zu extrahieren, und ein Massenspektrometer (MS), um die extrahierten Gasmengen zu quantifizieren. Im Unterschied zu den meisten MIMS Systemen (MIMS: "Membrane Inlet Mass Spectrometry"), in welchen das extrahierte Gas direkt in das vorherrschende Vakuum des Massenspektromters eingelassen wird, ist bei dem neu entwickelten System eine druckreduzierende Stufe zwischen Membran und MS geschaltet. Zwischen dieser Stufe und der Membrane erreichen die Gaskonzentrationen ein löslichkeitsnahes Gleichgewicht mit den in Wasser gelösten Gasen. Dank diesem Aufbau kann das entwickelte Messsystem direkt mit Umge-

bungsluft kalibriert werden, was einen Feldeinsatz erst ermöglicht.
Das neu entwickelte Instrument wurde in zwei Feldstudien eingesetzt. In einer ersten Studie wurde die Gasdynamik im Grundwasser eines durch einen voralpinen Fluss (Thur, Schweiz) gespeisten Aquifer untersucht. Die Studie zeigt, dass kontinuierliche Zeitreihen der Edelgaskonzentrationen Einblick in die Gasdynamik im Grundwasser geben. So konnte anhand der gemessenen Zeitreihen der Argon- und Sauerstoffkonzentrationen die Temperaturabhängigkeit des mikrobiellen Sauerstoffumsatzes quantifiziert werden. In einer weiteren Studie am selben Ort wurde der Sauerstoffeintrag durch "Excess Air"-Bildung während einer Pegelschwankung des Flusses in das Grundwasser untersucht. Die Resultate zeigen, dass der Sauerstoffeintrag durch "Excess Air"-Bildung wesentlich zur Belüftung von Grundwasser beiträgt und in Abhängigkeit des Abflussregimes des Flusses die biogeochemische Dynamik im Grundwasser beeinflusst. Entsprechend ist die Bildung von "Excess Air" ein wichtiger Faktor für die Trinkwasserqualität.
Zusammenfassend besitzt die Analyse von Zeitreihen der Edelgaskonzentrationen im Grundwasser, insbesondere in Kombination mit Sauerstoff-, Stickstoff- und Kohlendioxidkonzentrationen, ein beträchtliches Potential das Verständnis der Gasdynamik in Grundwasser zu erweitern. Diese Arbeit ist ein erster Schritt Edelgas-Konzentrationszeitreihen als ein neues und vielseitiges, analytisches Werkzeug in der Hydrogeologie zu etablieren.

1 Introduction

1.1 Motivation

Oxygen (O_2) concentration is probably the most important biological variable in groundwater because O_2 availability is the key constraint on respiration of aerobic organisms in groundwater environments (Schwoerbel, 1961; Husmann, 1971; Williams and Hynes, 1974; Poole and Stewart, 1976). Furthermore, O_2 turnover in groundwater —i.e. the microbially reduced amount of O_2 per mass of water— is directly linked to the consumption and hence availability of organic matter (Whitman and Clark, 1982; Rose and Long, 1988; Boulton et al., 1998; Malard and Hervant, 1999; Brunke and Gonser, 1997; Datry et al., 2004). Therefore, to asses groundwater quality, both the availability and the turnover of dissolved O_2 are important.

Surface-subsurface water exchange (e.g. infiltration of river water into the bank) is one major process to supply O_2 to the aquifer. The other important process that influences O_2 availability, is gas exchange within the unsaturated zone of the groundwater. Air/water partitioning in the unsaturated zone by the entrapment and the dissolution of air bubbles in response to water-table fluctuations or groundwater recharge (Heaton and Vogel, 1981; Stute et al., 1992; Beyerle et al., 1999; Kipfer et al., 2002; Holocher et al., 2003; Lippmann et al., 2003; Klump et al., 2007), not only leads to the formation of excess air (a surplus of atmospheric gases relative to atmospheric solubility equilibrium that is often found in groundwater), but also contributes to the overall input of O_2 into groundwater (Rose and Long, 1988; Beyerle et al., 1999; Klump et al., 2008; Massmann and Sueltenfuss, 2008).

Any quantification of O_2 turnover relies on the accurate determination of the total input of O_2. However, this input can only be determined using chemically conservative tracers, which are subject to the same physical gas transport and exchange mechanisms as O_2 — i.e. such tracers are only controlled by the Henry coefficients and the diffusion coefficients (e.g., Kipfer et al., 2002; Holocher et al., 2003; Lippmann et al., 2003; Klump et al., 2007, 2008; Sun et al., 2008). Atmospheric noble gases (i.e. helium, He; neon, Ne; argon, Ar; krypton, Kr and xenon, Xe) do not undergo any biogeochemical reactions. Furthermore, the diffusion coefficient and Henry coefficient of O_2 are within the range of values of the coefficients of the different noble gases (Wise and Houghton, 1966; Weiss, 1970; Broecker and Peng, 1974; Jähne et al., 1987). Hence, noble gases are suitable tracers to determine gas transfer, in particular O_2 transfer, into groundwater. Both field and laboratory based studies using noble gases as natural tracers, therefore played a key role in the investigation of excess air formation (Heaton and Vogel, 1981; Stute et al., 1992; Wilson and McNeill, 1997; Beyerle et al., 1999; Aeschbach-Hertig et al., 1999; Kipfer et al., 2002; Lippmann et al., 2003; Klump et al., 2007, 2008; Sun et al., 2008).

While there have been advancements in the understanding of gas exchange in groundwater in the last decade, the investigation of the impact of excess air formation on O_2 availability has been neglected. In particular, there have hardly been any field studies focused on this

subject (Massmann and Sueltenfuss, 2008). In particular, in riparian groundwater such field studies are rare and if presented rather as a minor part of an other study (e.g. Beyerle et al., 1999) than a major investigation. Therefore, the overall aim of this work is to combine O_2 with noble gas concentration measurements to determine O_2 turnover in groundwater, and to study excess air formation as a mechanism for the delivery of O_2 into groundwater.
However, dissolved O_2 and noble gas concentrations in riparian groundwater exhibit high variability, at both spatial and temporal scales (Whitman and Clark, 1982; Beyerle et al., 1999; Williams and Oostrom, 2000; Ingram et al., 2007; Massmann and Sueltenfuss, 2008). In particular, the hyporheic zone of a losing river is most likely prone to the same dynamical changes of chemical composition as the stream itself (for river dynamics see e.g. Kirchner et al., 2000), as during water recharge solvents are transported into the groundwater. Furthermore excess air formation due to river induced water-table fluctuations impact the dissolved gas concentrations. Hence the dynamic discharge behavior of a river is imposed on the dissolved concentrations in groundwater.
In contrast to O_2 concentration measurements, noble-gas analysis in environmental water samples is commonly conducted using laboratory-based static mass spectrometry. However, this approach is limited to the sequential analysis of individual water samples, taken in special air-tight containers (Weiss, 1968; Poole et al., 1997; Beyerle et al., 2000). With this method for sampling and analysis, the determination of noble-gas concentrations at a temporal resolution of less than one hour and over a time period of several days is therefore costly in terms of time, labor and finances. However, to study gas dynamics in the hyporheic zone of a dynamic river at an adequate enough temporal scale such high frequent noble gas concentration time-series (NGTS) are needed. Furthermore, NGTS would allow the temporal evolution of the environmental conditions at the last air/water partition to be reconstructed. Knowledge of the temporal evolution of the environmental conditions at the last air/water partition can help to determine the recharge origin and the residence time of the groundwater being studied.
To overcome these experimental limitations, in this thesis a membrane inlet instrument based on mass spectrometry is presented. The set-up is able to measure in-situ concentrations of dissolved O_2, Ar, He, Kr, and nitrogen (N_2) autonomously and quasi-continuously over several days.

1.2 Outline

This thesis is comprised of a description of the developed membrane inlet mass spectrometer (MIMS) and two studies on the gas dynamics, and in particular on O_2 turnover, in the riparian groundwater of a peri-alpine river. The sampling dates and locations of the two studies were chosen to cover the physical and biochemical gas dynamics in groundwater during a low flow period and a flood event of the river. The structure of the thesis is described in the following:

Chapter 2: Scientific background

This chapter is an introduction to dissolved gases in groundwater and to the principles of MIMS. In the first section, gas exchange processes in groundwater are discussed, whereby excess air is identified as an important gas source for groundwater. Synchronously with the discussion of excess air formation, noble gases are introduced as important environmental tracers to study gas exchange in groundwater. The introduction on dissolved gases concludes with a summary of redox processes which alter O_2, N_2 and CO_2 concentrations. The second part of the chapter includes a short description of the study site (Niederneunforn) and a short introduction to the principles of membrane inlet mass spectrometry.

Chapter 3: Membrane inlet mass spectrometer for quasi continuous on-site analysis of dissolved gases in groundwater

This chapter contains a characterization of the analytical capabilities and performance in the laboratory and in the field of the membrane inlet mass spectrometer (MIMS) developed for this thesis. In summary, the system permits quasi-continuous (every 12 min) measurements of dissolved gas concentrations (He, Ar, Kr, N_2, and O_2) in groundwater autonomously over several days. The system therefore enables the study of gas dynamics in the hyporheic zone of rivers.

Chapter 4: Argon concentration time-series as a tool to study gas dynamics in the hyporheic zone

In an initial field study, the O_2 dynamics in the hyporheic zone of a peri-alpine river (Thur, Switzerland) was investigated. Time-series of temperature and concentrations of dissolved Ar, O_2 and CO_2 were recored during a week of low flow conditions. The Ar concentration time-series was used to investigate physical gas transfer in the hyporheic zone, especially with respect to differences between gas and heat transport. Furthermore, the Ar concentrations were used to estimate travel times by cross-correlating the measured Ar concentrations with the calculated atmospheric solubility concentrations of the river. The physical gas transport information gained from the analysis of time-series of Ar concentrations was used to estimate the O_2 turnover in groundwater after water recharge.

Chapter 5: Excess air formation as a mechanism for delivering oxygen to groundwater

In a second field study we analyzed the temporal dynamics and the spatial distribution of dissolved gases (He, Ar, Kr, N_2, O_2 and CO_2) in an infiltrating groundwater system, being fed by a peri-alpine river (Thur, Switzerland), before, during and after a flood event. In particular, we investigated the injection of O_2 resulting from the formation of excess air during river-groundwater exchange, i.e. the entrapment and dissolution of air bubbles in the groundwater in response to groundwater level rise. The main result was that excess air injection contributes a significant portion of the O_2 available in groundwater.

Chapter 6: Conclusion and outlook

The last chapter includes a summary, where the most important findings are briefly discussed, and an outlook which discusses possible improvements and further uses of the method. The thesis is first summarized, focusing on the applicability of noble gas concentration time-series as a hydrological tool, followed by a conceptual discussion on the different sources and sinks of O_2 in the groundwater-river system discussed in Chapter 4 and 5. The chapter concludes with a list of suggestions for further conceptual applications of noble gas time-series and further technical applications of the MIMS developed for this thesis.

Appendix: Variables

The Appendix includes a list of variables, their units and a brief description.

2 Scientific background

2.1 Dissolved gases in water

Meteoric water contains dissolved gases originating from the atmosphere. These atmospheric gases not only contribute the major part to the amount of total dissolved gases in groundwater but, depending on their chemical properties, play an important role in many biogeochemical processes in groundwater environments. In this section, a short introduction is given to both the physical gas exchange mechanisms between atmosphere and (ground)water and to the most prominent biochemical reactions in groundwater involving dissolved gases. Please note that any other noble gas component in groundwaters, in particular the radioactive production of ^{3}He or ^{4}He is not discussed in this chapter. For a comprehensive review of noble gas abundances in water the reader is referred to Kipfer et al. (2002) or further to Morrison and Pine (1955); Mamyrin and Tolstikhin (1983); Schlosser et al. (1988).

2.1.1 Henry and diffusion coefficient

Table 2.1: Diffusion (Wise and Houghton, 1966; Broecker and Peng, 1974; Jähne et al., 1987) and Henry (Weiss, 1970; Weiss and Kyser, 1978; Weiss, 1971; Smith and Kennedy, 1983) coefficients for the stable noble gases and O_2 of water ordered by standard atomic mass (M_i).

i	M_i [g/mol]	$D_i(T_\mathrm{w} = 0\ ^\circ\mathrm{C})$ [$10^{-9}\mathrm{m^2 s^{-1}}$]	$H_i(T_\mathrm{w} = 0\ ^\circ\mathrm{C})$ [$(\mathrm{cm^3_{STP} g^{-1}})$/atm]
He	4.0026	4.74	0.0093
Ne	20.1790	2.34	0.012
O_2	31.988	1.17	0.0489
Ar	39.9480	1.44	0.053
Kr	83.8000	0.877	0.11
Xe	131.3000	0.664	0.22

Any surface water body exchanges gases with the atmosphere. Hence, dissolved gases of a well mixed water body with a constant temperature reach atmospheric solubility equi-

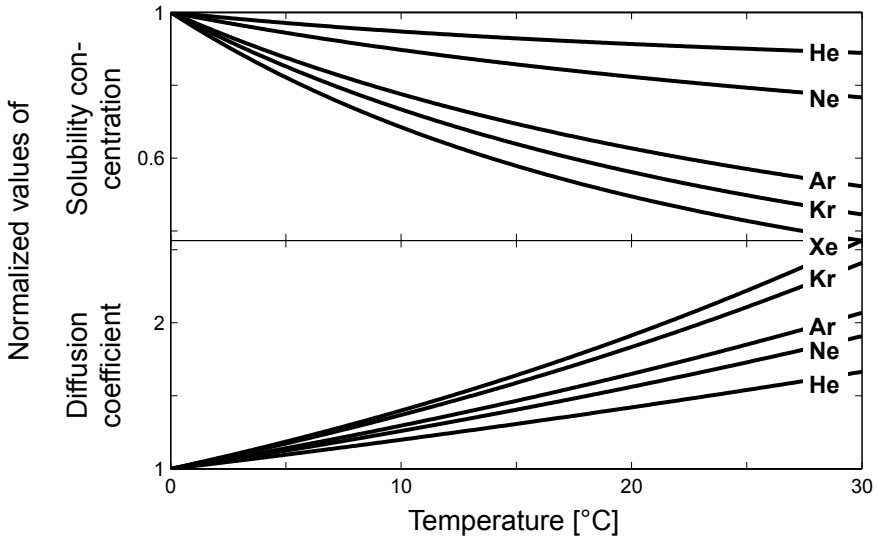

Figure 2.1: Temperature dependence of diffusion coefficients in water (Wise and Houghton, 1966; Broecker and Peng, 1974; Jähne et al., 1987) and the aquatic solubility equilibrium concentrations (Weiss, 1970; Weiss and Kyser, 1978; Weiss, 1971; Smith and Kennedy, 1983) of noble gases normalized to the respective value at 0 °C.

librium according to Henry's law, if gases are neither produced nor consumed (see e.g. Kipfer et al., 2002):

$$C_i^{\mathrm{ASW}} = H_i(T_{\mathrm{w}}, S_{\mathrm{w}}) \times p_i^{\mathrm{atm}}, \tag{2.1}$$

where C_i^{ASW} is the concentration of gas i in air saturated water (ASW), p_i^{atm} is the partial pressure of the gas in atmosphere and $T_{\mathrm{w}}, S_{\mathrm{w}}$ are temperature and salinity of the water. Besides the Henry coefficients (H_i), diffusion coefficients control the physics of air/water partitioning (see e.g. Kipfer et al., 2002). Diffusion is a transport phenomenon in which the gas flux is proportional (described by the diffusion coefficient D_i of gas i to the negative concentration gradient or more general to the negative gradient of the chemical potential. Diffusion is a kinetic and hence dynamic process in contrast to solubility which is a property of a system in equilibrium. Therefore, whether diffusivity or solubility, controls dissolved gas concentrations depends on the presence of processes or conditions influencing the dissolution process (e.g., water flow velocity or stagnant water layers) in the aqueous system studied.

To study gas exchange through the air/water boundary, noble gases are suitable tracers. Noble gases are biochemically inert and the only relevant terrestrial reservoir for noble gases in aquatic systems is the atmosphere (Kipfer et al., 2002). However, radon, which has no stable isotope, is not found in the atmosphere. From low to high mass the atmospheric noble gases are helium (He), neon (Ne), argon (Ar), krypton (Kr) and xenon (Xe). The diffusion coefficients and the Henry coefficients of the different atmospheric noble gases spread approximately over one order of magnitude (see Table 2.1). Furthermore, the temperature dependence of both coefficients increases considerably from the lighter to the heavier noble gases (see Figure 2.1, Weiss, 1970, 1971; Weiss and Kyser, 1978; Smith and Kennedy, 1983).

2.1.2 Excess air

Dissolved noble gases in groundwater are often found to be supersaturated (e.g. Heaton and Vogel, 1981; Wilson and McNeill, 1997; Beyerle et al., 1999; Aeschbach-Hertig et al., 1999; Kipfer et al., 2002). While an increase in temperature of the groundwater after initial gas exchange can lead to a supersaturation of the dissolved gases, the elemental composition of the found noble gas excess is closer to air than to air-equilibrated water. Therefore, the excess of atmospheric gases in groundwater commonly is referred to as "excess air" (Heaton and Vogel, 1981). Furthermore, the air-like composition led to the conclusion that excess air is produced by the complete dissolution of small entrapped soil air bubbles into the groundwater, e.g. due to injection of air.
Both geomorphic and hydraulic conditions influence excess air formation in groundwater. Because excess air commonly is produced at groundwater recharge or during water table rise, the local geomorphic conditions i.e. the shape and material of the aquifer (Wilson and McNeill, 1997; Holocher et al., 2003; Klump et al., 2007), plays a crucial role in trapping air and immobilization of the air bubbles (see Chapter 5). Therefore, the initial entrapped air volume and bubble size distribution depends on characteristic hydraulic properties of the aquifer such as porosity and particle size distribution (Wilson and McNeill, 1997; Holocher et al., 2003; Klump et al., 2007). Besides the bubble volume, the total pressure in the bubbles is the main factor in controlling the gas amount that dissolves in water during excess air formation. A higher pressure induces a larger solubility equilibrium concentration in the water and normally leads to a larger amount of gases being dissolved (Kipfer et al., 2002). The total pressure in the gas bubbles is a combination of atmospheric pressure (P_{atm}), hydrostatic pressure (P_{hyd}), pressure due to capillary forces and surface tension. Capillary forces and surface tension are only important if the bubble sizes are small ($\lesssim$ 0.1 mm, Klump et al., 2007). Hence, hydrostatic pressure is normally the main driver of an increased total pressure in the bubbles, e.g., a water table rise of 1 m induces an increase of 0.1 atm of total pressure.
Note that, for riparian groundwater excess air formation is to be expected, if the groundwater is hydraulically well connected to a river with dynamic discharge changes. Because the induced groundwater table rises not only lead to frequent entrapment of air bubbles but also to increased hydrostatic pressure at the location of entrapment. However, the local geomorphic conditions needs to favor the entrapment of air bubbles.

2.1.3 O_2 and excess air

Because there is no light in groundwater, no photosynthesis takes place and any O_2 must be transported into the groundwater from the surface or soil air. Rivers feeding the groundwater are such a source of O_2 for groundwater. However, the formation of excess air contributes also to the overall input of O_2 into groundwater (Rose and Long, 1988; Beyerle et al., 1999; Klump et al., 2008; Massmann and Sueltenfuss, 2008). The comprehension that O_2 is not only entering the groundwater by advection with the infiltrating river water is not new. In 1988, Rose and Long implicitly discussed excess air formation as a possible source of O_2. They did not use the term excess air, but by interpreting dissolved O_2 in groundwater they concluded that "oxygen can be transported to the phreatic zone from the overlying vadose zone". Beyerle et al. (1999) for the first time not only identified excess air formation as an O_2 source in groundwater, but also estimated the O_2 consumption

considering O_2 injection due to excess air formation. Inspired by the dynamics of the riparian groundwater of the Columbia river, Williams and Oostrom (2000) used laboratory experiments to show that a fluctuating water table can oxygenate anoxic groundwater by entrapping gas bubbles. Furthermore, Massmann and Sueltenfuss (2008) used Ne concentration measurements to study excess air formation due to water table fluctuations induced by a drinking water production well. The authors showed that, oxygenation occurred in the upper region of the aquifer where the fluctuating water table entrapped air. But below a certain depth, where the water was not affected by water table fluctuations, there was no observable excess air formation. Estimations of O_2 input at the site identified excess air as a major O_2 source whenever water table fluctuations were occurring (Massmann and Sueltenfuss, 2008).
The basis for the more recent studies (Beyerle et al., 1999; Williams and Oostrom, 2000; Massmann and Sueltenfuss, 2008) are models which enable the parameterization of excess air formation (see Section 2.1.4 or e.g. Kipfer et al., 2002). For the two field studies by Beyerle et al. (1999) and Massmann and Sueltenfuss (2008), the models were "calibrated" by noble gas concentrations. Noble gases are in particular suitable to study physical gas transport and exchange mechanisms of O_2, because the diffusion coefficient and Henry coefficient of O_2 are within the range of values of the coefficients of the different noble gases (see Table 2.1, Wise and Houghton, 1966; Weiss, 1970; Broecker and Peng, 1974; Jähne et al., 1987). In conclusion, the combined measurements of noble gas and O_2 concentrations is necessary to understand the lateral dynamics of O_2 in groundwater (see Chapter 4 and 5). However, models which enable the accurate parameterization of excess air formation need to be available.

2.1.4 Excess air models

In recent years excess air and its formation was thoroughly studied (e.g Stute et al., 1992; Beyerle et al., 1999; Aeschbach-Hertig et al., 1999; Cirpka and Kitanidis, 2001; Kipfer et al., 2002; Lippmann et al., 2003; Holocher et al., 2003; Klump et al., 2007, 2008). The resulting conceptual and numerical models describe the air/water partitioning in groundwater and yield mechanistic insight into the formation of excess air.

Simple excess air models

A good approach to excess air is to look at stationary air saturated water (ASW) containing unfractionated air bubbles. The first model of excess air formation (UA-model) describes the complete dissolution of the air bubbles into groundwater (Heaton and Vogel, 1981). Note that total dissolution is only possible as long as the final total dissolved gas pressure in water is smaller then the ambient pressure prevailing at the location. The final concentration C_i^f under these assumptions is the sum of the initial ASW concentration C_i^{ASW} and the (air) volume fraction z_i of the respective gas i of the total initial amount A of air in the bubbles per water mass:

$$C_i^f = C_i^{\mathrm{ASW}} + Az_i. \qquad \text{(UA-model)}$$

Figure 2.2 shows the changes in concentration being predicted by the UA-model or the respective models described in the following. The concentration evolution with increasing A for the UA-model is indicated with arrow ①.

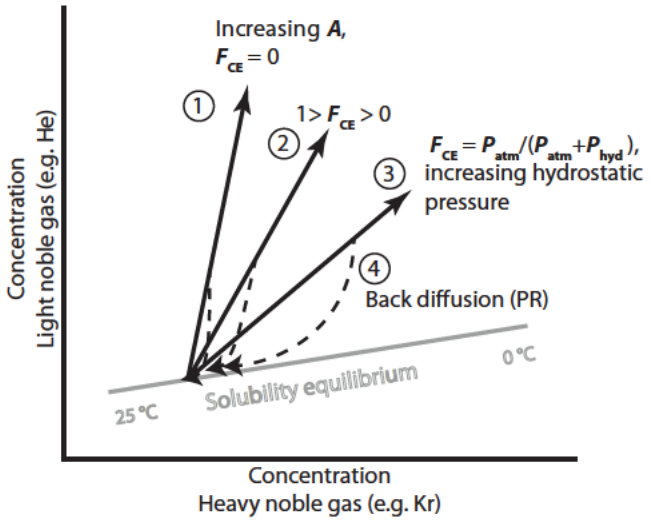

Figure 2.2: Impacts on concentrations affected by different excess air formation shown in a two elemental plot. Each arrow represents a concentration development of a specific excess air formation type. ① Total dissolution of an increasing amount of air. ② partial dissolution of an amount of air. ③ solubility concentration with increasing (hydrostatic) pressure in the entrapped air bubbles. 4. Diffusive loss after excess air formation through the air/water boundary. ①-③ normally have their origins on the solubility equilibrium line (grey). ④ Starts at the concentrations prevailing after excess air formation.

The simple UA-model is the starting point to the more complex partial re-equilibration (PR) model (Holmen and Liss, 1984; Stute et al., 1992; Aeschbach-Hertig et al., 1999; Kipfer et al., 2002). This model considers an additional diffusive loss of the dissolved gases back into the soil air after complete dissolution of the air. The diffusive loss is expressed by an exponential term multiplied by the excess air term of the UA-model equation:

$$C_i^f = C_i^{\mathrm{ASW}} + Az_i \exp\left(-F_{\mathrm{PR}}\left(\frac{D_i}{\Omega_{\mathrm{PR}}}\right)^{\beta}\right). \qquad \text{(PR-model)}$$

The diffusive degassing leads to a fractionation of the excess air composition due to differences in the diffusion coefficients of the different gases (D_i, see Table 2.1). The fractionation depends on the coefficient F_{PR} which is proportional to the time elapsed since complete dissolution. Ω_{PR} (cm^2/s) depends on the geometry and intrinsic time of the described system and β depends on the transfer of gases from bulk water through the near-surface water to the soil air (Holmen and Liss, 1984). In Figure 2.2, arrow ④ shows the evolution of the noble gas concentrations due to diffusive loss to the soil air in groundwater.

The PR-model is actually a special case of the more complex "multistep re-equilibration" (MR) model (Kipfer et al., 2002). The MR-model describes the cycling of various injection of gases and degassing steps (see Kipfer et al., 2002). This is physically more realistic, as in order to explain the same excess air pattern, the amount of injected air for each step is

much smaller than in the case of a single injection (several hundred percent in comparison to the typical range of 10-50 %, Kipfer et al., 2002).
Furthermore, the PR-model is very similar to the partial degassing (PD) model (Lippmann et al., 2003). The PD-model however describes a diffusive gas loss that affects the total gas concentration rather than only the excess air component, e.g. partial degassing of a gas happens if bubbles of an other gas are present in the water. In mathematical terms, the exponent describing degassing needs to be multiplied to the whole concentration of the UA-model (Lippmann et al., 2003).
The closed-system equilibration (CE) model is an expansion of the UA-model and takes into consideration that complete dissolution of the bubbles cannot per se be assumed. Instead, the dissolved gases in groundwater are assumed to be in solubility equilibrium with the gases in the bubble at an enhanced hydrostatic pressure. Note that due to the finite size of the bubbles, the gas composition in the bubbles normally differs from that of air due to the differences in solubility of the different (noble) gases. Using Henry's Law and mass conservation the final dissolved-gas concentrations are calculated to be (Aeschbach-Hertig et al., 2000; Kipfer et al., 2002):

$$C_i^f = C_i^{\mathrm{ASW}} + \frac{(1 - F_{\mathrm{CE}})Az_i}{1 + F_{\mathrm{CE}}Az_i/C_i^{\mathrm{ASW}}}, \qquad \text{(CE-model)}$$

where F_{CE} describes the degree of dissolution, i.e. F_{CE} is in the range of $[0, 1]$ and is proportional to A_t/A, where A_t is the remaining gas concentration in the bubbles. Furthermore, F_{CE} is inversely proportional to the pressure inside the bubbles (i.e. $F_{\mathrm{CE}} \sim 1/(P_{\mathrm{atm}} + P_{\mathrm{hyd}})$, with P_{atm} the atmospheric pressure and P_{hyd} the hydrostatic pressure at gas bubble location). The elementary composition of the dissolved noble gases in water heavily depends on F_{CE} (see Figure 2.2, arrows ①-③). In case of $F_{\mathrm{CE}} = 0$ all the bubbles are totally dissolved and $F_{\mathrm{CE}} \approx 1$ means that almost no migration of the gases in the bubble to the water has occurred. Furthermore, if F_{CE} values are near $P_{\mathrm{atm}}/(P_{\mathrm{atm}} + P_{\mathrm{hyd}})$, then the dissolved concentrations are near atmospheric solubility, but at an elevated total pressure (i.e. $P_{\mathrm{atm}} + P_{\mathrm{hyd}}$). On the other hand for $F_{\mathrm{CE}} = 0$ the model merges with the pure excess air model (UA-model).
There are further models which use the approach of the CE-model (i.e. solubility equilibrium and no advection), but consider a non-atmospheric composition of the initial gas phase, e.g. the depleted oxygen (DO) model considers O_2-depleted air due to microbial activity (Hall et al., 2005). A smaller O_2 partial pressure in the gas phase leads to higher partial pressures of the other gases, as the total pressure equals the total external hydrostatic pressure. However, the DO-model is equal to the CE-model if the air volume fractions z_i in the CE-model are changed accordingly
Note that in all models mentioned so far, the initial dissolved gas concentrations are implicitly assumed to be in atmospheric solubility equilibrium at the local groundwater temperature (e.g Stute et al., 1992; Beyerle et al., 1999; Aeschbach-Hertig et al., 1999; Kipfer et al., 2002; Lippmann et al., 2003; Hall et al., 2005). However, this assumption is not necessary fulfilled as groundwater temperature is often not conserved and changes during groundwater flow. The relation between heat and gas transport is further investigated and discussed in both Chapter 4 and 5.
In summary, these simple models enable the parameterization of excess air formation. Furthermore, the model parameters (T_{w}, A, F_{CE}, F_{PR},...) can be determined from the

observed noble gas concentration by least-squares regression (Aeschbach-Hertig et al., 1999). Therefore, in combination with noble gas concentration measurements these models enable the estimation of the excess air component of any other gas including O_2 (e.g. Kipfer et al., 2002). The excess air components for O_2 are needed to estimate the consumption rates of the reactive O_2. Because, such estimations depend on the knowledge of the initial gas concentrations, which are significantly biased if the respective excess air component is ignored (see Chapter 5).

Advective influences on excess air formation

All models introduced so far neglect the gas transport through advection with groundwater flow, i.e. both gas and water phase are thought to be immobile. In a real aquifer, especially near rivers, advective transport removes the gases from the location of gas exchange with the entrapped bubble, in the direction of the water flow (Fry et al., 1995; Cirpka and Kitanidis, 2001; Holocher et al., 2003; Klump et al., 2008).
In order to describe the gas/water partitioning, besides Henry's Law and mass conservation, dissolved gas transport needs to be considered. The equation describing gas transport (for a mathematical discussion see Cirpka and Kitanidis, 2001) introduces several new parameters which differ for different gases and depend on the local aquifer matrix. Such a local equilibrium (LE) model, that describes the physics of gas/water partitioning in moving water, cannot be calibrated by a simple analysis of the dissolved noble gas concentrations in a groundwater sample. However comparison of numerical solutions of the LE-model can be used to determine under which conditions the simple model fails to describe the gas input into groundwater if advection is present i.e., when does the inversion of the CE-model equation fail to deliver realistic physical quantities (e.g. T_{w}, A or F_{CE}). Such a discussion is given in Chapter 5 where the CE-model is used to determine O_2 input due to excess air formation in hypoxic or anoxic groundwater. The discussion is based on the results of Klump et al. (2008), who compared the CE-model to numerical solutions of the LE-model.

Kinetic influences on excess air formation

In general, local gas solubility equilibrium between gas bubbles and water cannot be assumed. Therefore, Holocher et al. (2003) developed an excess air model based on the kinetic mass transfer between entrapped, spherical air bubbles and the surrounding water phase (i.e., the kinetic bubble diffusion (KBD) model). The kinetic mass transfer between bubble and water is limited by a diffusion-controlled stagnant water film around the bubble (Holocher et al., 2003). The transfer coefficient k_i, which quantifies the gas flux (per concentration difference) of a gas i through the film is dependent on the diffusion coefficient D_i of the gas in water and the thickness of the stagnant water layer. This thickness increases with bubble radius and decreases with increasing velocity of the water flow (Epstein and Plesset, 1950; Holocher et al., 2003).
According to Epstein and Plesset (1950), k_i can be determined under these conditions as

$$k_i = D_i \left(\frac{1}{r} + \sqrt{\frac{v}{2\pi r D_i}} \right), \tag{2.2}$$

with v the seepage velocity of the groundwater and r the bubble radius. Equation 2.2 shows that the transfer coefficient is high for small r. Hence, if r is small, the time scale to establish a steady state between the gases in the bubble and in the surrounding water is short. Differences between the prediction of the KBD-model and the equilibrium models (e.g., CE-model or LE-model) are expected if the gas transfer is slow, i.e. if k_i is small or more specific if the ratio of the characteristic timescales of advection to that of kinetic gas transfer (i.e. the dimensionless Dahmköhler number) is small.
To estimate the influence of kinetic effects Klump et al. (2008) determined the dimensionless Dahmköhler number for several different hydrological scenarios. The authors found that the higher the Dahmköhler number is, the less pronounced the influence of kinetic effects on the final dissolved gas concentrations are. The numerical study further showed that for Damköhler numbers larger than 100, the differences in the results of the KBD model to that of the local equilibrium models become negligible. For excess air formation by regional groundwater recharge, the Dahmköhler ernumber is normally high ($\gg 100$) and hence the local equilibrium model is valid. However, in the hyporheic zone or in riparian groundwater where water table fluctuations are fast (i.e. small characteristic timescale of advection), the Dahmköhler number may be significantly lower than 100 and kinetic effects are prone to play an important role.

2.1.5 Gases related to redox processes

Most of the important biochemical processes in groundwater, involve reactants or products in gaseous form (e.g., Streeter and Phelps, 1925; Whitman and Clark, 1982; Korom, 1992; Malard and Hervant, 1999; Rivett et al., 2008). Microbial respiration of O_2 (i.e., aerobic respiration) is one important example of such a process. In general, microbes in groundwater obtain their energy from redox processes, i.e., by inter-compound electron transport. Dissolved organic matter is typically the most common electron donor in groundwater (Rivett et al., 2008). Microbes preferentially use the electron acceptor with the highest Gibbs free energy, which is normally O_2. Therefore aerobic respiration leads to the fast depletion of dissolved O_2 and infiltrated nutrients along the lateral hyporheic flow path in groundwater (Brunke and Gonser, 1997; Malard and Hervant, 1999). Vice versa, the reduction of O_2 is an indicator for microbial metabolic activity and is a key parameter for evaluating the quality of groundwater and drinking water (Malard and Hervant, 1999). This can be generalized for other electron donors. However, O_2 plays a key role because of its high abundance in the atmosphere, its production by photosynthesis in surface water and its leading role as an electron acceptor in redox processes.
If O_2 is depleted, the reduction of the electron acceptors with the next highest Gibbs free energy becomes energetically favorable i.e. Nitrate NO_3^- (see e.g Schwarzenbach et al., 2003). The nitrate found in groundwater is mostly derived from agriculture activities (Defra, 2002), but there are other significant sources (Wakida and Lerner, 2005). Nitrate is reduced trough a series of intermediate nitrogen oxide products to N_2 i.e., dentrification. Note that not all microbes are able to use all the steps in the denitrification chain as an energy source.
In most redox processes involving organic matter CO_2 occurs as an end-member. In particular in respiration the consumed O_2 is stochiometrically linked one-to-one to CO_2. However, CO_2 reacts with calcite ($CaCO_3$), which is often present in aquifers, and liberating dissolved Ca^{2+} and HCO_3^- ions. Hence, the biologically produced CO_2 is not preserved in

groundwater. The relationship between CO_2 and H_2CO_3, H^+, HCO_3^- and Ca^{2+} (and further Mg^{2+}) is complex and is discussed in detail e.g. by Stumm and Morgan (1995).
In conclusion, only the direct quantification of O_2 consumption (see Section 2.1.3) is a measure for microbial activity, as changes in CO_2 concentrations can be significantly biased (Deffeyes, 1965; Stumm and Morgan, 1995). Note that CO_2 concentrations still serve as an important indicator for O_2 consumption if in the interpretation the interaction with carbonic acid is considered (see Chapter 5).

2.2 Study site: Niederneunforn at river Thur

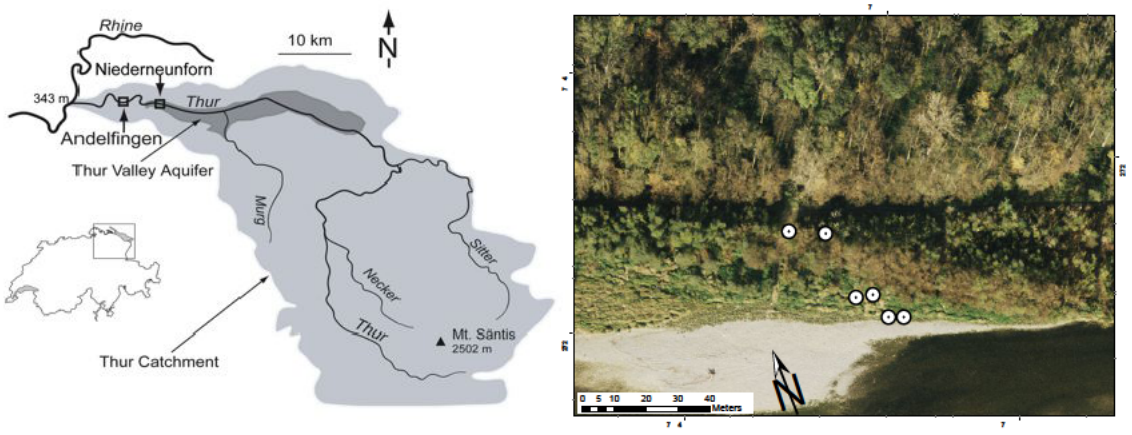

Figure 2.3: The river Thur and an aerial photograph of the field site at Niederneunforn with the groundwater piezometers (filled circles with black dot) used during this work.

Most of the investigations of this work where carried out at the RECORD (Restored Corridor Dynamics, 2007-2011) project field site at the river Thur (Switzerland). Due to river revitalization, the river Thur strongly interacts with the local groundwater at this site. The goals of the RECORD project were the assessment and modeling of coupled ecological and hydrological dynamics in the restored corridor of a river (i.e., the river Thur). For further information on the RECORD project the reader is referred to Schneider et al. (2011) or to www.cces.ethz.ch/projects/nature/Record.
The river Thur, a tributary of the Rhine river (Figure 2.3), is located in the northeast of Switzerland. Its catchment area of 1700 km^2 includes the limestone formation of Säntis with an elevation over 2500 meter asl. The high elevation difference between the confluence of the river (343 m) and Säntis and the fact that there is no lake or reservoir along the course, allows the Thur to have the very dynamic flow regime of an alpine river. The river Thur is known for rapidly occurring changes in water discharge of 2 m^3/s to 1130 m^3/s (mean 50 m^3/s, recording period: 1904-2005 Binderheim-Banakay et al., 2000; BAFU, 2010).

In the late 19$^{\text{th}}$/early 20$^{\text{th}}$ century most of the river stretch was channelized for flood protection. However, since the early 1990s, several 1-3 km long river sections were widened to ensure flood protection with ecological demands (Schneider et al., 2011). One of these revitalized sections is located at the RECORD field site in Niederneunforn where the studies for Chapter 4 and Chapter 5 were conducted on several piezometers of the northern river bank (Figure 2.3). The aquifer at Niederneunforn, a deep sandy gravel layer of 5-6 m, is sealed by impervious lacustrine clays at the bottom and covered by a low permeable sand/loam layer at the top. Bank infiltration from the river Thur is the main source recharging the aquifer ("losing river", see Vogt et al., 2010a). The good hydraulic and hydrological connectivity of the aquifer results in fast flowing groundwater (Vogt et al., 2010a). The groundwater travel times are small, i.e. they range from less than one day to reach the nearest piezometer and up to approximately 4.5 days to reach the most distant piezometer (Vogt et al., 2010a).

2.3 Membrane inlet mass spectrometry

Membrane inlet mass spectrometers (MIMS) are used to quantify volatile species in water. In recent years such "classical" MIMS have been successfully applied for the on-site quantification of dissolved gases in surface water (Tortell, 2005; Schlüter and Gentz, 2008; Gueguen and Tortell, 2008; Camilli and Duryea, 2009; Etzkorn et al., 2009) and in groundwater (Eschenbach and Well, 2011; Visser et al., 2011). Thus the developed system to measure noble gas concentration is based on the MIMS technology (see Chapter 3). The following sections briefly introduce the main principles of MIMS.

2.3.1 Ion source, separator and detector

A mass spectrometer (MS) is an analytical instrument which is used to determine the elemental composition of an analyte. The general principle behind a MS is the separation of ionized particles with an electro-magnetic field. A MS consists of four major components: inlet, ion source, separator and detector.

Ion source: The term ion source refers to the device where the analytes are ionized, i.e. where at least one electron is separated from the atoms, molecules or compounds. The ionization method used in the MIMS developed for this work is ionization by electron impact, i.e. by removing electrons of the highest orbit of the particles by collision with accelerated electrons. During ionization, molecular compounds often fragment, and double ionization occurs if the electrons have enough kinetic-energy.

Separator: After leaving the ion source, the ions are spatially (or temporally) separated by using electromagnetic fields ($\mathbf{E}, \mathbf{B}$). The acceleration $\mathbf{a}$ of a point charge Q with mass m can be calculated using Lorentz's force law and Newton's second law of motion:

$$\mathbf{a} = \frac{Q}{m}(\mathbf{E} + \mathbf{v_p} \times \mathbf{B}), \tag{2.3}$$

where $\mathbf{v}_\mathrm{p}$ is the velocity of the particle. In our case Q is $+ze$ with z= 1, 2, and the electron charge $e = 1.602176565(35) \times 10^{-19}$ C. The dependency of $\mathbf{a}$ on m/Q means that particles are separated based on their mass-charge ratio i.e. according to their specific mass.

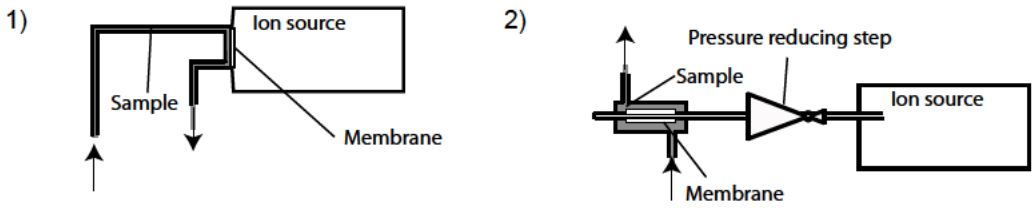

Figure 2.4: Comparison of a "classical" flow through membrane inlet (Kotiaho, 1998) to the membrane inlet used in this work (GE-MIMS, see Chapter 3).

Hence, particles with different masses are not necessarily separated, e.g. $^{40}Ar^{++}$ and $^{20}Ne^{+}$ have a very similar mass-charge ratio.
In the quadrupole mass spectrometer, which was used in this work, voltages applied to 4 parallel circular rods generate an oscillating electric field i.e. a quadrupole field. The ions are separated based on the stability of their trajectories in the quadrupole field (stable means the trajectory does not hit the rods). The stability of the trajectories and hence the filtered mass-charge range depends on the setting of the voltages and the frequency of the field oscillation. Quadrupole mass spectrometers are favored for environmental in-situ MIMS applications because of the reasonable price and the lower weight than other types of MS.
Detector: The MS used in this work contains two different detectors to measure the current of the ion beam after passing the separator: the Faraday cup (Brown and Tautfest, 1956) and an electron multiplier (EM, Allen, 1947). The Faraday cup, which is held at a constant potential over a high ohmic resistor ($> 10^9\ \Omega$), catches the ions. The small electrical current in the resistor is approximately equal to the current of the beam. The high ohmic resistor is needed to determine currents down to 10^{-13} A, i.e., by measuring the voltage across the resistor (which then ranges above 1 mV). Faraday cups are very robust and linear detectors but not very sensitive.
For smaller ion beams an EM is used to amplify the measured beam. In principle, the EM is a "charge multiplier". It uses special resistive glasses to produce, from the impact of an accelerated ion, an avalanche of electrons. Depending on the chosen acceleration voltage (1 kV to 2 kV), the impact of a single ion results in up to 10^7 electrons, i.e. an amplification of approximate 10^7.
Both the ion source and the separator need high vacuum conditions, and therefore, MS are equipped with sophisticated pump systems (Leybold, 1987). For further informations on mass spectrometry in general, we refer the reader to de Hoffmann and Stroobant (2007).

2.3.2 Membrane inlets

Through the MS inlet a sample of the analyte is introduced into the high vacuum environment of the ion source. The inlets set-up will vary depending on the physical or chemical properties of the sample. The inlet used in this work uses a membrane to selectively transport gases to the MS. In particular, the semi-permeable membrane blocks water but

permits the dissolved gases to enter the ion source. Membrane inlets have therefore been commonly used to determine concentrations of dissolved gases in water (Johnson et al., 2000; Ketola et al., 2002; Davey et al., 2011; Tortell, 2005; Schlüter and Gentz, 2008; Gueguen and Tortell, 2008; Camilli and Duryea, 2009; Etzkorn et al., 2009; Eschenbach and Well, 2011; Visser et al., 2011).
The efficiency and the selectivity of the permeation (i.e. the membrane diffusion coefficient D_m^i of gas i) depends on the membrane material, temperature and pressure, and on the physical and the chemical properties of the analyte (Kotiaho and Lauritsen, 2002). The transport process of a given molecule i through a flat membrane with thickness l_m and surface area S_m is described by Fick's equation of diffusion. In steady state the flux J_{ss}^ithrough the membrane is calculated by:

$$J_{\mathrm{ss}}^i = \frac{S_m D_m^i}{l_m} \Delta C_i, \tag{2.4}$$

where $\Delta C_i = C_i - H_i p_i$, with the partial pressure p_i on the MS side of the membrane and C_i the concentration of gas i in water. Two special cases of Equation 2.4 are important for membrane inlets: $p_i = 0$ and $\Delta C_i = 0$.
$\boldsymbol{p_i = 0}$: The case of a negligible small partial pressure p_i, results in a flow of gas i to the ion source that is proportional to the concentration C_i in water (see Figure 2.4, Type 1). The inherent problem of such MIMS is that the total diffusivity of the membrane is highly dependent on temperature and on the clogging of the membrane. Hence, J_{ss}^i depends on water temperature and on the water quality. Note that, all types of membrane inlets listed in the reviews of Kotiaho (1998) and Davey et al. (2011) belong to this case.
$\boldsymbol{\Delta C_i = 0}$: The gases in the water and on the MS side of the membrane are in solubility equilibrium. The partial pressure of the gas on the MS side is then proportional to the concentration C_i in water. The "gas equilibrium" MIMS system (GE-MIMS, see Chapter 3) that was developed for this work is based on this approach. However, the MS is coupled to the membrane via a pressure reduction inlet, as the partial gas pressures need to be greatly reduced for final gas analysis in the MS (see Figure 2.4, Type 2).

3 Membrane inlet mass spectrometer for the quasi continuous on-site analysis of dissolved gases in groundwater

Chapter 3 has been published as:
Mächler, L., Brennwald, M. S. and Kipfer, R. (2012). Membrane inlet mass spectrometer for the quasi-continuous on-site analysis of dissolved gases in groundwater. *Environ. Sci. Technol.* **46**, 8288–8296.

Abstract

We developed a stand-alone system based on a membrane inlet mass spectrometer (MIMS) for measuring dissolved gas concentrations in groundwater under field conditions. The system permits the concentrations of dissolved gases (He, Ar, Kr, N_2, and O_2) in groundwater to be determined quasi-continuously (every 12 min) with a precision of better than 4% for He and Kr, and with a precision of 1% for Ar, N_2 and O_2 in air-saturated water. The detection limits are below 3×10^{-9} cm^3_{STP}/g for the noble gases and below 400×10^{-9} cm^3_{STP}/g for N_2 and O_2. The results of a first deployment of the system in the field indicate that changes in the concentration of Ar that result from diel fluctuations of 3 °C in the river water temperature was still able to be resolved in groundwater, although the corresponding temperature signal almost vanished.

3.1 Introduction

The hyporheic zone — the transition zone between a river and the groundwater underlying it — is itself an active and dynamic bio-geochemical aquatic system (Kirchner et al., 2000). Exchanges of water, nutrients, and organic matter occur in response to variations in discharge, bed topography and porosity. Feeding rivers which recharge adjacent aquifers are highly dynamic, being characterized by high variability in their discharge rates and in their chemical composition; e.g., in dissolved oxygen and organic matter (Uehlinger and Naegeli, 1998; Kirchner et al., 2000; Uehlinger, 2006). The hyporheic zone is an important habitat for the microbes which chemically reduce nutrients and substrates infiltrated into the groundwater (Brunke and Gonser, 1997; Malard and Hervant, 1999; Boulton et al., 1998; Hayashi and Rosenberry, 2002).
Of the chemical variables investigated in relevant studies (Schwoerbel, 1961; Husmann,

1971; Williams and Hynes, 1974; Poole and Stewart, 1976) oxygen (O_2) is probably the most important biologically, and often the most variable (Whitman and Clark, 1982). O_2 depletion in the hyporheic zone reflects microbial activity and is directly linked to the availability of organic matter and to water quality (Whitman and Clark, 1982; Rose and Long, 1988; Boulton et al., 1998; Malard and Hervant, 1999; Brunke and Gonser, 1997; Datry et al., 2004).

However, bio-geochemically induced O_2 depletion is difficult to determine because the total input of O_2 into the groundwater, either dissolved in the infiltrating river water or resulting from gas exchange within the aquifer, is often unknown (Kipfer et al., 2002; Holocher et al., 2003; Klump et al., 2008). In particular, it cannot normally be calculated by assuming atmospheric solubility equilibrium, as the equilibrium concentration is controlled mainly by local soil temperature and not necessarily by the temperature prevailing during the last occurrence of gas partitioning (Beyerle et al., 1999). Gas partitioning in porous media by the entrapment and dissolution of air bubbles in response to water-table fluctuations or groundwater recharge (Heaton and Vogel, 1981; Klump et al., 2007, 2008) not only leads to the formation of excess air (a surplus of atmospheric gases relative to atmospheric solubility equilibrium that is typical of groundwater), but also contributes substantially to the overall input of O_2 into groundwater (Beyerle et al., 1999; Klump et al., 2008). In conclusion, initial O_2 availability in the hyporheic zone may be much larger than expected based on atmospheric equilibrium considerations alone.

Measurements of atmospheric noble-gas concentrations are useful in quantifying physical gas exchange and gas transport in groundwater. Specifically, such measurements enable the soil temperature at recharge to be reconstructed by calculating equilibrium concentrations as well as the amount of excess air (Klump et al., 2007, 2008; Beyerle et al., 1999; Aeschbach-Hertig et al., 1999; Kipfer et al., 2002).

Focusing on O_2, we note that argon (Ar) in particular represents an almost ideal conservative tracer for O_2 dynamics. This is because both the diffusion coefficients and Henry coefficients, which control the physics of air/water partitioning (Kipfer et al., 2002; Klump et al., 2007, 2008), are very similar for Ar and O_2 (Wise and Houghton, 1966; Broecker and Peng, 1974; Jähne et al., 1987; Weiss, 1970).

Noble-gas analysis is commonly conducted using laboratory-based mass spectrometers. However, this approach allows only the sequential analysis of individual water samples, taken in special air-tight containers (Weiss, 1968; Poole et al., 1997; Beyerle et al., 2000). With the available experimental protocol for sampling and analysis, the determination of noble-gas concentrations at a temporal resolution of less than one hour and over a time period of several days is therefore costly in terms of time, labor and finances.

To overcome these experimental limitations, we present here a membrane inlet instrument based on mass spectrometry which is able to measure concentrations of dissolved O_2, Ar, helium (He), krypton (Kr), and nitrogen (N_2) on-site in the field autonomously and quasi-continuously (with a time resolution of 12 min per measurement) over several days.

Membrane inlet mass spectrometers (MIMS) are used to quantify volatile species in water. In general the membrane separates the water from the high vacuum environment of the mass spectrometer (Johnson et al., 2000; Ketola et al., 2002; Davey et al., 2011). In recent years such “classical” MIMS have been successfully applied for the on-site quantification of dissolved gases in surface water (Tortell, 2005; Schlüter and Gentz, 2008; Gueguen and Tortell, 2008; Camilli and Duryea, 2009; Etzkorn et al., 2009) and in groundwater (Eschenbach and Well, 2011; Visser et al., 2011).

"Classical" MIMS systems enable measurements of dissolved gases in groundwater at high temporal resolution. On-site calibration of such systems is required, as the total diffusivity of the membrane is highly dependent on temperature and on the clogging of the membrane, and sensitivity fluctuations of the MS are to be expected. However, calibration is technically challenging because it requires water with known dissolved gas concentrations, which prevents autonomous long-term use of this method in the field.
Besides MIMS, other systems that measure the concentrations of dissolved radon or carbon dioxide in water also rely on membranes. In these systems, an equilibrium is established between the dissolved gas concentrations in water and the gas phase to be analyzed. The partial pressures in the gas phase are then determined with a gas analyzer — e.g., an infrared gas analyzer (IRGA, Carignan, 1998) or a radon sniffer (Schmidt et al., 2008) — which consumes virtually no gas, so the solubility equilibrium is not disturbed (Demarty et al., 2011; Huxol et al., 2012).
The "gas equilibrium" MIMS system (GE-MIMS) that we have developed is based on this approach. An MS, used as a gas analyzer, is coupled to the membrane via a pressure reduction inlet. The GE-MIMS is suited to long-term operation in the field, because fluctuations in the sensitivity can be controlled by calibrating it with ambient air.
In the following sections we introduce the basics of the GE-MIMS and discuss the performance of the instrument based on several laboratory experiments and on a field study that illustrates the performance of the instrument under field conditions.

3.2 Method

The GE-MIMS system is based on establishing a gas equilibrium between the water and the extraction chamber (EC) in which the gases accumulate after migrating from the water through the membrane (see Figure 3.1 B). In order to establish an equilibrium between the dissolved gases in the water and the respective gases in the EC, the gas flux extracted for detection from the EC must be negligible. The influence on the gas equilibrium of a non-negligible, but very low gas flux from the EC — i.e., of a slightly lower pressure in the EC — is discussed in the next section. If the flux is negligible, the partial pressure of a gas i in the EC ($p_{\mathrm{i}}^{\mathrm{EC}}$) and its concentration C_i in the water establish an equilibrium according to Henry's law (Aeschbach-Hertig et al., 1999; Weiss, 1970; Weiss and Kyser, 1978; Weiss, 1971; Smith and Kennedy, 1983); i.e., the values of p_{i}^{EC} depend on the solubility of the gases in the water, but not on the permeability of the membrane (Manning et al., 2003).
For air-saturated water, the total pressure in the EC is equal to the atmospheric pressure. However, for final gas determination in the MS, the pressure needs to be strongly reduced (by a factor of 10^9). We therefore connected the GE-MI to the MS via two pressure-reducing stages (Figure 3.1 A). The first stage, a 3 m long capillary (VR1), reduces atmospheric pressure to a medium vacuum ($\sim$ 1 hPa). The medium vacuum is maintained by a diaphragm pump, in which most of the gas extracted from the EC ends. In the second stage, the remaining gas is introduced through a pressure-reducing valve (VR2) into the high vacuum of the MS ($< 10^{-6}$ hPa), which is maintained by a hybrid turbo-molecular drag pump (Figure 3.1 A). This two-stage set-up results in a gas flow of $\sim$ 1 $\mathrm{cm}^3_{\mathrm{STP}}$/min extracted through the capillary from the EC. This flow ensures that the portion of the gas that is introduced into the mass spectrometer is a representative sample of the gas in the EC and is not simply gas which may have accumulated in front of the inlet, for instance

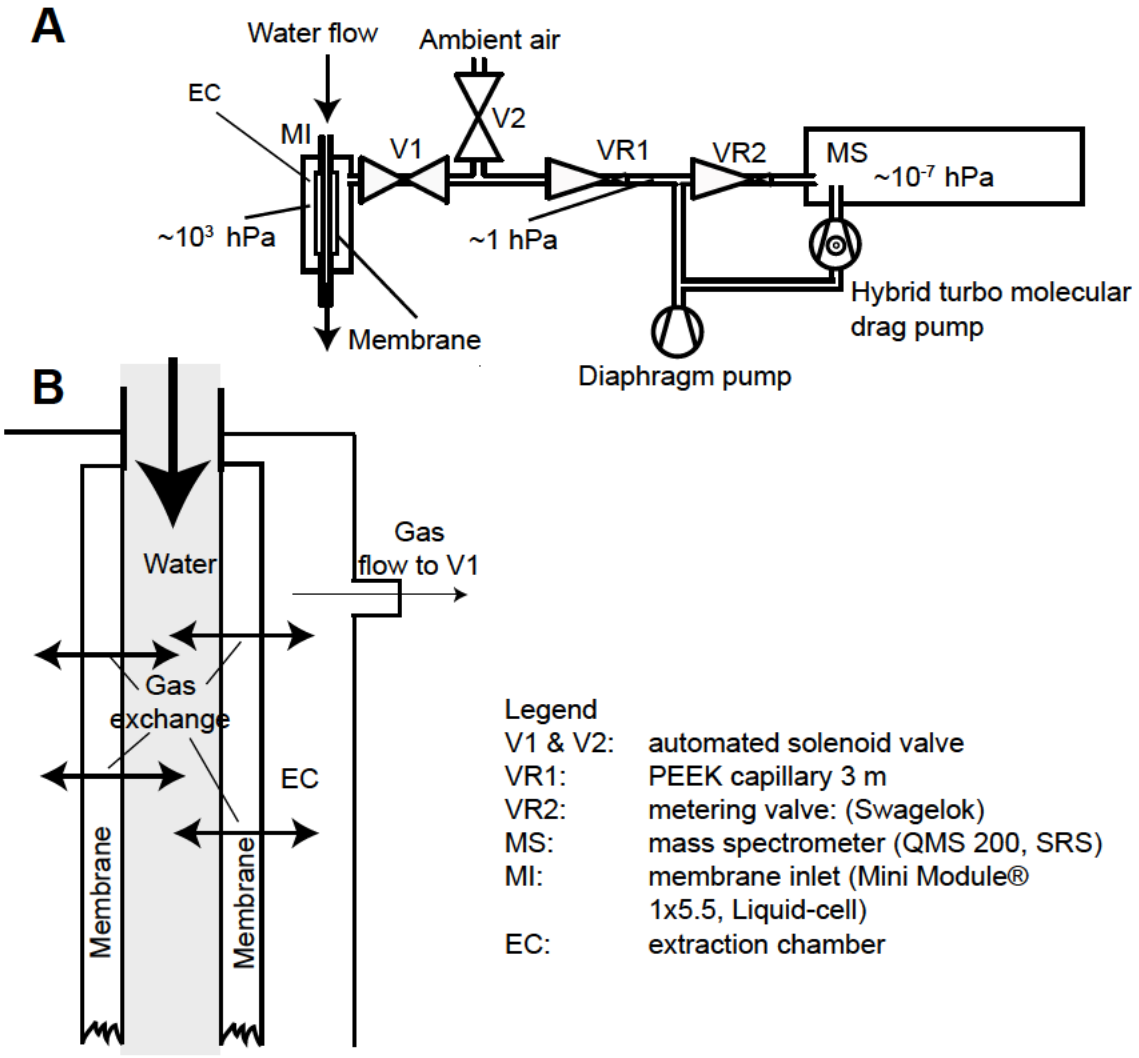

Figure 3.1: **A)** Diagram of the GE-MIMS. **B)** Diagram of the membrane inlet device separating the dissolved gases from the liquid water. For technical details see the appendix of this chapter.

from the previous gas content of the EC. The result of the final gas analysis in the MS are signals (i.e., currents) which, for each given gas species i, are proportional to $p_{\mathrm{i}}^{\mathrm{EC}}$, and hence to C_i.
As a further result of this instrumental setup, for atmospheric gases the GE-MIMS can be calibrated by connecting the capillary to ambient air instead of to the EC. The valves V1 and V2 of the inlet system (see Figure 3.1) enable the apparatus to be switched between the two modes of dissolved gas measurement (V1 open, V2 closed) and air calibration (V2 open, V1 closed).
As a membrane inlet we used a mini module (Liqui-Cel®, Membrane Contactor) which consists of a polyurethane fiber-membrane placed in a polycarbonate housing (dimensions: 178 mm $\times$ 40 mm). The use of a fiber membrane results in a relatively large active surface area (0.18 m^2) compared to the volume of the EC (25 mL). The valves V1 and V2 are automated solenoid valves (Minisol, fluid automation systems), which allow fast valve operation.
The mass spectrometer used in our GE-MIMS is a commercially available portable (44 cm $\times$ 20 cm $\times$ 61 cm, 35 kg) residual gas analyzer (QMS 200, Stanford Research Systems, SRS, 2000), equipped with an electron impact ion source, a quadruple mass filter and a dual faraday/electron-multiplier detector. To adjust the gas flux into the MS, the switching inlet valve was replaced by a metering valve (VR2). The gas analyzer is operated using an external computer program that was developed at ETH Zürich to control static noble gas spectrometers (Beyerle et al., 2000). Once installed at the field site, the system can operate and record dissolved gas concentrations for several days without further maintenance. Further technical details of our GE-MIMS are given in the appendix of this chapter.

3.3 Measurement procedure

The instrumental setup described above enables the partial pressure of a gas i in the extraction chamber (p_i^{EC}) to be determined if the partial pressure of the gas in the free atmosphere is known. For the case of a non-negligible but very low gas flux out of the EC, the procedure to determine p_i^{EC} is similar. In this case, however, Henry's law does not fully describe the gas partitioning in the membrane inlet (see below). In this section we discuss in detail the p_i^{EC} determination procedure for He, Ar, Kr, N_2 and O_2.
The strength of the signal of a gas i measured by the MS is proportional to p_i^{EC}. For a given mass/charge ratio, the signal is defined as the peak value of the output current at the selected detector. For each gas, we chose this ratio to be equal to the mass/charge ratio of a single ionized particle. The values of these ratios are as follows: 4 m/z for He, 28 m/z for N_2, 32 m/z for O_2, 40 m/z for Ar, 84 m/z for Kr, 18 m/z for H_2O and 44 m/z for CO_2 (where m is the relative molecular mass in unified atomic mass units and z is the electrical charge measured in units of the absolute value of the charge on an electron). A channel electron-multiplier is used to detect the noble gases, and a Faraday cup to detect N_2 and O_2. In a measurement cycle of 20 s the signal of each of the seven gases was measured for 1 s. The remaining 13 s were used to read the zero levels of the detector signals (peak base line).
The partial pressures of the gases in the EC need time to reach steady state after the EC has been connected to the MS (Figure 3.2). The typical half-life of the decline to steady state was determined to be around 1 min. For all gases analyzed, the half-life ($t_{1/2}$) was

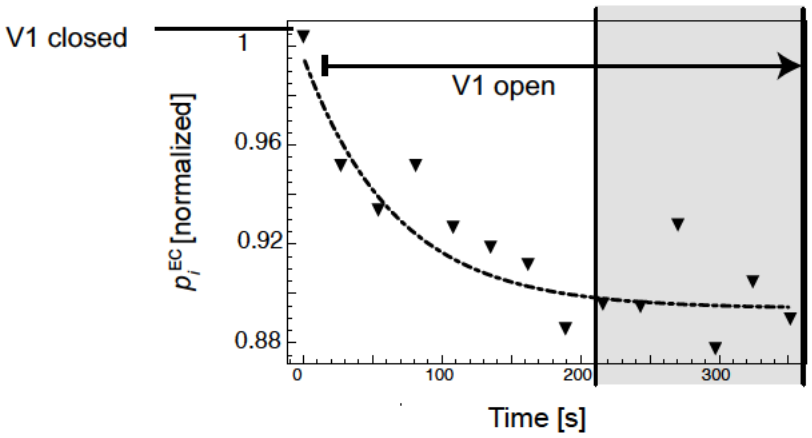

Figure 3.2: The decline in the partial pressure p_i^{EC} of a gas i in the extraction chamber from the undisturbed gas equilibrium condition to the steady state that eventually results when a small amount of gas is extracted from the extraction chamber by opening valve V1. Only data from the shaded region are used for calculating the dissolved-gas concentrations in the water sample.

found to be independent of the water flow rate Q_w as long as Q_w exceeded 0.5 L/min. The signals measured during the first 210 s $= 3.5t_{1/2}$ (waiting time) after connecting the EC to the MS (V2 closed, V1 open), when the gas exchange is not yet in steady state, are therefore not used for quantitative gas determination. The data acquired over the next 150 s are used to calculate a mean signal. We note that the concentration change (ΔC_{max}) between two measurements that can be resolved depends on the duration of the waiting time. For instance, a waiting time of 500 s ($\approx 8.3t_{1/2}$) is required to achieve a deviation of 3 ‰$\times\Delta C_{max}$ from the steady state concentration. For a typical water analysis this signal is at least one order of magnitude higher than twice the standard deviation of the background noise, even for the least abundant gases He and Kr (see Table 3.1 for estimated detection limits). To calculate the partial pressure p_i^{EC}, the signal of the partial pressure in the EC acquired from the MS is compared to the corresponding signal measured during the air calibration procedure. Apart from connecting the capillary to ambient air (V2 open, V1 closed), calibration measurements are treated the same as EC measurements. In the case of calibration a stable gas flux is established within 10 s, which is the time required for the gas to be transferred from valve V2 into the MS.
During operation, each EC measurement is preceded and followed by a calibration measurement. Thus, for each measured gas, two measurements of the ratio of the signal to the partial pressure in the free atmosphere are obtained. The partial pressure p_i^{EC} of each gas was determined by assuming that any sensitivity shift that would result in a difference in the ratios is linearly dependent on time.

3.4 Laboratory-based measurements

We performed several laboratory experiments to determine the deviation of the real partial pressures from those calculated using Henry's Law in response to the small amount of gas extracted from the EC. We introduce the nondimensional deviation function $F_i^f = p_i^{\mathrm{equ}}/p_i^{\mathrm{EC}}$ to quantify the ratio of the equilibrium partial pressure p_i^{equ} to p_i^{EC}, where the superscript f denotes the chosen experimental configuration of the GE-MIMS (e.g., F_i^f is expected to be different for a capillary length other than 3 m). In general, F_i^f depends on the flow rate Q_{w} of water through the membrane inlet and on the water temperature T_{w}. From Henry's Law and the definition of F_i^f, it follows that:

$$C_i = H_i(T_{\mathrm{w}})F_i^f(Q_{\mathrm{w}}, T_{\mathrm{w}})p_i^{\mathrm{EC}}, \tag{3.1}$$

where $H_i(T_{\mathrm{w}})$ is the Henry coefficient of the gas i. Hence if $F_i^f(Q_{\mathrm{w}}, T_{\mathrm{w}})$ is known, the concentrations of gas i dissolved in the water can be calculated from its partial pressure p_{EC}^i determined with our GE-MIMS.
Furthermore, Equation 3.1 is the result of a simple mass balance model. This model describes the steady state of the gas system of the membrane inlet in terms of the equality of the following three gas fluxes:

1. The total gas flux of a gas from the water through the membrane into the EC;
2. the gas flux pumped out of the EC through the capillary into the MS;
3. and the gas flux removed from or delivered to the dissolved gases in the water pumped through the membrane inlet.

In particular this model yields the dependence of $F_i^f(Q_{\mathrm{w}}, T_{\mathrm{w}})$ on the water flow Q_{w}:

$$F_i^f(Q_{\mathrm{w}}, T_{\mathrm{w}}) = \Gamma_i(1 + \alpha_i/Q_{\mathrm{w}}), \tag{3.2}$$

where Γ_i (dimensionless) and α_i (cm^3/s) are coefficients that depend on the total effective permeability of the membrane, the flow resistance of the capillary and the Henry coefficient H_i only. For more information on the derivation of Equation 3.2 we refer to the appendix of this chapter.

3.4.1 Dependence of the nondimensional deviation function F_i^f on the water flow rate Q_{w}

The dependence of $F_i^f(Q_{\mathrm{w}}, T_{\mathrm{w}})$ on Q_{w} was investigated by pumping air-saturated water at 22 °C through the membrane-inlet device at different flow rates. Specifically, C_i was kept constant and Q_{w} was varied from 0.5 L/min to 3 L/min.
Air-saturated water was produced by slowly stirring deionized water in a 100-L basin to equilibrate its gas concentrations with the ambient air in a temperature-controlled room (Klump et al., 2008). Attainment of solubility equilibrium with the ambient air was ascertained using a total dissolved gas probe (Manning et al., 2003) and by measuring the dissolved oxygen concentration with an optode probe (DOL, HACH, Chu et al., 2011) calibrated using the Winkler method. Both control measurements confirmed that solubility

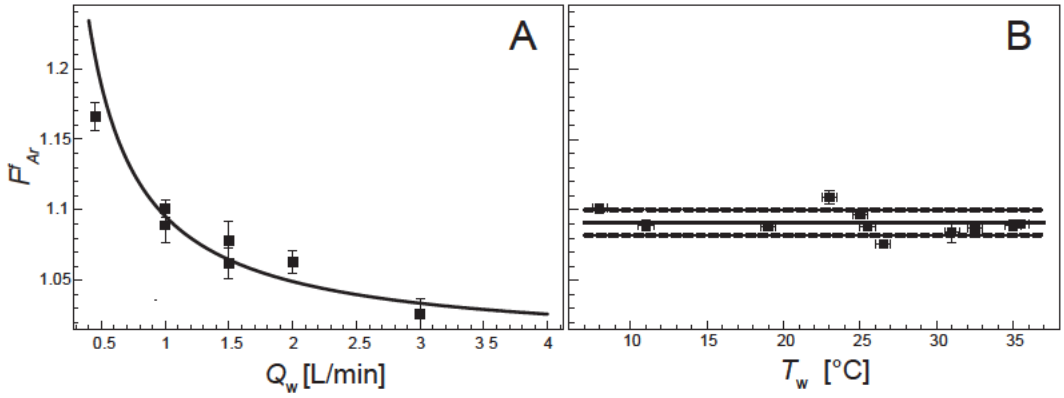

Figure 3.3: Dependence of the deviation function F^f_{Ar} on (**A**) water flow rate Q_{w} and (**B**) water temperature T_{w} for $Q_{\mathrm{w}} = 2$ L/min. In (**A**) the solid line corresponds to a fit of Equation 3.2 to the data. In (**B**) both the mean (solid line) and standard deviation (dashed lines) are shown.

equilibrium was attained to within the precision of the instruments ($\approx 1\%$) during the entire experiment. The air-saturated water was pumped through a silicone tube to the membrane inlet using a submersible pump in the tank. No gas bubbles were observed in the silicone tube. We note that the calibration measurements were conducted under the same ambient air conditions as those which prevailed during the production of the air-saturated water. In particular the barometric pressure remained constant, which is important to ensure constant concentrations of dissolved gases in the basin during the measurements.
The dependence of F_i^f on Q_{w} for all gases (Figure 3.3) is strong for $Q_{\mathrm{w}} < 1$ L/min, but becomes negligible at higher flow rates, as predicted by Equation 3.2. Note that the Ar data shown are representative of all gases measured. For all subsequent measurements we therefore chose $Q_{\mathrm{w}} = 2$ L/min because fluctuations of a few percent in Q_{w} do not significantly alter F_i^f; e.g a 5% change in Q_{w} at 2 L/min results in a change of $< 1\%$ in F_i^f. Note that we used the water temperature in the basin to calculate F_i^f. However, the temperature of the water passing through the membrane inlet was probably slightly higher than in the basin because the water was heated by the submersible pump. In evaluating the following experiments the temperature we refer to is therefore always that of the water entering the membrane inlet.

3.4.2 Dependence of the nondimensional deviation function F_i^f on water temperature T_{w}

The dependence of F_i^f on T_{w} was determined in two temperature runs. In each run, the temperature of the water entering the membrane inlet was varied by heating it externally without changing its gas content. Each run started with air-saturated water at a given temperature T_{ASW} (8 °C or 23 °C). The water was then heated to the desired temperature T_{w}

by forcing the water to flow through a long, heated copper tube to avoid any change in the dissolved-gas concentrations before it entered the membrane-inlet device. In the first run the water was heated stepwise from 23 °C to 36 °C and in the second run from 8 °C to 25 °C.

The sensitivity of F^f_{Ar} to T_{w} over the temperature range from 8 °C to 36 °C is shown in Figure 3.3 B. The mean values and relative standard deviations (rSD) of F^f_i for all temperatures and for all gases measured are listed in Table 3.1. For these gases, F^f_i shows no detectable temperature dependence over the entire temperature range investigated. Furthermore, F^f_i is virtually independent of the gas specimen analyzed.

The data from this experiment in combination with the values of F^f_i listed in Table 3.1 can be used to recalculate the concentrations of dissolved gases in the original air-saturated water in the basins. While the concentration as such does not deliver additional information, the standard deviation of the ratio of the determined concentrations to the equilibrium concentrations of the original air saturated water yields an estimate of the relative error of a single measurement which was found to be similar to the rSD of F^f_i listed in Table 3.1.

Estimated detection limits (Table 3.1) were not determined in a series of measurements , but instead were set to twice the standard deviation of the peak base line at the respective mass/charge ratio.

However interfering ions — i.e., ionized fragments of molecules or doubly charged ions — may contribute to the signal measured at a particular mass/charge ratio. Such interference can, to a certain extent, be corrected by determining the ionization pattern of the particle the interfering ions originate from. For gas measurements, the ion fragments CO^+ and O_2^+ of CO_2 interfere with N_2 signals at 28 m/z and with O_2 at 32 m/z. In particular, the CO_2 gas concentration in groundwater can be as high as atmospheric O_2 concentrations, and may therefore pose a problem in classical MIMS gas analytics.

However, in contrast to classical MIMS, the signal ratio of two gas species in GE-MIMS is not proportional to the ratio of their concentrations, but to the ratio of their respective partial pressures in the EC. GE-MIMS is therefore more sensitive to poorly soluble gases (O_2,N_2, noble gases) than to highly soluble gases (CO_2, Weiss, 1974). Hence for CO_2 the partial pressure in the EC is around 20 times (Weiss, 1974) smaller than for O_2 at the same (molar) concentration in water. Around 10 % of the ionized CO_2 gas contributes to the 32 m/z signal which is used for O_2 determination. Detection limits of the measured O_2 concentration in water therefore corresponds to approximately 0.5 % of the CO_2 concentration in the water, if not corrected for interferences. However, this inherent suppression of CO_2 because of its high solubility explains why the interference of ion fragments originating from CO_2 at 32 m/z (O_2^+) and 28 m/z (N_2^+) was shown to be negligible based on interference estimates from signals at 44 m/z (CO_2^+).

The concentrations of dissolved gases in lake water as determined using the GE-MIMS were compared to the results obtained using the accepted analytical protocol for noble-gas analysis using static mass-spectrometry (Beyerle et al., 2000). Both measurements agree for all noble gases analyzed within the error of the respective method (see Table 3.2).

In conclusion, the GE-MIMS, with a small gas flux to be extracted for final gas detection, operates at a steady state close enough to gas equilibrium to enable the dissolved-gas concentrations in the analyzed water to be recalculated (using Equation 3.1) from the measured partial pressures in the extraction chamber (p_i^{EC}). Note that to do so, no profound knowledge of the exact physical behavior of the membrane with regard to its gas transport

Table 3.1: Experimentally determined values for the deviation function F_i^f, and its relative standard deviation (rSD) along with the estimated detection limits of the GE-MIMS (defined as twice the standard deviation of the peak base line: see text).

Gas	$F_i^f(Q_w = 2$ L/min) [-]	rSD [%]	Detection limit [10^{-9} cm^3_{STP}/g]
^{4}He	1.13	3	0.6
$^{28}(N_2)$	1.11	1	200
$^{32}(O_2)$	1.12	1	400
^{40}Ar	1.09	1	3
^{84}Kr	1.10	4	3

or transfer is needed.
In summary, our system developed for the online determination of dissolved gases in groundwater yields concentration with a typical overall error (taking into account both precision and accuracy) of 1 % - 4 % (Table 3.1). This error is adequate to resolve concentration changes corresponding to a temperature change at groundwater recharge of about 1 °C at a sampling frequency of 5 measurements per hour (6 min for a gas measurement in the EC plus 6 min for a calibration). Our portable dissolved-gas detection system therefore enables the concentrations of dissolved atmospheric gases (He, Ar, Kr, O_2, N_2) in groundwater and surface waters to be determined quasi-continuously in the field.

Table 3.2: Comparison of GE-MIMS measurements with measurements of dissolved noble gases in lake water conducted at ETH Zürich, based on the accepted analytical protocol for noble-gas analysis using static mass-spectrometry (Beyerle et al., 2000).

Gas	GE-MIMS [cm^3_{STP}/g])	MS ETH Zürich [cm^3_{STP}/g])	Relative difference [%]
^{4}He	4.5 10^{-8}	4.40 10^{-8}	2
^{40}Ar	3.8 10^{-4}	3.84 10^{-4}	1
^{84}Kr	9.0 10^{-8}	9.20 10^{-8}	2

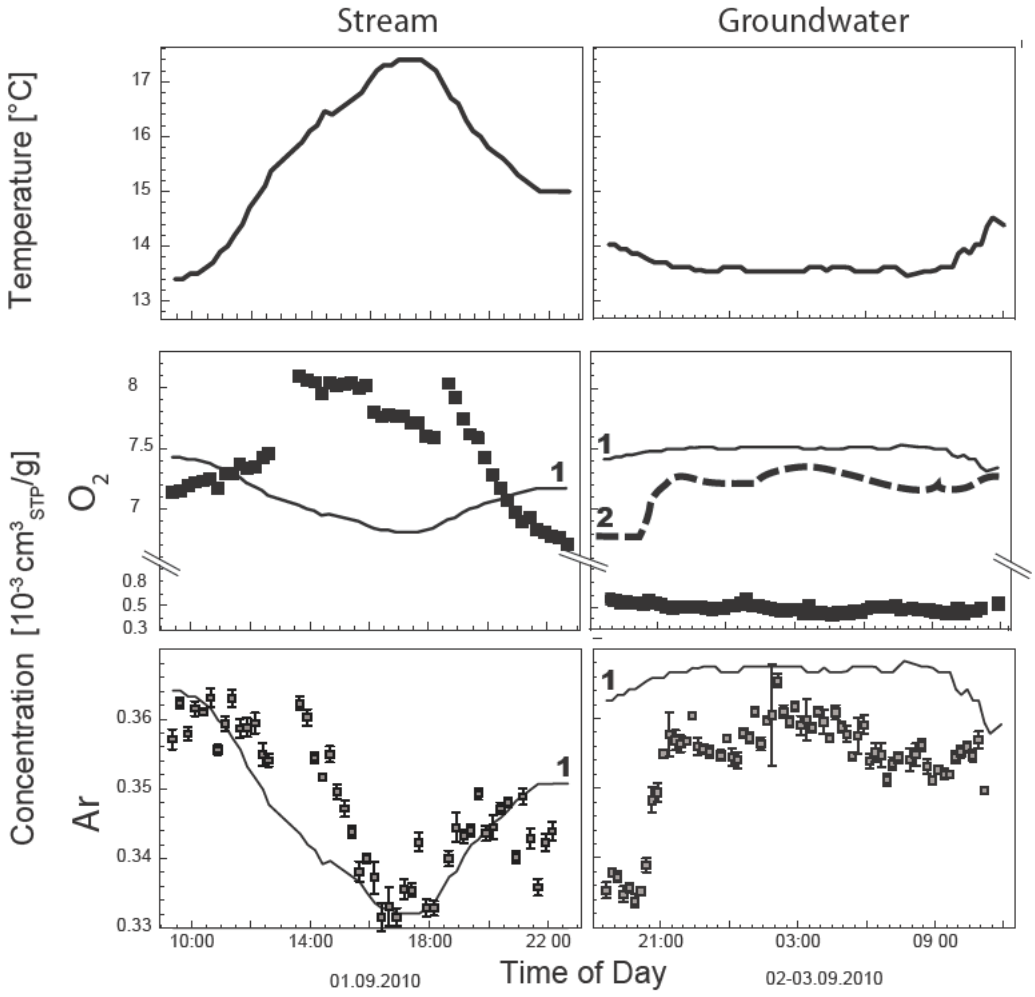

Figure 3.4: Water temperature and the concentrations of oxygen (O_2) and argon (Ar) measured in the Chriesbach (north-east Switzerland) and in the neighboring groundwater. The error bars indicate standard errors. If no error bar is shown (as in the case for the O_2 data) the standard error is smaller than the symbol representing the data. **1**: Atmospheric equilibrium concentrations for O_2 and Ar calculated from water temperature. **2**: Initial atmospheric equilibrium concentration for O_2 in the hyporheic zone calculated from the measured Ar concentration.

3.5 Field measurements: Oxygen dynamics in the hyporheic zone of a stream

We conducted an experiment to test the performance of the GE-MIMS system under field conditions and to analyze whether the system's resolution with respect to concentration and time was sufficient to study gas dynamics and O_2 turnover during the exchange of water between a stream and groundwater through the hyporheic zone. The study site was located at the downstream end of Chriesbach, a macrophyte-rich stream on the Swiss Plateau with a catchment area comprised mainly of agricultural, industrial and residential land (Kaenel et al., 2000). Concentrations of major nutrients (P, N) are high because of effluents from a wastewater treatment plant 4 km upstream from the study site.
The measurements were made in a groundwater observation well 2 m from the stream (0.5 m below the groundwater table) during the night (2. - 3. November) and in the stream itself during the day (1. November, at 0.3 m water depth), during base flow conditions (~ 0.5 m$^3/s$) and stable weather conditions (sunny with no rain) that had prevailed for more than two days before commencement of the measurements.
The same instrumental setup as in the laboratory experiments was used. However the groundwater measurements were conducted with longer waiting times (500 s) to account for low oxygen concentrations. Furthermore, optode probe measurements of O_2 concentration were conducted at the beginning and the end of both the groundwater and stream measurements, and were found to agree always within 5 % with the O_2 concentrations determined by GE-MIMS. This further validates the statement that high CO_2 concentrations that occur in groundwaters or rivers with high nutrient loads do not affect the performance of the GE-MIMS.
The results of the field experiment (Figure 3.4) show that the stream was supersaturated with O_2 during the day and undersaturated during the night. Ar concentrations in the stream, which were close to the atmospheric equilibrium concentration, fluctuated by 10 % in response to the diel water temperature fluctuations (stream temperatures were 17 °C during the day and 13 °C during the night). However, from morning until early afternoon there was a significant delay in the response of the Ar concentration to the changing stream temperature.
Atmospheric gas exchange, governed by changing water temperature, was the major driver of the concentrations of both O_2 and Ar in the stream. However, the observed delay in the response of the Ar concentration with respect to stream temperature reflects the different temporal response of temperature and gas concentration that results from the heat transport rate significantly exceeding the gas-exchange velocity (Schwarzenbach et al., 2003; Aeschbach-Hertig et al., 1999). In particular, direct solar radiation incident on the stream can lead to a difference in the behavior of heat transport and gas exchange (Schwarzenbach et al., 2003). In addition, photosynthesis during the day and respiration during the night resulted in O_2 concentrations in the stream deviating from the atmospheric equilibrium concentration (Streeter and Phelps, 1925; Schurr and Ruchti, 1975; Livingstone, 1991; Uehlinger, 2006). Note that the anomaly in O_2 and Ar concentration — i.e., the data gap in the stream at 13:00 — is due to cleaning of the membrane inlet by back-flushing.
In the groundwater, measured O_2 concentrations were very low (hypoxic conditions), whereas Ar concentrations were as high as in the stream. In particular, the Ar concentrations in the groundwater showed the same diel fluctuation as in the stream, and were

lower than the atmospheric equilibrium concentrations calculated from the groundwater temperature.

We concluded that the temporal evolution of the Ar concentration in the stream was imposed on the groundwater as a result of the advective transport of water from the stream to the groundwater through the hyporheic zone. Furthermore, the observation that the concentration of Ar in the groundwater was determined by physical processes occurring directly at the interface between stream and groundwater rules out the possibility of any secondary gas exchange having occurred within the porous medium; in particular, it rules out any significant injection of air as a result of the formation of excess air within the hyporheic zone. Hence, the steep increase in the Ar concentration in the groundwater around 21:00 h apparent in Figure 3.4 can only be related to a decrease in water temperature at recharge similar to the decrease in stream temperature that occurred at around 19:00 h. Because weather conditions were stable, we can assume that a decrease in water temperature always occurred at around 19:00 h, and hence the travel time of the groundwater since recharge must have been 2 hours plus an unknown number of whole days.

By using the knowledge gained from the measured Ar concentrations and the fact that the transport behavior of O_2 is similar to that of Ar, the fate of O_2 in the hyporheic zone can be analyzed conceptually. First, the initial concentration of O_2, entering the groundwater was set in the stream, with no additional O_2 input resulting from the formation of excess air. Second, the initial atmospheric equilibrium concentration of the O_2 at recharge (plotted in Figure 3.4) can be calculated from the concentrations of dissolved Ar in the groundwater. We note that the ratio of the atmospheric equilibrium concentrations of O_2 and Ar is constant to within 1 ‰ in the temperature range from 10 °C to 20 °C (Wise and Houghton, 1966; Weiss, 1970). Third, the effective O_2 consumption can be calculated from reconstructed initial O_2 concentrations in the stream at the time of infiltration (as determined from the travel time derived from Ar concentrations), along with the measured O_2 concentrations in the stream and in the groundwater. This calculation shows that the amount of O_2 consumed in the hyporheic zone was subject to the same diel fluctuations as the concentrations of dissolved O_2 in the stream.

In conclusion, the study described here yields insight into the gas dynamics of the stream and the groundwater. In particular, the assumption that the concentrations of dissolved gases in the water are in atmospheric equilibrium with respect to water temperature is not only not valid in groundwater, but is also erroneous in river water because the transfer velocities of heat and gases differ. Both limitations make a strong case for conducting a combined analysis of Ar and O_2 when studying O_2 consumption in the hyporheic zone and other aquatic environments. We note that quantifying the formation of excess air as an additional potential source of O_2 is crucial to the quantification of real O_2 consumption (in this field experiment the formation of excess air was able to be excluded). Ar concentration measurements are therefore crucial to the determination of O_2 turnover during riverbank infiltration, and also yield insights into the travel time of the infiltrating water, the determination of which is of key importance in hydrology (e.g. Silliman et al., 1995; Anderson, 2005; Cirpka et al., 2007; Vogt et al., 2010a).

The GE-MIMS was used during three days to record time-series in a stream and its hyporheic zone. This field study demonstrated that the GE-MIMS is able to resolve diel fluctuations in gas concentrations during river-groundwater exchange. In groundwater our instrument determined dissolved gas concentrations for 15 h without interruption, and in the stream the measurements were interrupted once only to clean the membrane by back-

flushing. Hence the time interval of operation could have been extended to days with no problem.

3.6 Discussion

The GE-MIMS system enables the simultaneous, quasi-continuous (5 measurements per hour) measurement of dissolved He, Ar, Kr, O_2, and N_2 concentrations in groundwater with a standard error of less than 4 % (see Table 3.1). The system allows changes in gas concentration to be studied in dynamic aquatic environments, such as the hyporheic zone, where gas concentrations in the groundwater change rapidly in response to variations in the physical conditions prevailing in the losing river (e.g., discharge rate and temperature). The sensitivity and precision of the GE-MIMS enables the resolution of Ar concentration changes in response to water-temperature fluctuations of $\pm$ 1 °C. Furthermore, by taking into account all the concentrations of all gas species analyzed, the instrument enables the real consumption rates of O_2 in groundwater to be estimated.
The GE-MIMS is suitable for use in field conditions, as fluctuations in the sensitivity of the system can be controlled by periodic calibration using ambient air as a gas standard. Avoiding the use of a large, bulky tank for a calibration gas standard greatly simplifies the field work. This calibration method is unique to membrane-inlet systems that work similarly to the GE-MIMS system and is not feasible for the common types of MIMS system in which the gases are extracted directly into the vacuum of the ion source of an MS (Beste et al., 1975; Lloyd and Scott, 1983; Harland et al., 1987; Lloyd et al., 1992; Kana et al., 1994; Lloyd et al., 1996; Johnson et al., 2000; Lloyd et al., 2002; Kotiaho and Lauritsen, 2002; Bell et al., 2007; Schlüter and Gentz, 2008). Compared to "classical" MIMS setups however, our system has a longer response time and requires higher water flows (2 L/min). The method used in our field study, focusing on O_2 dynamics in groundwater, can be applied without further modification to other research areas. For instance, the combined analysis of dissolved N_2 and noble gases enables N_2 production by denitrification to be distinguished from N_2 injection resulting from excess air formation. Furthermore, the analysis of CO_2 in groundwater, which is possible without modifying the GE-MIMS, allows the mass balances of chemicals in processes where O_2, N_2, and CO_2 occur as products or reactants to be constrained. Additionally, time-series of noble gas concentrations in river/groundwater systems acquired using the GE-MIMS may contain groundwater travel-time information similar to that contained in time-series of water temperature or salinity (e.g. Silliman et al., 1995; Anderson, 2005; Cirpka et al., 2007; Vogt et al., 2010a).

Acknowledgement

The authors thank H. Surbeck for helpful discussions about technical details and for providing a total dissolved gas pressure probe. We are also grateful to U. Menet, A. Süsli and D. Niederer for technical support and H. Baur for adapting the IONIC MS control program to our system. Furthermore we thank D. M. Livingstone for improving the clarity and accuracy of the manuscript. This work was performed within the framework of the RECORD project (Assessment and Modeling of Coupled Ecological and Hydrological Dynamics in the Restored Corridor of a River (Restored Corridor Dynamics)), and was funded by Eawag (Swiss Federal Institute of Aquatic Science and Technology) and

CCES (Competence Center Environment and Sustainability of the ETH Domain). The manuscript benefited substantially from the comments and suggestions of the editor and three anonymous reviewers.

3.7 Appendix

3.7.1 Gas flux calculation

The partial pressure p^i_{EC} of a gas i in the extraction chamber (EC) of the membrane inlet, in steady state, is described in terms of three gas fluxes:

1. The total gas flux J^i_{Me} of a gas from the water through the membrane into EC, which is proportional to the total effective permeability D^i_m of the membrane and to the difference of the normalized concentration $\overline{C}^i_{\mathrm{wa}}$ of the water flowing through the extraction chamber and the equilibrium concentration given by Henry's law ($H_i p^i_{\mathrm{EC}}$):

$$J^i_{\mathrm{ME}} = D^i_m \left(\overline{C}^i_{\mathrm{wa}} - H_i p^i_{\mathrm{EC}} \right). \tag{3.3}$$

2. The gas flux J^i_{MS} pumped out of the EC through the capillary into the MS, which is proportional to p^i_{EC}:

$$J^i_{\mathrm{MS}} = R^{\mathrm{cap}}_i p^i_{\mathrm{EC}}, \tag{3.4}$$

   with R^{cap}_i the coefficient describing the gas flow-resistance of the capillary. Note that the pressure at the end of the capillary is three orders of magnitude smaller than at the inlet of the capillary and can therefore be neglected.

3. The flux of gas J^i_{wa} removed from the dissolved gases of the water flow (Q_{w}) pumped through the membrane inlet:

$$J^i_{\mathrm{wa}} = Q_{\mathrm{w}} \Delta C^i_{\mathrm{wa}}, \tag{3.5}$$

   with ΔC^i_{wa} the concentration loss during through flow:

$$\Delta C^i_{\mathrm{wa}} = \frac{C^i_{\mathrm{wa}} - \overline{C}^i_{\mathrm{wa}}}{2}, \tag{3.6}$$

   with C^i_{wa} the water concentration at the inlet of the EC.

In steady state i.e. if p^i_{EC} does not change with time all fluxes are equal ($J^i_{\mathrm{ME}} = J^i_{\mathrm{MS}} = J^i_{\mathrm{wa}}$). Therefore in steady state there is a direct relation of C^i_{wa} to p^i_{EC} i.e. we can recalculate $F^f_i(Q_{\mathrm{w}}, T_{\mathrm{w}})$ of Equation 3.1:

$$F^f_i(Q_{\mathrm{w}}, T_{\mathrm{w}}) = \Gamma_i(1 + \alpha_i / Q_{\mathrm{w}}), \tag{3.7}$$

where Γ_i ([-]) and α_i ([cm^3/s]) are coefficients depending on D_m^i,R_i^{cap} and H_i only:

$$\Gamma_i = \frac{R_i^{\mathrm{cap}}}{D_m^i H_i} + 1,$$
$$\alpha_i = 2D_m^i(1 - \frac{1}{\Gamma_i}).$$

Note that, in case of $Q_{\mathrm{w}} \gg \alpha_i$, F_i^f becomes independent of Q_{w} and equal to Γ_i.

3.7.2 Part list

Table 3.3: List of parts used, for details we refer to the respective company.

System	Item	Specification	Description
Inlet system			
Membrane inlet			
	Mini module: Membrana contractors	Membrane	Polyurethane X50 Fiber (OD/ID 300/220 µm) with 0.18 m^2 active surface area.
		Housing	Polycarbonat ca 178×40 mm
		Volume	Shellside (EC) 25 mL, Lumenside (Water) 15 mL
Valves			
	Solenoid valves: Minisol, fluid automation systems.	Number of ways	2 Way
		Function	Normally closed
		Action	Direct acting
		Cycling rate	2000 cpm
		Body material	Stainless steel
		Part number	06-211-107-45
	Capillary:VICI PEEK	length	3 m
		ID	0.13 mm
		Part number	JR-T-6007-M3
	Metering valve: L-series, Swagelok	Part number	SS-4L-MH

continued on next page

System	Item	Specification	Description
MS			
	QMS 200, SRS (2000)		
	Ion source	Operation	Electron impact ionization
		Filament	Thoriated Iridium
		Electron energy	90 eV
	Separator	Typ	Quadrupole
		Rod diameter	0.25”
		Rod length	4.5”
	Detector	Faraday cup	
		Electron multiplier	off axis configuration
	Resolution		0.5 m/z @ 10 % peak hight
	Power	max	600 W
		mean	300 W
	Weight		34 kg
	Dimensions		44 cm $\times$ 20 cm $\times$ 61 cm
Pumps			
	Hybrid turbo-molecular/drag pump Varian V 81-M	pumping speed	70 L/s
	Diaphragm pump KNF M613	Stages	4

4 Argon concentration time-series as a tool to study gas dynamics in the hyporheic zone

Chapter 4 has been submitted for publication in Environmental Science and Technology:
Mächler, L., Brennwald, M. S. and Kipfer, R. (2012). Argon concentration time-series as a tool to study gas dynamics in the hyporheic zone.

Abstract

The oxygen dynamics in the hyporheic zone of a peri-alpine river (Thur, Switzerland), were studied through recording and analyzing the concentration time-series of dissolved argon, oxygen, carbon dioxide and temperature during low flow conditions, for a period of one week. The argon concentration time series was used to investigate the physical gas dynamics in the hyporheic zone. Differences in heat and gas transport were observed by comparing the diel temperature evolution of groundwater to the dissolved argon concentrations measured. These differences were most likely caused by vertical heat transport which influenced the local groundwater temperature. Furthermore, the argon concentration time-series were used to estimate travel times of the water by cross correlating the measured argon concentrations with the argon concentrations of the river. The information gained from the physical gas transport was used to estimate the oxygen turnover in groundwater since water recharge. The resulting consumed oxygen amounts showed strong diel variations, which correlated with the water temperature at groundwater recharge. Hence, the variation in the consumption rate were most likely caused by the temperature dependence of microbial activity.

4.1 Introduction

The hyporheic zone, the transition zone between surface water and groundwater, is important for the water quality of both the river and groundwater. It is an important habitat for microbes which consume organic material, and therefore chemically reduce nutrients infiltrated into the groundwater (Brunke and Gonser, 1997).
Most of the important biochemical processes in groundwater, involve reactants or products in gaseous form (Streeter and Phelps, 1925; Whitman and Clark, 1982; Korom, 1992; Malard and Hervant, 1999; Rivett et al., 2008). Microbial mediated aerobic respiration, with oxygen (O_2) as a reactant and carbon dioxide (CO_2) as a product, is a prominent example of such process. In order to determine the O_2 turnover in groundwater, i.e., the

amount of O_2 per unit mass of water that has been consumed, since recharge, the in-situ O_2 concentration as well as the total input of O_2 into the respective water mass need to be quantified. The main O_2 sources are advection with the infiltrating river water and gas injection into groundwater in the unsaturated zone including excess air formation. Excess air, a surplus of atmospheric gases relative to atmospheric equilibrium that is typical of groundwater, forms during gas partitioning in the unsaturated zone of an aquifer by the entrapment and dissolution of air bubbles in response to water-table fluctuations or groundwater recharge (Heaton and Vogel, 1981; Aeschbach-Hertig et al., 2000; Klump et al., 2007, 2008). Therefore, to study the fate of O_2 in groundwater both river and excess air contribution to the O_2 budget need to be determined. Thus, a tracer for O_2 is needed which shows no biochemical reactivity.

Noble-gases are ideal tracers to study gas exchange in ground and surface water, as noble gases are chemically inert, present in the atmosphere and prone to the same physical processes as O_2. Measurements of atmospheric noble-gas concentrations enable to quantify physical gas exchange and gas transport in groundwater. In particular, such measurements allow the water temperature of last gas exchange to be reconstructed and the amount of excess air to be estimated (Beyerle et al., 1999; Ballentine and Hall, 1999; Aeschbach-Hertig et al., 1999; Kipfer et al., 2002; Beyerle et al., 2003; Hall et al., 2005; Klump et al., 2007, 2008). Noble gas analysis of groundwater therefore yields the information needed to reconstruct the effective input of O_2 into the groundwater, i.e., O_2 input due to both advection with water from the river and injection due to excess air formation. In particular argon (Ar) represents an almost ideal conservative tracer for O_2 dynamics. This is because both the diffusion coefficients and Henry coefficients, which control the physics of air/water partitioning (Kipfer et al., 2002), are very similar for Ar and O_2 (Weiss, 1970; Wise and Houghton, 1966; Broecker and Peng, 1974; Jähne et al., 1987).

In addition to O_2 availability, aerobic microbial respiration is regulated by temperature (O'Connell, 1990; Kirschbaum, 1995; Greskowiak et al., 2006). Groundwater temperature therefore is a key factor in O_2 turnover. Water temperature is controlled by heat transport, i.e., advection with water and conduction in water and the aquifer. Examples of heat conduction are the heat exchange of the groundwater with the aquifer material (Stallman, 1965) or the transport of heat from the surface to the groundwater (vertical conduction) in shallow aquifers in particular (Smith et al., 1964; Beyerle et al., 2003; Vogt et al., 2010b; Molina-Giraldo et al., 2011).

Combined temperature and noble gas concentration measurements contain information on heat transport. Heat exchange of a water body with its surroundings changes its temperature from the initial temperature set at water recharge. As noble gas concentrations depend on the temperature prevailing during last gas/water partitioning, the initial temperature and hence the temperature changes thereafter can be determined without knowing the exact location and time of infiltration (Kipfer et al., 2002).

Quasi-continuous noble gas measurements allowing short term fluctuation of dissolved gas concentration to be determined, however have only recently become technically feasible (Mächler et al., 2012). As a result hitherto, combined gas and heat transport studies in dynamic groundwater systems, like the hyporheic zone of a dynamic river, have not been possible. Therefore, in this work we present up to our knowledge the first study on both (noble) gas and heat transport in the hyporheic zone of a dynamic river (Thur, Switzerland) and its implications for O_2 concentrations. The goal of the study is to analyze the temporal evolution of O_2 turnover during a measurement period of 5 days and to reconstruct

the temperature dependence of O_2 consumption. The field site where we conducted the measurements is known to exhibit diel O_2 fluctuations and non horizontal heat transport (Vogt et al., 2010b) and is therefore an ideal location to study O_2 dynamics. The Ar, O_2 and CO_2 concentrations were determined in situ and continuously over the entire measurement period with a recently developed membrane inlet mass spectrometer (Mächler et al., 2012, see Chapter 3).

4.2 Methods

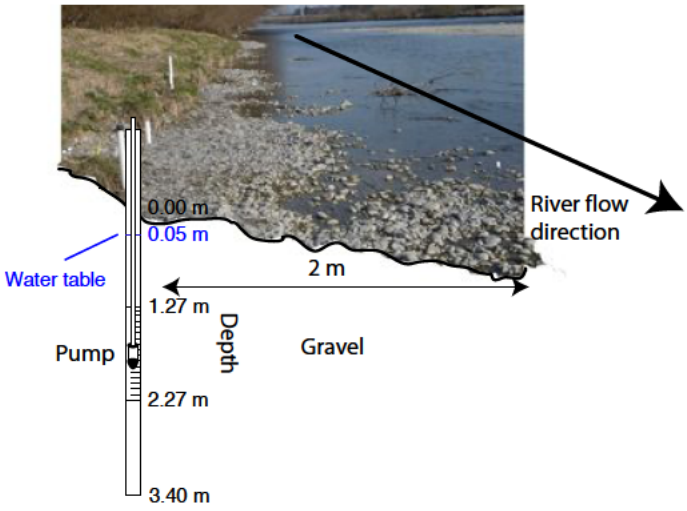

Figure 4.1: Piezometer at the study site in Niederneunforn (Switzerland) where the measurement was conducted.

4.2.1 Study site

The peri-alpine Thur river is located in the north-east of Switzerland. The catchment includes an area with an elevation up to over 2500 m asl and its estuary leads into the river Rhine at 345 m asl. Most of the river was channelized for flood protection in the late 19^{th}/early 20^{th} century. However, as part of revitalization measures, in recent years the over-banks over a length of approximate 2.5 km were removed and the riverbed was widened to allow small meanders to develop (BAFU, 2010).
The groundwater observation well where we conducted the gas concentration measurements was located approximately 1 m from the river shore (for screening and pump-head depth see Figure 4.1). The groundwater at this location has a travel time since recharge of less than one day (Vogt et al., 2010a). At this location the unconfined aquifer is approximately 6 m thick, and consist of sandy gravel with impervious clay below, and is hydraulically and hydrologically well connected with the river Thur (Vogt et al., 2010a).

There is no top soil covering the aquifer at this location, hence the uppermost gravel layer of the aquifer is in direct contact with the atmosphere (see Figure 4.1).

4.2.2 Dissolved gas measurement system

The membrane inlet mass spectrometric system used is described in detail in Mächler et al. (2012) (see Chapter 3). In brief the water is pumped (rate = 2 L/min) to the membrane inlet with a submersible pump. The extracted gases are analyzed with a quadrupole mass spectrometer and the acquired data processed according to Mächler et al. (2012). The measurement frequency is approximately four measurements per hour. For this work we included dissolved CO_2 into the measurement procedure, following the experimental set up and calibration procedure of Mächler et al. (2012). The overall error of the CO_2 concentration measurements are approximately 3 % at atmospheric equilibrium concentration. The overall errors of the other analyzed gases are given in Mächler et al. (2012).

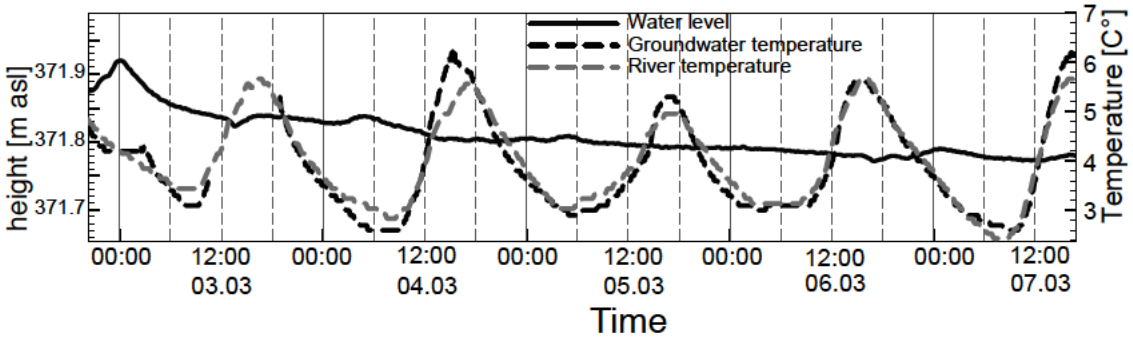

Figure 4.2: Temperature of groundwater in the observation well and river water, right axis. Water level of the river Thur, left axis.

4.3 Results and Discussion

4.3.1 Temporal evolution of temperature and Ar concentration

The measurements started two days after a minor flood with a maximum river discharge of 100 m^3/s and were conducted from the 2^{nd} to the 7^{th} of March 2011. During the measurements the water level in the river decreased by 10 cm and the discharge of the river Thur declined from 30 m^3/s to 20 m^3/s.
The temperature of the groundwater and of the river, as well as the water level in the observation well are depicted in Figure 4.2. Both temperatures exhibited similar temporal evolutions with the same diel variation. However, the temperature variations in the groundwater were slightly larger than in the river. This enhanced amplitude of the water

Table 4.1: Maxima of the cross correlation of the temporal evolutions 1.) of measured Ar concentration $[Ar]_{GW}^{MES}$ and Ar atmospheric equilibrium concentration $[Ar]_{GW}^{ASW}$ of the groundwater, and 2.) of the Ar atmospheric equilibrium concentration of the river $[Ar]_{RIV}^{ASW}$ and $[Ar]_{GW}^{MES}$. Henry coefficients to calculate atmospheric equilibrium concentration were taken from Wise and Houghton (1966)

.

	Data sets	1.Maximum	2. Maximum	3. Maximum
1.	$[Ar]_{GW}^{MES}$ vs $[Ar]_{GW}^{ASW}$	4.4 h	5.4 h	6.2 h
2.	$[Ar]_{GW}^{MES}$ vs $[Ar]_{RIV}^{ASW}$	5.3 h	5.5 h	6.5 h

temperature in the hyporheic zone is an indication of an additional heat source during day and a heat sink during night, i.e., advection with infiltrating river water was not the only process controlling temperature in the groundwater.

The Ar concentrations (see Figure 4.3) in the groundwater exhibited diel fluctuations reaching minima during night and maxima around noon. The amplitude, frequency, and to a lesser extent the shape, of the dissolved Ar concentration fluctuations were similar to the diel fluctuations of the atmospheric equilibrium concentration at the respective groundwater temperatures. However, the two concentration evolutions were separated by a phase-shift of around 4.5 to 6 h (see Table 4.1 for cross correlation results), i.e., the Ar concentrations in the groundwater were not in atmospheric equilibrium with the ambient water temperature. Furthermore, the temporal evolution of the Ar-concentration was also, up to a delay of approximately 5 to 6.5 h (see Table 4.1), similar to the atmospheric equilibrium concentration of the river (not shown in Figure 4.3 due to the similarity of the groundwater- and the river temperature).

The Ar concentrations in the groundwater were not in atmospheric equilibrium in respect to the ambient water temperature. Hence, heat and dissolved gases were affected by different exchange processes during the transport from the river (surface) to the observation well.

Excess air is an exchange process exclusively affecting gas concentrations. However, the similar temporal evolution of atmospheric equilibrium concentration of Ar in river to Ar-concentration in groundwater, indicates that the air/water partitioning in the coupled river-groundwater system occurred in the river. In particular, as is apparent from Figure 4.3, the daily mean of the Ar-concentration in groundwater is similar to the respective daily mean of the river. This rules out any injection of air as a result of the formation of excess air, since the formation of excess air would lead to a surplus of dissolved-gas concentrations (Zartman et al., 1961; Heaton and Vogel, 1981; Beyerle et al., 1999; Aeschbach-Hertig et al., 1999; Kipfer et al., 2002; Klump et al., 2007). In summary, the temporal evolution of the Ar concentration in the stream was imposed on the groundwater as a result of the advective transport of water from the stream to the hyporheic zone. The comparison of the dissolved Ar concentrations in the river and the groundwater shows that the riverine water is transported within 5-6.5 h ($\approx$ delay in the groundwater concentration) to the observation well. Furthermore, excess air formation was not the cause for the dissolved Ar concentrations deviating from atmospheric equilibrium.

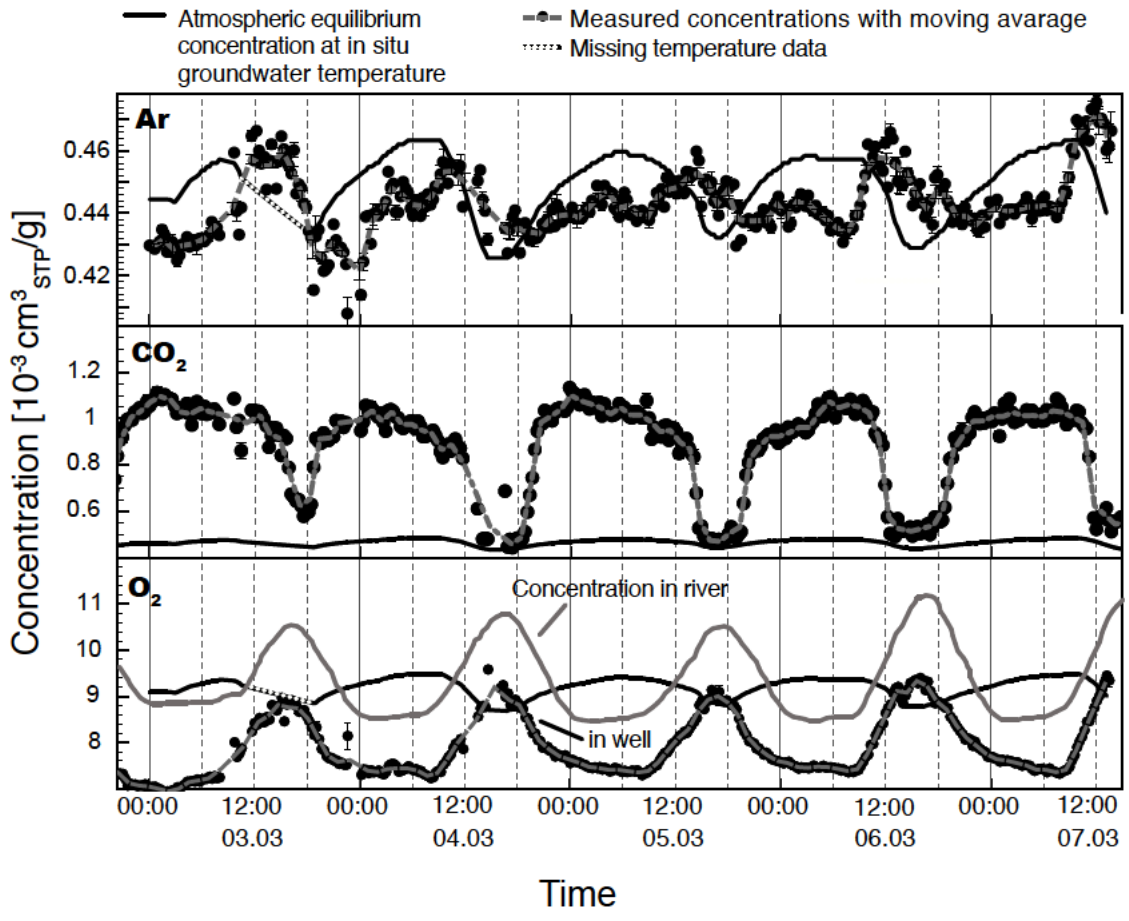

Figure 4.3: Gas concentrations in the observation well. The O_2 concentration of the river, additionally shown in the lowest plot, was recored 10 km downstream (BAFU, 2011).

In groundwater near the surface, besides (lateral) heat advection, vertical heat transport is known to play a significant role in the overall heat budget (Vogt et al., 2010b; Molina-Giraldo et al., 2011). In particular in our case where the aquifer top exhibits hardly any vegetational cover, direct solar radiation heats the uppermost gravel layer. Similarly during the night, the uncovered upper most gravel layer cools rapidly. In both cases the missing vegetational cover results in a high temperature gradient from aquifer top to the groundwater, and hence enforces vertical heat conduction (Smith et al., 1964; Beyerle et al., 2003). We can therefore identify vertical heat transport as having an influence on the measured groundwater temperatures. Indeed, in our study the synchronous temperature evolution of river and groundwater (Figure 4.2) indicates that groundwater temperatures were mainly controlled by vertical heat exchange. An advective heat transport of water from the stream to the hyporheic zone would impose the rivers diel temperature variations with a delay onto the groundwater temperature. This delay is due to the travel time of the infiltrating water of approximately 5 to 6.5 h.
We note that in a river the heat transport rate may exceed the gas-exchange velocity (Schwarzenbach et al., 2003; Aeschbach-Hertig et al., 1999) resulting in a delay in response of the Ar concentration in the river with respect to water temperature. However, such delay in the response of the Ar concentrations is coupled to a dampening of the amplitude in the Ar concentration variations (see the supporting information for the dependence of the amplitude dampening on the time lag). Such dampening is not present in the Ar-concentrations measured in groundwater in comparison to the atmospheric equilibrium concentration of the river (see Figure 4.3), therefore our assumption of the argon concentration in the river being in atmospheric equilibrium is valid.

4.3.2 Temporal evolution of O_2 and CO_2 concentrations

The O_2 concentrations of the river showed the typical diel fluctuation resulting from photosynthesis during the day and respiration during the night (Streeter and Phelps, 1925; Schurr and Ruchti, 1975; Livingstone, 1991; Uehlinger, 2006). Note that the O_2 concentrations of the river were recorded at a national observation station about 10 km downstream of the field site (BAFU, 2011). We assume the shape of the diel O_2 concentration fluctuation in the river at the study site to be similar to the diel fluctuation at the monitoring station, as both sites are exposed to the same daily solar irradiation and at low flow conditions the river water and its quality and clarity (clear water) is the same at both locations. However, the absolute amplitude of the O_2 concentration variations were possibly different, as the biological production of O_2 may vary locally due to changes in algae growth and river depth (Livingstone, 1991).
The CO_2 concentrations (Figure 4.3) in the observation well showed strong diel fluctuations. The observed maxima of the CO_2 concentrations exceeded the respective atmospheric solubility concentration by over 100 %. Such high amounts of CO_2 are very common in groundwater and are the result of DOC degradation with O_2 (Whitman and Clark, 1982; Korom, 1992; Malard and Hervant, 1999). As expected, the O_2 concentrations in the groundwater were lower than in the river and exhibited diel fluctuations, with a temporal evolution inverse to that of the CO_2 concentrations. Note that, the synchronous evolution of the O_2 concentration in the groundwater and in the river is not due to a constant consumption rate, as a O_2 concentration evolution with a constant consumption rate would exhibit a delay due to the travel time.

Furthermore, both O_2 and CO_2 concentrations synchronously reached atmospheric equilibrium concentration around 18:00. However, the amplitude of the O_2 concentration fluctuations was more than twice as high as that of CO_2. The inverse concentration evolution of CO_2 and O_2 indicates that, as expected, O_2 turnover and hence microbial activity showed diel variations. However, CO_2 concentrations are only a qualitative indicator for the O_2 turnover, as CO_2 is chemically reactive.

4.3.3 Oxygen turnover

To quantify the O_2 turnover within the groundwater, besides the local O_2 concentration, the total effective O_2 input at groundwater recharge must be known. In our study, the initial concentration of O_2, entering the groundwater was set in the stream, with no additional O_2 input resulting from the formation of excess air. Thus, the O_2 turnover can simply be calculated by subtracting the measured O_2 concentration in groundwater from the respective initial O_2 concentration at recharge, i.e., the O_2 concentration in the river around 5.5 h (travel time of the water) prior to the groundwater measurement. The calculated O_2 turnover (ΔO_2) since groundwater recharge, is shown in Figure 4.4 in comparison to the measured CO_2 super saturation (ΔCO_2).

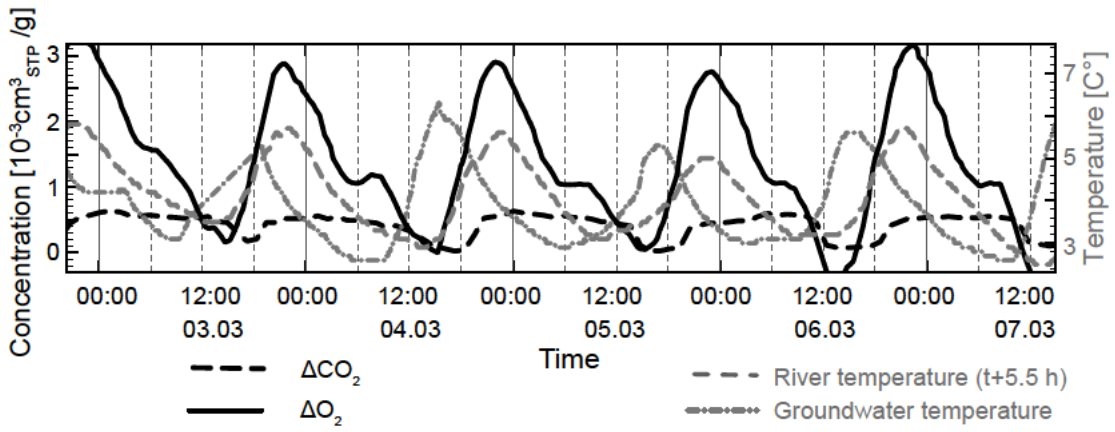

Figure 4.4: Results of calculated O_2 turnover (ΔO_2) compared to the CO_2 super saturation (ΔCO_2). Groundwater temperature and the river temperature shifted for 5.5 h hour to compensate for groundwater residence time are displayed in grey.

As expected, ΔO_2 as well as ΔCO_2 show diel fluctuations and the amplitude of ΔCO_2 is significantly (around 5 times) smaller. Dissolved CO_2 tends to react with water and calcium carbonate to form the soluble calcium bicarbonate. Vogt et al. (2010b) observed that the HCO_3^- concentration in a nearby observation well differs from HCO_3^- concentration in the river, hence confirming the presence of such a process. We further note that in the calculation of ΔCO_2 any CO_2 concentration variations of the river Thur (Hayashi et al., 2012) were not considered.

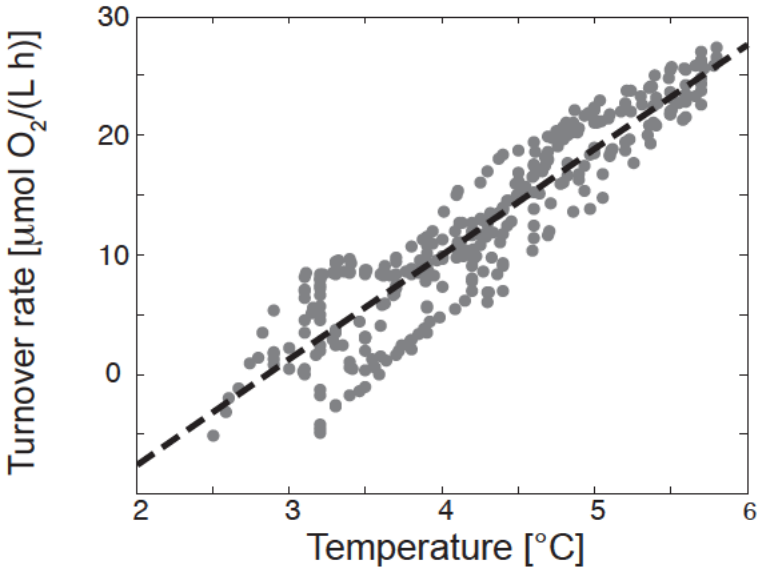

Figure 4.5: O_2 turnover rate, over the total travel distance from the river to the observation well, compared to temperature of the infiltrating river. Linear regression yields a slope of 8.8 ± 0.4 µmol/(L h K).

During its daily minimum, ΔO_2 reaches zero (negative values are due to the inaccuracy in travel time). Hence, consumption seemed to have stopped. This is remarkable as O_2 (and presumably also DOC) is still available. On the other hand, bacterial activity is controlled by temperature (O'Connell, 1990; Kirschbaum, 1995; Greskowiak et al., 2006). The initial water temperature at recharge, i.e. river temperature (shifted 5.5 h backwards), was almost in phase with ΔO_2, which is in contrast to the measured local groundwater temperature which leaped around 5 h ahead of ΔO_2. While we neither know the evolution of ΔO_2 nor of the temperature of the water in between river and observation well, the initial groundwater temperature was set by the river temperature. If we assume that most of the O_2 turnover happened in the first few cm after infiltration of the water into the aquifer (Malard and Hervant, 1999), or more generally if we assume that the turnover predominantly occurred while (vertical) heat conduction did not yet significantly alter the initial temperature in groundwater, we can estimate the temperature dependence of ΔO_2 (see Figure 4.5). Our calculations show that the ΔO_2 increases with temperature between 3 and 6 °C (with a slope of 8.8 ± 0.4 µmol/(L h K)), and ceases at temperatures below 3 °C.
Note that in case that O_2 is consumed at a constant rate through out the aquifer such a temperature relation could not be found.

4.3.4 Discussion

We investigated the diel gas fluctuations in the hyporheic zone of a losing river. We were able to exclude any relevant influences of secondary gas exchange on the concentration measured in the hyporheic zone, in particular excess air formation was not present. Therefore the temporal evolution of water temperature at the location, where the last air/water partitioning occurred, the river, was identified as the major control of the Ar concentra-

tions in the hyporheic zone.
The Ar concentrations measurements in the hyporheic zone in combination with the temperature measurements in the river and in the hyporheic zone enabled us to investigate the difference in heat and gas transport. In particular we found that temperature in the hyporheic zone was controlled mainly by vertical heat transport and advection with groundwater flow only had an insignificant contribution. Diurnal temperature fluctuations were therefore not suitable for travel time estimation of the water. However, by cross correlating the Ar concentrations in groundwater to the atmospheric solubility concentrations of Ar in the river, we were able to estimate the groundwater travel time at the observation well to approximately 5 - 6.5 h.
Using the gained knowledge of the gas transport, we quantified the O_2 turnover in the groundwater. With the assumption that most microbial activity consuming O_2 occurred just after infiltration of the water, we were able to relate the changes in O_2 turnover to changes in the water temperature that prevailed during the consumption of O_2. Whereby from 3 °C to 6 °C, O_2 turnover increased with temperature and it stopped at temperature below 3 °C indicating that no aerobic microbial activity occurred anymore.
In general, we recommend noble-gas concentration time-series (NGTS), similar to the Ar concentrations of this work, to be used for the study of dynamics of gas exchange in river groundwater systems. In particular, NGTS contain information about temporal evolution of geochemistry and heat budget of the water at infiltration and in the aquifer. Furthermore, as documented in our work, NGTS can be used to determine groundwater travel-time, analogous to travel time determination with time-series of water temperature or salinity (Silliman et al., 1995; Anderson, 2005; Cirpka et al., 2007; Vogt et al., 2010a). In terms of combined noble gas and O_2 quantification, O_2 turnover can be quantified with high temporal resolution. Hence microbial activity which is in direct relation of O_2 turnover can be studied in-situ and in real time and compared to the prevailing condition of the groundwater (e.g., temperature as in this work, or chemical composition in general).

Acknowledgments

We thank B. Doulatyari for improving the manuscript and S. Diem for assistance in collecting the temperature data. This work was performed within the framework of the RECORD project (Assessment and Modeling of Coupled Ecological and Hydrological Dynamics in the Restored Corridor of a River (Restored Corridor Dynamics)), and was funded by eawag (Swiss Federal Institute of Aquatic Science and Technology) and CCES (Competence Center Environment and Sustainability of the ETH Domain).

4.4 Appendix

4.4.1 Diel evolution of the dissolved Ar concentration in a river

In the following section we will look at gas exchange in a river with a diel temperature evolution $T_{\mathrm{w}}(t)$. The gas exchange of Ar is parameterize with the exchange rate k_r which is equal to the ratio of the gas exchange velocity v_f, depending on wind-speed and river morphology, to the river depth h_r. The mean dissolved Ar concentration in the river ($C_{\mathrm{Ar}}(t)$,

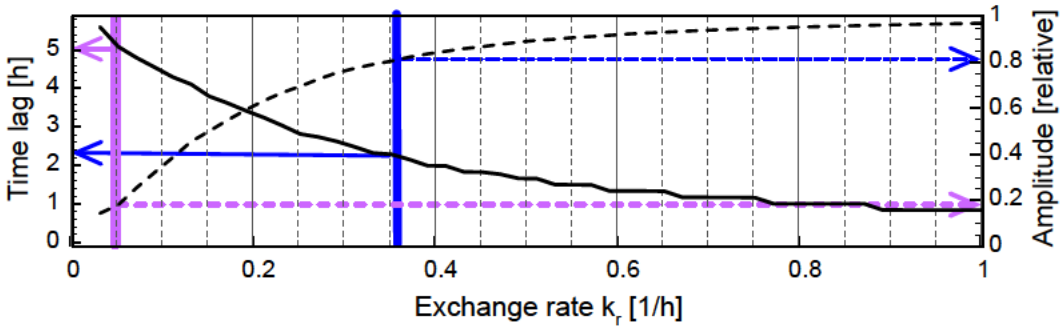

Figure 4.6: Numerical solutions for time lag (solid line) and Amplitude (dashed line) Numerical solutions of Equation 4.1 for different exchange rate k_r. The blue and the violet marks show a k_r value of 0.38 h^{-1} and of 0.05 h^{-1}. The latter is calculated by assuming a time lag of 5 h.

which can be assumed to be equal to the concentration at any location in the river due to turbulent mixing) is than given by the following rate equation (Schurr and Ruchti, 1975):

$$\frac{dC_{Ar}(t)}{dt} = k_r \left(H_{Ar}(T_w(t)) \times p_{Ar} - C_{Ar}(t) \right), \tag{4.1}$$

with p_{Ar} the partial pressure in air and H_{Ar} the Henry constant of Ar.
We numerically solved Equation 4.1 with the assumption that $T_w(t) = T_0 + T_{var} \sin(\frac{2\pi}{24h} t)$, for $T_0 = 4.5$ °C, $T_{var} = 1.5$ °C and $k_r = 0...1$ h^{-1}. The resulting concentration amplitudes and time lags, in respect to river temperature, are shown in Figure 4.6. The solution shows that a delay or time lag of the temporal evolution of Ar concentration in comparison to river temperature is linked to a dampening of the Ar concentration amplitudes ande vice versa.
To explain a phase shift of 5 h as observed in our Ar concentrations, a k_r value of approximately 0.05 h^{-1} is needed. This rate is very low compared to the determined k_r of other studies, e.g. of the Aare river with 0.24 h^{-1} (Schurr and Ruchti, 1975) and a mean depth of $h_r \approx 2.4$ m (Schweizer et al., 2007) which is more than the double of the Thur river ($h_r \approx 1$ m). Furthermore a river with such a small k_r value exhibits a concentration evolution with a reduced amplitude of only 20 % compared to the concentration evolution of immediate gas exchange ($k_r \to \infty$). However, such a reduced amplitude was not observed, hence gas exchange and heat transfer velocity of the Thur river must have had similar values during the entire study.

5 Excess air formation as a mechanism for delivering oxygen to groundwater

Chapter 5 has been submitted for publication in Water Resources Research:
Mächler, L., Peter, S., Brennwald, M. S. and Kipfer, R. (2012). Excess air formation as a mechanism for delivering oxygen to groundwater.

Abstract

The temporal dynamics and spatial distribution of the concentrations of dissolved gases (He, Ar, Kr, N_2, O_2 and CO_2) in an infiltrating groundwater system fed by the peri-alpine River Thur (Switzerland) were analysed before, during and after a single, well-defined flood event. The analysis was based on measurements taken in five different groundwater observation wells that were located approximately 10 m apart and tapped the same groundwater body, but were situated in three different riparian zones. The input of O_2 into the groundwater as a result of the formation of excess air was found to be of the same order of magnitude as that resulting from the advection of river water, although the amount of excess air formed and the amount of O_2 delivered varied significantly among the riparian zones. The results suggest that the input of O_2 into groundwater as a result of excess air formation is controlled not only by the hydraulic conditions prevailing in the river and the groundwater, but also by the thickness of the confining bed at the top of the aquifer, which is revealed to be a key factor controlling the trapping and dissolution of air in groundwater.

5.1 Introduction

A significant part of Switzerland's drinking water (over 30 % Hartmann and Michel, 1992; SVGW, 2002) is produced from riparian aquifers. Rivers which recharge their adjacent aquifers are highly dynamic, and are characterized by high variability with regard to discharge rates and the chemical composition of the solutes e.g., dissolved oxygen (Uehlinger and Naegeli, 1998; Kirchner et al., 2000; Uehlinger, 2006).
In groundwater, dissolved oxygen (O_2), carbon dioxide (CO_2) and nitrogen (N_2) are essential reactants and products of biogeochemical processes, in particular of microbiological activity, which remove nutrients and pollutants and are therefore an important control of water quality (Whitman and Clark, 1982; Korom, 1992; Brunke and Gonser, 1997; Boulton et al., 1998; Malard and Hervant, 1999; Hayashi and Rosenberry, 2002; Rivett et al., 2008). In particular, CO_2 is produced in both aerobic respiration —the consumption of

O_2— and during denitrification, whereby in case of complete denitrification also N_2 is produced. However, CO_2 concentrations are not a direct quantitative measure for bacterial activity, as part of the produced CO_2 is often transformed into calcium bicarbonate (see e.g., Hynes, 2001).
During floods, biogeochemical changes in the river are transmitted to the groundwater. Furthermore, the varying hydraulic conditions can activate interaction of the groundwater with the soil, e.g. input of DOC (Baker et al., 2000; Peter et al., 2012a), and trigger gas input from the soil air into the groundwater (Vogel et al., 1981; Stute et al., 1992; Aeschbach-Hertig et al., 1999; Williams and Oostrom, 2000; Kipfer et al., 2002; Klump et al., 2007).
Therefore, to quantitatively and qualitatively interpret subsurface biogeochemical processes, not only the concentrations of N_2, O_2 and CO_2, need to be measured, but it is also necessary to determine the total amount of each gas injected per water mass (effective gas input). Gas transport by infiltrating river water into the aquifer and gas exchange through the unsaturated zone within the aquifer contribute to the effective gas input. Both contributions are often unknown (Vogel et al., 1981; Stute et al., 1992; Kipfer et al., 2002; Lippmann et al., 2003; Holocher et al., 2003; Klump et al., 2008). In particular, the initial concentration cannot usually be determined by assuming atmospheric solubility equilibrium, as the equilibrium concentration is controlled mainly by local soil temperature and not necessarily by the temperature prevailing during the last occurrence of gas partitioning (Vogel et al., 1981; Heaton and Vogel, 1981; Beyerle et al., 1999).
Gas partitioning in an aquifer by the entrapment and dissolution of air bubbles, in response to water-table fluctuations or groundwater recharge, leads to the formation of excess air i.e. a surplus of atmospheric gases relative to atmospheric solubility equilibrium (Heaton and Vogel, 1981; Kipfer et al., 2002; Lippmann et al., 2003; Klump et al., 2007). Excess air formation therefore contributes substantially to the effective input of O_2 and N_2 into groundwater (Rose and Long, 1988; Beyerle et al., 1999; Williams and Oostrom, 2000; Massmann and Sueltenfuss, 2008). In conclusion, initial O_2 availability in groundwater may be much larger than expected based on atmospheric equilibrium considerations alone (Beyerle et al., 1999).
Atmospheric noble gases (He, Ne, Ar, Kr and Xe) are biogeochemically inert and are therefore excellent tracers to analyze gas exchange in porous media, such as excess air formation (e.g., Kipfer et al., 2002). In particular, measured noble gas concentrations enable the amount of injected excess air to be reconstructed (Beyerle et al., 1999; Aeschbach-Hertig et al., 1999, 2000; Kipfer et al., 2002; Ingram et al., 2007; Klump et al., 2007, 2008), and hence allow the effective O_2 and N_2 input into groundwater to be estimated.
Both in laboratory experiments (Williams and Oostrom, 2000) and in few field studies, excess air formation was documented to influence O_2 availability in groundwater (Beyerle et al., 1999; Massmann and Sueltenfuss, 2008). However, no field study up to our knowledge investigated in detail O_2 injection into riparian groundwater due to the hydraulic fluctuations of the river. Therefore, in this work we studied excess air formation as a mechanism for the delivery of O_2 to groundwater in different riparian zones near an infiltrating peri alpine-river responding to a flood incident. Furthermore, in order to quantify possible biochemical production of N_2 due to denitrification processes, we determined the injection of atmospheric N_2 into the groundwater.
Our study was conducted during a small flood event of an alpine river (Thur, Switzerland), and included the quantification of different dissolved gas concentrations (N_2, O_2,

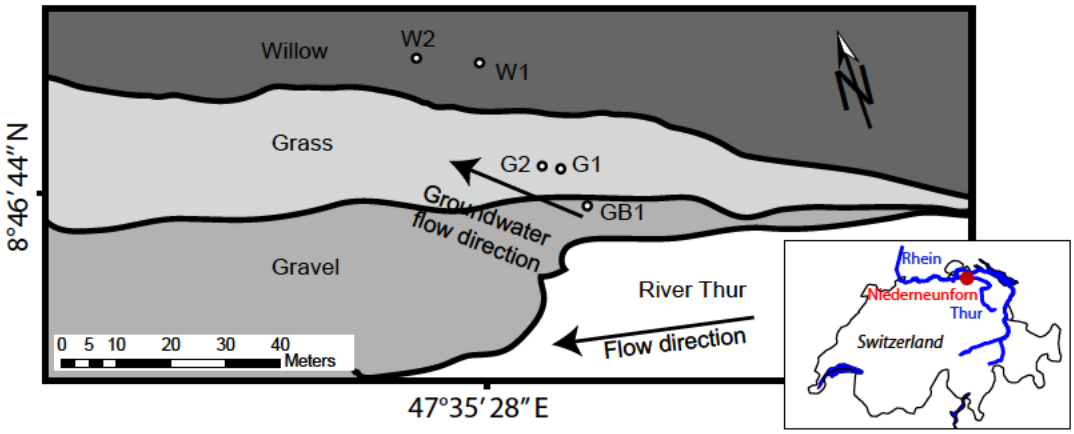

Figure 5.1: Schematic map of the field site (Niederneunforn at river Thur, Switzerland) during low flow. During high flow the gravel banks were flooded. The groundwater wells in the different functional process zones are also shown. Groundwater flow direction is taken from Vogt et al. (2010a). Note that, a more recent work (Peter et al., 2012c) suggested a groundwater flow with a less steep angle to the river flow direction.

CO_2, He, Ar, Kr) in several groundwater wells. The wells were located, between 1 and 50 m away from the river, covering three different functional process zones i.e., individual types of hydrogeomorphic patches that differ in their physiochemical characteristics, size, shape and internal structural complexity, and therefore fulfill different ecological functions (Thorp et al., 2006).
The results of our work set the basis for an accompanying study to analyze the turnover of organic carbon and nitrogen in the different riparian zones in response to the flood event (see companion article, Peter et al., 2012b). In this study, our determined CO_2 and O_2 concentrations and the calculated O_2 and N_2 injections due to excess air formation are embedded in a broader biochemical context.

5.2 Methods

5.2.1 Study site

The river Thur is located in the northeast of Switzerland. The catchment area of the river Thur includes an elevation of over 2500 m asl and the rivers estuary leads in to the river Rhine at 345 m asl. The high elevation difference and the fact that there is no lake along its course, makes the river Thur a very dynamic river. In particular, precipitation events in the catchment trigger immediate increases in water discharge, which often leads to floods (BAFU, 2010; Vogt et al., 2010a). Therefore, most of the river was channelized for flood protection in the late 19^{th}/early 20^{th} century (Binderheim-Banakay et al., 2000; BAFU, 2010). In recent years, the overbanks were removed over a length of approximate 2.5 km and the riverbed was widened to allow small meanders to develop in order to revitalize the river (BAFU, 2010; Schneider et al., 2011).

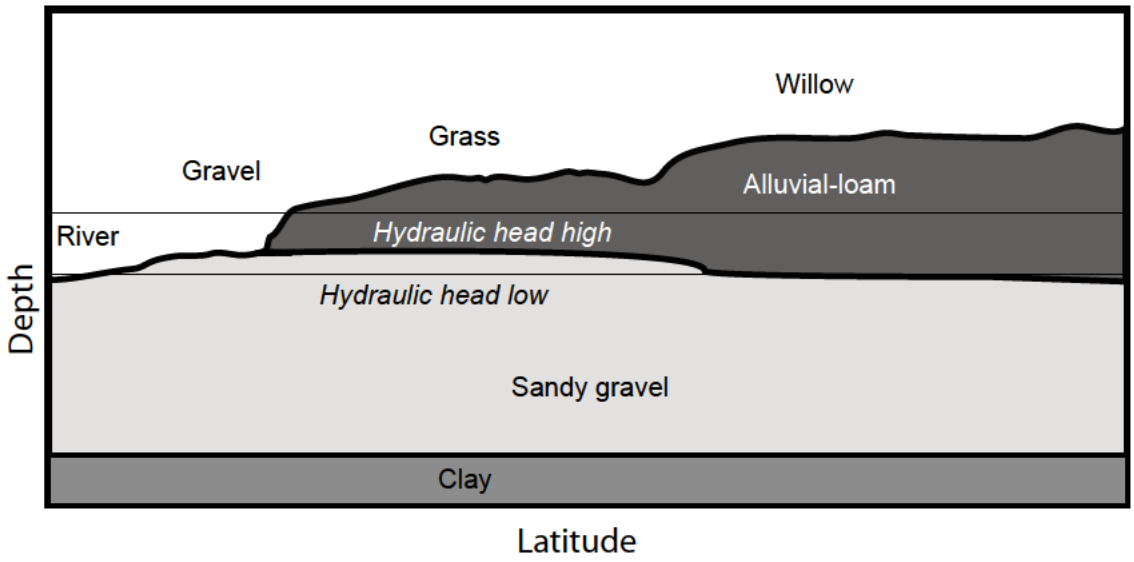

Figure 5.2: Schematic view of the transversal section of the Aquifer. Aspect ratios of the different objects are to scale.

The underlying Thur-Valley aquifer spreads over the entire valley and constantly exchanges water with the river. At our study site (Niederneunforn, Canton Thurgovia) this riparian aquifer is approximately 6 meter thick (see Figure 5.2). It consists of sandy gravel with impervious clay below and with a 0.5-2 m thick alluvial loam layer forming the aquifer-top. Depending on the water table and the thickness of the top layer, the groundwater at our study site exhibits unconfined and confined conditions (Vogt et al., 2010a). The studied observation wells are less than 50 m away from the river and were set in three different riparian zones (see Figure 5.1): gravel (well GB1), grass (well G1 and G2) and willow (well W1 and W2). The groundwater residence time in the different wells ranges from less than one day in the gravel zone to more than 4 days in the two wells in the willow zone (Vogt et al., 2010a).

5.2.2 Measurements

The Gas Equilibrium Membrane Inlet Mass Spectrometer (GE-MIMS) system used for the in situ determination of the gas concentrations in groundwater is described in detail in Mächler et al. (2012). The system permits to quasi continuously (every 12 min) determine concentration of dissolved gases (He, Ar, Kr, N_2, and O_2) in groundwater. For this work we included dissolved CO_2 into the measurement procedure, following the experimental set up and calibration procedure of Mächler et al. (2012). The overall error of the CO_2 concentration measurements is about 3 % at atmospheric solubility concentration. The observed CO_2 concentration in groundwater was always larger than the detection limit of the system (Mächler et al., 2012). The overall measurement errors of the other analyzed gases are $\pm$ 1 % for Ar, N_2 and O_2, $\pm$ 3 % for He and $\pm$ 4 % for Kr (Mächler et al., 2012).

5.2.3 Gas exchange in porous media

In open water, gases are exchanged through the interface between the water body and the atmosphere and commonly attain gas partitioning equilibrium which is described by Henry's law (see e.g. Kipfer et al., 2002):

$$C_i^{\mathrm{ASW}} = H_i(T_\mathrm{w}, S_\mathrm{w}) p_i^{\mathrm{atm}}, \tag{5.1}$$

where p_i^{atm} is the partial pressure of a gas i in air, C_i^{ASW} the gas concentration in air-saturated water (ASW), and H_i is the Henry coefficient of gas i at the temperature T_w and salinity S_w.
In contrast, gas exchange in the unsaturated zone of a riparian groundwater not only occurs with the atmosphere, but also with entrapped air bubbles that are captured in the unsaturated zone (i.e., excess air formation), e.g. during water-table fluctuations (Vogel et al., 1981; Stute et al., 1992; Aeschbach-Hertig et al., 1999; Williams and Oostrom, 2000; Kipfer et al., 2002; Klump et al., 2007). Aeschbach-Hertig et al. (2000) proposed a simple but widely accepted parameter model of excess air formation, which assumes the gases in the gas bubbles and the dissolved gases to be in solubility equilibrium with respect to the elevated pressure in the gas phase. Under such conditions, and further with the given water temperature T_w and by assuming a negligible groundwater salinity ($S_\mathrm{w} \approx 0$), the dissolved gas concentration C_i^f of a gas i can be described by the closed-system equilibration model CE-model (CE-model, see Aeschbach-Hertig et al., 2000):

$$C_i^f = C_i^{\mathrm{ASW}}(T_\mathrm{w}) + \frac{(1 - F_{\mathrm{CE}})\, A z_i}{1 + F_{\mathrm{CE}} \dfrac{A z_i}{C_i^{\mathrm{ASW}}(T_\mathrm{w})}}, \tag{5.2}$$

where A is the amount of dry air per unit mass of water initially entrapped in the water and z_i is the volume fraction of the gas i in dry air. The fractionation F_{CE} describes the "degree" of bubble dissolution. In case of $F_{\mathrm{CE}} = 0$ all the bubbles are completely dissolved and $F_{\mathrm{CE}} \approx 1$ means that virtually no gas of the air bubbles dissolved in the surrounding groundwater. For $F_{\mathrm{CE}} > 0$ the excess air component is elementally fractionated with respect to the complete dissolution of air. As during the partial dissolution of air bubbles, the more soluble (noble) gases are enriched in the water phase. Aeschbach-Hertig et al. (2000) showed that the model parameters (T_w, A, F_{CE}) can be determined from the observed noble gas concentration by least-squares regression using Equation 5.2 (Aeschbach-Hertig et al., 1999, 2000).
In Equation 5.2 the concentrations prevailing before excess air formation C_i^0 are assumed to be equal to the ASW concentration i.e., $C_i^0 = C_i^{\mathrm{ASW}}(T_\mathrm{w})$. However, this is not necessarily true (see introduction) and hence Equation 5.2 needs to be modified:

$$C_i^f = C_i^0 + \frac{\left(1 - F_{\mathrm{CE}} \dfrac{C_i^0}{C_i^{\mathrm{ASW}}(T_\mathrm{w})}\right) A z_i}{1 + F_{\mathrm{CE}} \dfrac{A z_i}{C_i^{\mathrm{ASW}}(T_\mathrm{w})}}. \tag{5.3}$$

Note that the derivation of Equation 5.3 follows exactly the derivation of the CE-model given by Aeschbach-Hertig et al. (2000). However, the initial concentration is now an

arbitrary concentration C_i^0 instead of C_i^{ASW}.
The results obtained from Equation 5.3 differs significantly from Equation 5.2, if C_i^0 deviates significantly from $C_i^{\mathrm{ASW}}(T_{\mathrm{w}})$. In such a case, only the modified CE-model (i.e., Equation 5.3) is appropriate to qualitatively describe the gas injection. However, if C_i^0 in Equation 5.3 corresponds to a ASW concentration at a similar temperature as T_{w}, the CE-model regression will deliver reasonable values for A and F_{CE}. Note that in case of total dissolution (i.e., $F_{\mathrm{CE}} = 0$), the value A is actually determined correctly. However, in this case the resulting value for C_i^{ASW} needs to be interpreted as the ASW concentration at the water temperature that prevailed during the air/water partitioning before excess air formation, which is in general different form the groundwater temperature during excess air formation. In case of a elemental fractionation ($F_{\mathrm{CE}} > 0$), the excess air is in principle temperature dependent. However, in strong contrast to temperature reconstruction from dissolved noble gases, the determination of A and F_{CE} is mainly controlled by light and hence poorly soluble noble gas species (He). As the Henry coefficient of He hardly depends on temperature, the determination of A and F_{CE} are only marginally affected by the water temperature at which the noble gas concentrations prior to the excess air formation were preset. In our case of a losing river the initial concentration for noble gases are given by the ASW concentration at river temperature. Temperature differences of the river and groundwater are reasonably small (see Section 5.3.3) and hence the CE-model (i.e. Equation 5.2) can be used to determine A and F_{CE}. Also for calculating N_2 injection the original CE model can be used, as the initial N_2-concentrations are near the ASW concentrations of the river. However, to estimate O_2 input we used Equation 5.3, as initial O_2 concentrations in the hypoxic groundwater were very low.
To calculate O_2 input by using Equation 5.3 in case of $F_{\mathrm{CE}} > 0$, we implicitly assume that no O_2 is consumed during the actual formation of excess air. In the case of significant O_2 consumption during excess air formation, O_2 is constantly extracted from the bubbles to attain local equilibrium between the dissolved gases and the entrapped gas phase, until the bubbles are void of O_2. In that limiting case, the effective O_2 input is equal to Az_{O_2}. Therefore, the quantification of the effective O_2 input using Equation 5.3 represents a conservative estimate.

5.3 Results and calculations

5.3.1 Changes in dissolved gas concentrations in response to the flood

The field campaign started in the middle of May (2011) after a dry period of several weeks. At that time, the discharge of the river Thur was below 10 m^3/s (Figure 5.3). On 15 May, after heavy precipitation in the catchment, a small flood (discharge approximately 100 m^3/s) passed our study site at Niederneunforn and forced the water table to rise approximately 1 m. At peak flood, the gravel zone was flooded. The groundwater table in the grass and the willow zones remained below the soil surface. After the peak flow the discharge rapidly decreased and was three days later was again below 20 m^3/s.
The dissolved gas concentrations measured in the three functional process zones are shown in Figure 5.4. All measured O_2 concentrations in all wells were found to be below ASW concentration. Especially low O_2 concentrations were found in well W1 throughout the

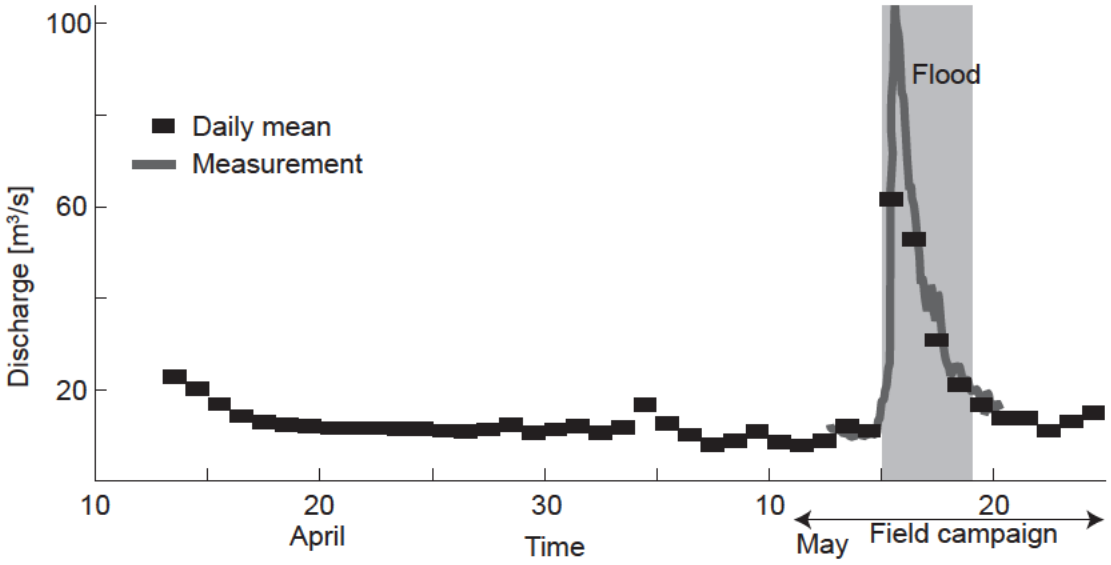

Figure 5.3: Discharge of the river Thur at Niederneunforn during April-Mai 2011.

entire measurement period except for 2 days after the flood. Also particularly low O_2 concentration were found in well W2 during the period after the flood, as well as in the grass and gravel zones during the flood. In all zones the dissolved CO_2 concentrations were significantly higher than ASW concentration and increased in response to the flood.
In the groundwater of the grass and gravel zones the temporal evolutions of CO_2 and O_2 were anti-correlated, whereby the observed increase in CO_2 concentration during the flood was similar to the O_2 concentration decrease. Assuming that the initial concentrations of O_2 in the grass and gravel zones remained the same and did not change at all, the CO_2 concentration increases can be explained by the consumption of the initially available O_2. However, in the willow zone the CO_2 concentrations increased much stronger during the flood than in the other zones. Due to the initially prevailing low O_2 concentrations, the increase in CO_2 concentrations cannot be explained by consumption of the initially available O_2.
Noble-gas concentrations also increased in response to the flood event. The synchronous temporal concentration evolution of all dissolved noble-gases in the first day of the flood points to a gas input, triggered by the flood event, i.e., excess air formation. Furthermore, for well W1 and W2 gas transport from the river (or the hyporheic zone) to the different groundwater wells takes up to 4 days (Vogt et al., 2010a) and hence a change in river gas concentrations takes far longer than 1 day to reach well W1 and W2. We therefore conclude that excess air was formed within the aquifer and not in the river during infiltration. Due to the direction of groundwater flow (see Figure 5.1, Vogt et al., 2010a; Peter et al., 2012c) the excess air observed in well GB1 was formed in-situ in the gravel zone. Furthermore, the typical Darcy velocity at the field site is approximately 10 m/day (Vogt et al., 2010a). Thus the water sampled in the willow and gravel zone in the first and probably also in the second day after the peak flood, was already in the respective zone during the flood (see Figure 5.1). In conclusion, the observed excess air was generated in the same zone where the respective observation well is located. However, for longer time scales concentrations might be affected by advective transport from other zones and hence do

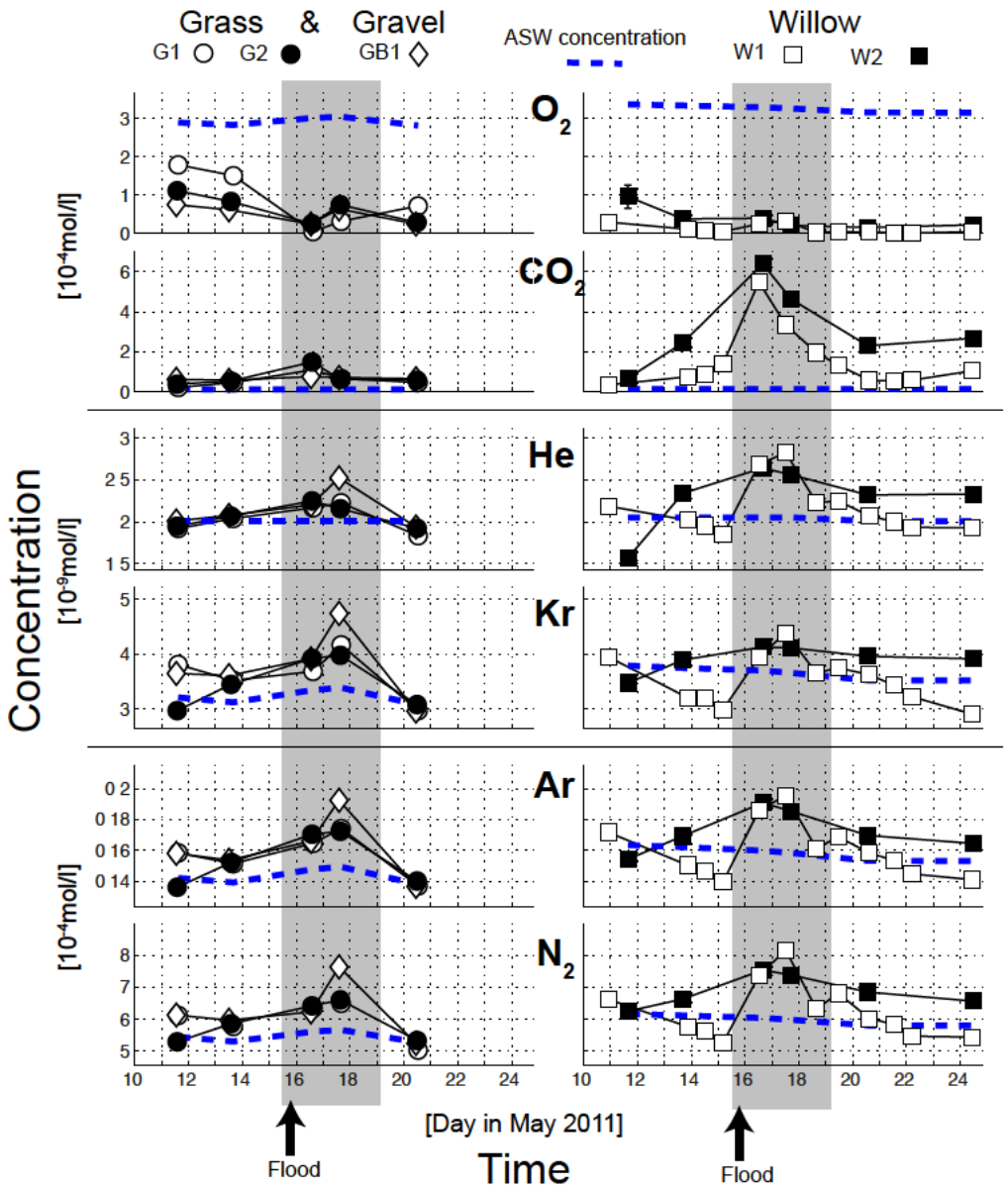

Figure 5.4: Dissolved gas concentrations in the wells. For each measured gas specimen, two panels are shown: the left panel with the dissolved gas concentrations determined in the wells positioned in the willow zone and the right panel with the concentrations in the grass and gravel zones. The grey area corresponds to the grey area in Figure 5.3.

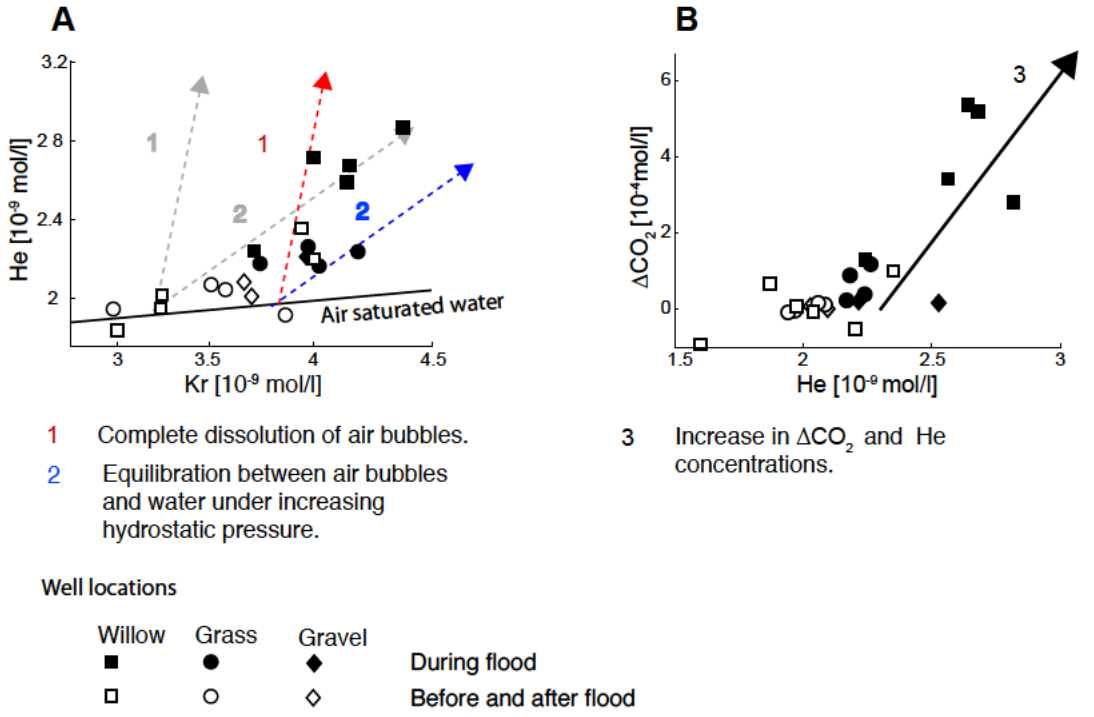

Figure 5.5: **A**) Two-elemental plot of He and Kr and **B**) plot of ΔCO_2 agains He concentrations. The ΔCO_2 is the difference of the measured CO_2 concentrations and the expected ASW concentration. The arrows in Figure **A** indicate the concentration increase of dissolved noble cases in response to different dissolution processes (see 1 & 2 in the legend, Kipfer et al., 2002). The arrow origins are set the atmospheric solubility concentration at the water temperature during the process of dissolution. Arrows of the same process, but with different origins (on different atmospheric solubility concentrations) are approximately parallel (grey arrows).

not only reflect excess air formation or any other process within the zone itself.
To analyze the temporal evolution of excess air formation, the evolution of He and Kr concentrations are illustrated in Figure 5.5 A. Especially during the flood (filled points) the determined He and Kr concentrations are higher than ASW concentrations, as they do not fall on the line the respective ASW concentrations span. The noble gas surpluses during the flood have an elemental composition which follows a pressure trend (dashed arrow 2 in Figure 5.5, Beyerle et al., 1999; Kipfer et al., 2002). That means the noble gas concentrations during the flood event can be interpreted as a combination of an ASW component and an excess noble gas component, generated by the (partial) dissolution of entrapped air bubbles under elevated pressure.
Figure 5.5 A also indicates higher Kr and He concentrations in the willow zone than in the grass and gravel zones, which implies an enhanced excess air formation in the willow zone. Furthermore, Kr concentrations in the excess air components of the groundwater in the willow zone are enriched with regard to the He concentrations, i.e., the Kr/He concen-

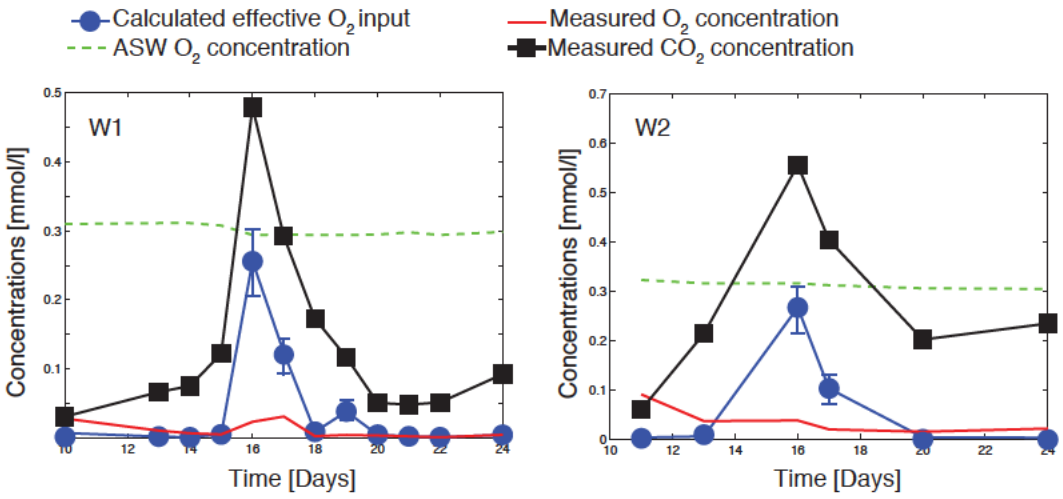

Figure 5.6: Measured CO_2 and O_2 concentration in comparison to the calculated O_2 concentration accounting for excess air formation. The error bars indicate 1-σ errors of the calculated values for A and F_{CE}.

tration ratio exceeds the ratio of dissolved atmospheric air. The excess air components, hence, are elementally fractionated with regard to complete dissolution of air in groundwater at 15 °C. Thus only partial dissolution of the gas bubbles occurred (i.e. $F_{CE} > 0$). He concentrations and the excess CO_2 concentrations (see Figure 5.5 B) show a strong positive correlation, which indicates that the CO_2 rise is closely linked to excess air formation. We hypothesize that the CO_2 increase during the flood event resulted from O_2 input due to excess air formation, whereby the injected O_2 was respired to CO_2. Under such conditions the measured CO_2 increase therefore must balance the O_2 input, unless a significant part of the produced CO_2 is transformed to calcium bicarbonate or transferred as a free gas into the remaining gas bubbles.
In summary, the measured dissolved gas concentrations indicate local excess air formation. However, both the amount and the elemental composition of the excess air differs between the different functional process zones, influencing the dissolved O_2 and the CO_2 concentrations. To confirm and quantitatively discuss these statements, both excess air and effective O_2 input needs to be determined.

5.3.2 Calculations of O_2 input due to excess air formation

The determined CE-model parameters F_{CE} and A are given in Table 5.1. The model calculations confirm that only in the willow zone large air entrapment occurred (i.e., $A \gg 0$ cm^3_{STP}/kg) during the flood: the values of A in the other zones are almost two orders of magnitudes smaller than in the willow zone. Furthermore, in the willow zone the composition of the excess air component is elementally fractionated ($F_{CE} > 0$), whereby in groundwater of the grass and gravel zone the excess air is of atmospheric composition ($F_{CE} = 0$). These findings are in agreement with the observed noble gas excesses in the willow zone during the flood event, which are enriched in the more soluble and heavier

noble gas species (see Figure 5.5).
The enhanced excess air formation in the willow zone injected significantly more O_2 into the groundwater in this zone than in the grass and gravel zones, where hardly any O_2 injection occurred (see Table 5.1). The comparison of calculated effective O_2 input with the measured O_2 and CO_2 concentrations in the groundwater of the willow zone (Figure 5.6) reveals that the effective O_2 input was similar to the CO_2 concentration increase during the flood ($|\Delta[CO_2]| \approx |[O_2]|$).
We assume the initial CO_2 concentration in well W1 and W2 to be equal to the measured CO_2 concentration before the flood, because, before the flood, the sum of the measured O_2 and the CO_2 concentrations in the grass zone was constant in time, and similar to the measured CO_2 concentration in the willow zone. Thus, assuming advection of the gases with water from the grass zone to the willow zone and complete reduction of O_2, the initial CO_2 concentration of the water in the willow zone must have been very similar to the measured CO_2 concentration before the flood. However, the sum of the initial CO_2 and the CO_2 produced by the local respiration of the injected O_2 explain about 90 % of the measured CO_2 concentration during the flood. The other remaining 10 % of CO_2 needs to be explained by another CO_2 source, e.g. CO_2 production due to denitrification.
We estimated the N_2 injection due to excess air formation in order to determine whether the measured N_2 concentrations can be fully explained by the physical exchange during air/water partitioning (e.g., excess air formation), or wether any biogeochemical reactions affected the N_2 concentration. The analysis shows that excess air formation completely accounts for the elevated dissolved N_2 concentrations in the groundwater body at our field site, i.e. the differences (ΔN_2) of measured N_2 and the calculated N_2 concentrations are within measurement uncertainty in all zones (see Table 5.1).
Hence, complete denitrification does not seem to significantly contribute to the observed CO_2 variations. However, incomplete denitrification which does not produce N_2 and therefore cannot be address by dissolved gas measurements may contribute to CO_2 formation.

Table 5.1: Determined model parameters (with Equation 5.2), the effective O_2 input (with Equation 5.3) and the relative deviation of calculated to the measured N_2 concentration (ΔN_2). Our wells corresponds to the wells analyzed by Vogt et al. (2010a) (names are given in the brackets after our nomenclature of the wells).

Well		A [cm^3_{STP}/kg]	F^1_{CE} [-]	O_2 input [µmol/l]	$\Delta N_2{}^2$ [%]	Day in Mai 2011
Gravel						
GB1	(r050)	0.2 ± 0.2	0	2 ± 2	2	11
		0.6 ± 0.2	0	5 ± 2	0	13
		1.0 ± 0.2	0	10 ± 2	-3	16
		2.2 ± 0.2	0	20 ± 2	0	17
		0.2 ± 0.2	0	2 ± 2	0	20
Grass						
G1	(r042)	0.7 ± 0.2	0	7 ± 1	2	11
		1.1 ± 0.2	0	10 ± 2	0	13
		1.8 ± 0.2	0	16 ± 2	-3	16
		1.3 ± 0.2	0	12 ± 2	0	17
		0.5 ± 0.2	0	5 ± 2	0	20
G2	(r072)	0.2 ± 0.4	0	2 ± 4	2	11
		0.9 ± 0.4	0	9 ± 4	0	13
		1.4 ± 0.4	0	13 ± 4	0	16
		1.5 ± 0.4	0	14 ± 4	-3	17
		0.1 ± 0.4	0	1 ± 4	-4	20
Willow						
W1	(r041)	0 ± 0.1	0	0 ± 1	0	10
		0 ± 0.2	0	0 ± 2	0	13
		0 ± 0.1	0	0 ± 1	2	14
		0 ± 0.1	0	0 ± 1	0	15
		89 ± 14	0.68 ± 0.05	232 ± 40	-1	16
		17 ± 9	0.55 ± 0.09	69 ± 30	0	17
		1.2 ± 0.3	0	12 ± 3	0	18
		3.5 ± 0.3	0	33 ± 3	4	19
		0.5 ± 0.1	0	5 ± 1	-1	20
		0.3 ± 0.1	0	3 ± 1	0	21
		0.1 ± 0.1	0	1 ± 1	0	22
		0.2 ± 0.1	0	2 ± 1	2	24
W2	(r058)	0 ± 0.1	0	0 ± 1	0	11
		1.6 ± 0.2	0	15 ± 2	-1	13
		91.8 ± 0.5	0.69 ± 0.01	218 ± 9	-1	16

continued on next page

Well	A	F_{CE}[1]	O_2 input	ΔN_2[2]	Day
	44 ± 30	0.72 ± 0.05	122 ± 30	-1	17
	1.5 ± 0.1	0	14 ± 1	3	20
	1.5 ± 0.1	0	14 ± 1	2	24

1, Only if the unfractionated excess air model (i.e. $F_{\mathrm{CE}} \triangleq 0$) did not yield an acceptable fit, the CE model (i.e., F_{CE} is unconstrained) was used (see also Klump et al., 2008).
2, Total error, including the measurement error and the model error, is around 2 %.

5.3.3 Accuracy and reliability of the used CE-model

The CE approach used to parameterize excess air is based on assumptions about the excess air formation which are not always justified, meaning that the results obtained by the CE approach may not be accurate (see Klump et al., 2008). We will therefore develop in this section some arguments that our simplified approach to approximate excess air formation by applying the CE model (Equation 5.2) is nevertheless reasonable in quantitative terms and produces valid and acceptable results. As noted in the method section of this work, in Equation 5.2 the initial noble gas concentration are assumed to be in solubility equilibrium with the ambient water temperature (Aeschbach-Hertig et al., 2000). In our case the initial concentrations in the studied groundwater were most likely set in the river Thur and therefore correspond to the atmospheric equilibrium at river temperature. But, the river temperatures (15 - 19.5 °C) were higher than the temperatures of the groundwater where the excess air formation took place (e.g. 13 - 16 °C in the willow zone). As pointed out earlier, only in case of a strong elemental fractionation ($F_{\mathrm{CE}} \approx 0$), the composition of the injected atmospheric gas component due to excess air formation is temperature dependent, i.e. only in the willow zone. The effect of a temperature discrepancy on the less soluble noble gas species is however low ($\lesssim$10 % for Ar and $\lesssim$2 % for He). Thus, the determination of the effective input of O_2 and N_2 with the CE-model parameters A and F_{CE} is therefore justifiable and reasonably adequate.
Both the CE-model (Equation 5.2) and the modified CE-model (Equation 5.3) implicitly assume that the exchanging water and the entrapped gas phase are at any time and at any location in atmospheric solubility equilibrium. Hence, the kinetics of gas dissolution as well as any transport within the water (and gas) phase are neglected. However, these basic assumptions are not always fulfilled during gas water partitioning in an aquifer (Klump et al., 2008). Klump et al. (2008) experimentally studied excess air formation in column experiments and compared the results with the outcome of numerical studies of different models describing the physics of gas exchange during the gas/water partitioning in porous media, accounting for both advective-dispersive transport and kinetic effects during gas dissolution (Holocher et al., 2003; Klump et al., 2008). Klump et al. (2008) documented that the kinetics of gas dissolution can be neglected and hence the assumption of local gas equilibrium is valid, as long as the advective gas transport (with the water flow) is slow compared to the effective gas transfer from the gas phase into the water. At our site, the observed groundwater table fluctuation of around 1 m occurred in about one day, whereas a local gas equilibrium between the entrapped air bubbles and the surrounding air water is established within about an hour (Holocher et al., 2003). Therefore, the ratio of the rates of gas exchange and advective gas transport (i.e. the Damköhler number) is large which

justifies the assumption of a local gas equilibrium (Klump et al., 2008).
Besides the kinetics of dissolution, the CE-model furthermore neglects advection with groundwater flow i.e., assumes global solubility equilibrium rather than local equilibrium (for a local equilibrium model see e.g., Cirpka and Kitanidis, 2001). Klump et al. (2008) found that in an advection dominated regime the CE-model tends to overestimate the initial amount of entrapped air (A) and its elemental fractionation (F_{CE}). However, such deviation only occurs at very strong advection when groundwater flow extracts and removes significant amounts of the gases from the air phase and hence significantly depletes the gas phase. Under such conditions the heavier, more soluble noble gases are far less enriched in the flowing groundwater than the light noble gases (Klump et al., 2008). However, in our study, in particular in the willow zone where most excess air was generated, the heavy and soluble Kr shows a similar supersaturation as the light and only poorly soluble He ($F_{\mathrm{CE}} \approx 0.7$, see Table 5.1). We note that even the given high groundwater velocity of up to 10 m/day (Vogt et al., 2010a) does not significantly deplete the Kr excess with regard to the He excess. Again, we therefore conclude that the determined values for A and F_{CE} are not strongly subjected to any bias due to groundwater advection.
Moreover, Klump et al. (2008) showed that the formation of unfractionated excess air is not only related to the complete dissolution of air bubbles. Rather, the stronger impact of advection on the more soluble gases leads to a depletion of the heavier and more soluble gases in the gas phase. After reaching a new steady state between gas phase and water phase, elemental fractionation of the dissolved noble gas excess due to differences in solubility are counteracted by the elemental fractionation of the gases in the gas phase. At such steady state the produced noble gas excess has an elemental composition of unfractionted air, although a trapped "non-atmospheric" gas phase is still present and dissolving. Under such conditions the CE-model is shown to (slightly) underestimate A and therefore the injected O_2 is underestimated (Klump et al., 2008). Our calculations therefore present a conservative estimate of the minimum O_2 input.
In summary, in our case the use of the CE model to quantify excess air formation and the modified CE-model to estimate the according O_2 injection yields reasonable results even when accounting for the physically unrealistically assumptions of the CE-model (Klump et al., 2008).

5.4 Conclusion

To our knowledge this field study is the first which estimates the input of O_2 due to excess air formation into a riparian groundwater during a flood event. Our noble gas measurements allowed us to determine injection of atmospheric O_2 and N_2 into groundwater because dissolved noble gas concentrations in groundwater enable the amount of initial entrapped air and the state of its dissolution to be quantified (Kipfer et al., 2002). Such measurements hence allow the determination of the excess of any other atmospheric gas like O_2 or N_2 (Kipfer et al., 2002).
Our calculations show that in the case of the riparian groundwater near the river Thur, the O_2 increase due to excess air formation in response to flood events is of the same order of magnitude as the atmospheric solubility concentration of O_2. However, during the flood the measured O_2 concentrations in the groundwater remained low, in contrast to the CO_2 concentrations which increased considerably. The calculated O_2 inputs were similar

to the observed CO_2 production. Hence, we conclude that the O_2 introduced by excess air formation was consumed immediately after injection, whereby CO_2 was produced. Similarly, our quantification of excess air yields an adequate estimate of the dissolved atmospheric N_2 concentrations, which need to be known to detect and study complete denitrification processes.
In conclusion, in riparian groundwaters that respond directly to hydraulic changes in the feeding river with water table fluctuations, excess air formation contributes significantly to the O_2 input into the groundwater. Excess air is therefore relevant for groundwater quality. In particular its formation may represent the only mechanism for the delivery of O_2 into groundwater far away from the feeding river.
The amount of dissolved excess air that was generated in response to the investigated flood, as well as its elemental composition, were observed to vary between the different functional process zones. Excess air formation and hence O_2 injection in the willow zone was found to be significantly larger than in the grass or gravel zones.
Excess air formation in groundwater is constrained to the quasi-saturated zone at the boundary between the saturated and the unsaturated zone, where air bubbles can be entrapped by water table fluctuations (Kipfer et al., 2002; Holocher et al., 2003; Klump et al., 2008). As a result of the increasing thickness and depth of the loam layer covering the Thur aquifer with distance from the river, measured hydraulic heads indicate that the groundwater in the willow zone is always confined (see Figure 5.2). In the grass zone however, a confined groundwater body is only present during the flood, while during normal flow conditions of the river Thur unconfined conditions prevail. In the gravel zone the groundwater body is always unconfined as no loam layer is present. These different hydraulic conditions may set a conceptual frame to explain why excess air formation differs between the different zones. The unconfined conditions in the gravel zone do not effectively trap air (due to high gas permeability of the gravel) and prevent excess air from being generated. Similarly, in the grass zone the soil air can be pushed towards to the gravel zone which again prevents effective air trapping. In contrast, in the willow zone, the rising groundwater table in response to enhanced river discharge exerts a higher hydrostatic pressure on the entrapped gas phase, as the confining loam layer prevents the entrapped air to escape.
Besides the confining loam layer, additional factors that affect the texture of the soil and hence influence the "mobility" of the entrapped air bubbles will impact the formation of excess air. Such differences in soil texture and geomorphology, which may have a certain influence on the ecological function (e.g. due to different vegetative cover or root growth of the willows), may further explain the difference in excess air formation in the grass and the willow zone.
In conclusion, our study demonstrates that excess air formation contributes significantly to O_2 occurrence in riparian groundwater and hence crucially controls the redox condition and therefore the quality of groundwater. Furthermore, our study demonstrates that morphology is the structural key to excess air formation and controls a substantial part of O_2 availability in groundwater.

Acknowledgments

This work was performed within the framework of the RECORD project (Assessment and Modeling of Coupled Ecological and Hydrological Dynamics in the Restored Corridor of a

River (Restored Corridor Dynamics)), and was funded by Eawag (Swiss Federal Institute of Aquatic Science and Technology) and CCES (Competence Center Environment and Sustainability of the ETH Domain).

6 Conclusion and outlook

6.1 Noble gas concentration time series

Single-sample based noble gas analysis to study gas/water partitioning in groundwater and in surface water is well established. From the noble gas concentrations of a single water sample, information about the past conditions at the time of air/water partitioning (e.g. temperature, hydrostatic pressure or salinity) can be reconstructed (e.g. Kipfer et al., 2002). In riparian groundwater, changes in both the chemical composition and the hydraulic condition of the adjacent river often influence groundwater chemistry. The temporal evolution of gas concentrations cannot be adequately resolved by a single-sample based analysis. Therefore, to study dissolved gas concentration changes on short time scales, characteristic of riparian groundwaters, an autonomous instrument which "quasi-continuously" measures dissolved noble gas concentrations in groundwater is needed.
The first target of this thesis was therefore to develop an instrument to autonomously quantify dissolved (noble) gases with a time resolution of less than 15 min, which could operate in the field over several days. To accomplish this, a membrane inlet system with a mass spectrometer for the gas analysis was combined (see Chapter 3). More precisely, a pressure reduction step between the membrane inlet and the mass spectrometer was included to ensure that the gases on the MS side of the membrane are (nearly) in solubility equilibrium with the water. This design solves the problem of in field calibration as the pressure reduction step allows ambient air to be used as a gas standard for calibrating the mass spectrometer. As the gas exchange is defined by Henry's law and is not influenced by membrane properties, the membrane inlet does not need any calibration. Thus, the problem of in field calibration is solved, which finally enables the instrument to be operated in-situ and autonomously.
The developed instrument was successfully deployed in two case studies investigating the O_2 dynamics in the riparian groundwater of a peri-alpine river (Chapter 4 & 5, see also Section 6.2). The first study (Chapter 4) investigated the origin of O_2 concentration fluctuations observed in the hyporheic zone. The measured time series of Ar concentrations contained information on the origin and the residence time of the water in the aquifer. By combining the Ar data with the time-series of measured O_2 concentration, the temperature dependence of O_2 consumption in the hyporheic zone was reconstructed.
The second study analyzed O_2-injection into groundwater due to excess air formation. The measurements were conducted at several groundwater observation wells during a flood event. The results revealed that there are lateral differences in excess air formation, and hence in O_2 injection. These differences are explained by geomorphic variability across the different riparian zones. Furthermore, it was shown that in riparian groundwater, excess air formation enhances O_2 availability considerably and therefore significantly influences the biochemical conditions as well as the quality of the groundwater.
In conclusion, noble gas concentration time series (NGTS) enable gas dynamics in ground-

water to be studied in real time and in particular to investigate the formation of excess air. For example, NGTS helped to determine the influence of the local geomorphic conditions on the gas exchange (Chapter 4 & 5). Furthermore, NGTS can be used to validate the reliability of simple models describing air/water partitioning in groundwater, (e.g. the CE-model), as the evolution of dissolved concentrations in response to the hydraulic conditions can be investigated in quasi-continous manner (Chapter 4 & 5).
Similar to a single set of noble gas concentrations, NGTS contain information on water temperatures and salinities during the last gas exchange. However, NGTS also allow the temporal evolution of the the environmental conditions at the last air/water partition to be reconstructed. Knowledge of the temporal evolution of the environmental conditions at the last air/water partition can help to determine recharge origin and residence time of the groundwater being studied (see Chapter 4).
As a major conclusion, the thesis identifies NGTS to be essential to the study of O_2 turnover in groundwater. As NGTS lead to a quantification of the physical exchange processes that control inputO_2 in groundwater. Only if the physical boundary conditions of the occurrence of O_2 are properly defined, any kind of bio-geochmical modification of the O_2 concentration can be studied. The same argument holds for any other reactive gas (e.g., CO_2 and N_2) dissolved in groundwater.

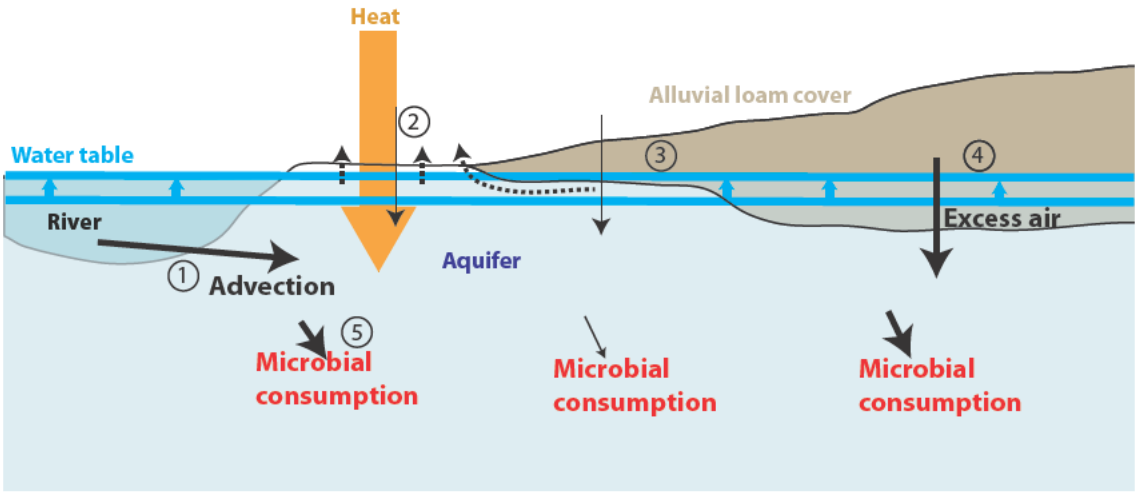

Figure 6.1: Schema of the river Thur with O_2 fluxes (solid and dashed black arrows).

6.2 Oxygen dynamics at the field site

The two field studies conducted as part of this thesis give insight into the gas exchange and the O_2 turnover rates of a dynamic riparian groundwater system. Figure 6.1 summarizes the findings.

As documented in Chapter 4, O_2 is supplied by bank infiltration from the river into the groundwater (Figure 6.1 ,①). As there is no O_2 input from excess air formation at a constant river discharge, bank infiltration is in this case the only source of O_2 to the groundwater. Consumption of O_2 in groundwater is strongly dependent on the water temperature, because microbial activity is a function of temperature (O'Connell, 1990; Kirschbaum, 1995; Greskowiak et al., 2006). Thus, if the temperature is high (e.g., 15 °C) most of the O_2 is consumed in the first few meters in the ground after infiltration (Chapter 5). However between temperatures of 6 °C and 3 °C consumption rates declines rapidly to zero (Chapter 4).
In contrast to O_2, heat (orange arrow in Figure 6.1) is not only entering the groundwater by advection with the infiltrating river water, but also by vertical conduction, especially during low flow conditions. This is a result of the uncovered gravel forming the top of the aquifer in the first meter after the river bank (Figure 6.1 ,②), i.e., there is no alluvial loam cover attenuating the heat exchange.
The alluvial loam cover also plays an important role in excess air formation. The second study (Chapter 5) shows that there was no excess air produced in zones without a confining alluvial loam cover (②, indicated by a thin solid arrow). This is a result of the high gas permeability of the gravel aquifer, which prevented air bubbles from being trapped. Therefore, as occurred during the studied flood event, the gas is able to escape from the aquifer (dashed arrows in Figure 6.1). In zone ③ although a alluvial loam cover is present, no excess air was observed. However, the groundwater was unconfined during the study, except during peak floods period. Thus, the air was pressed through the highly permeable gravel between the groundwater table and the alluvial loam cover to zone ② (indicated by dashed arrows in Figure 6.1), from where the air escaped. Note that the air in the topsoil did not produce any excess air (very thin solid arrow).
In the zone ④ the aquifer is covered by a alluvial loam layer which confines the groundwater at all times. In this zone, significant amounts of excess air were generated (indicated by a bold solid arrow) in response to a flood. Hence, a rising groundwater table in response to enhanced river discharge exerted a higher hydrostatic pressure on the entrapped gas phase, and the confining alluvial loam layer prevented the entrapped air from escaping.
In conclusion, at the study site the alluvial loam cover is the relevant medium allowing excess air to be produced. Close to the river where a deep enough cover is lacking, the O_2 in the groundwater only enters from the river. Further away from the river, where a confining layer is present, excess air formation is identified as the main source of O_2 for groundwater. In this zone, O_2 availability is controlled by river discharge fluctuations and by the local geomorphic structure i.e., the presence of a alluvial loam cover.
In comparison, the conclusions of this thesis agree with the results of previous works (see Section 2.1.3, Rose and Long, 1988; Beyerle et al., 1999; Williams and Oostrom, 2000; Massmann and Sueltenfuss, 2008), which identified exceed air formation as a source of O_2 in groundwater and fluctuating water table as a possible cause of it. However, in this thesis, the geomorphological condition was identified as another key element that controls the excess air formation and hence the O_2 injection. In the Niederneunforn study site the alluvial loam cover is important for excess air formation, as without it there would be no excess air formation and therefore no essential amount of oxygen entering the groundwater outside the river zone.

6.3 Outlook

The following section lists suggestions for future research in which the deployment of the GE-MIMS can further improve current knowledge (Suggestion A-C). Furthermore, a brief list of possible improvements of the GE-MIMS is given (Suggestion D). This thesis then concludes by discussing other fields of deployment of MIMS (Suggestion E).

Suggestion A: High resolution study of excess air formation
In Chapter 5, the role of excess air formation on O_2 availability in a riparian groundwater in response to a single flood event was investigated. While the temporal resolution of one measurement per well per day was sufficient to understand the gas dynamics in a quantitative manner, a time series similar to the one used in Chapter 4 would give insight into excess air formation in "real" time. Such a gas concentration time series could be used to determine the parameter of complex numerical models like the LE-model or KBD model. Such models capture the impact of different flow conditions and physical properties of the aquifer on excess air formation. Thus, in the long term, an evaluation standard for estimating excess air formation from the hydrological and geomorphical properties of the river and groundwater system could be achieved.

Suggestion B: Noble-gas concentration time series as a tool for residence time determination
Time series of conductivity and temperature are valuable tools in determining residence times of riparian groundwater. In a similar way, NGST can also be used to determine residence times (Chapter 4). This aspect of NGST should be further investigated with field studies and with the application of the mathematical tools of time series analysis e.g. Fourier analysis. Furthermore, heat, salinity and gas are each exposed to different processes along a flow path in groundwater. Most of these processes depend on the geomorphic conditions of the aquifer (i.e. heat exchange, solute exchange and excess air formation). In a single time series of only one observable (i.e. temperature, conductivity or noble gas concentration) different processes are often entangled. However, a combined time series analysis of all observables has the potential to untangle the different processes and may lead to a better quantification of the processes influence on the respective quantity (e.g. vertical heat transport on temperature, see Chapter 4).

Suggestion C: Gas dynamics in surface waters
The GE-MIMS is not limited to groundwater applications — dissolved gas concentrations in lakes can be measured by the same method. Problems like methane production in lakes or aeration of lakes can be studied in-situ and in real-time with the GE-MIMS.

Suggestion D: Improvement of the GE-MIMS
There are several ways to improve the performance of the method and to broaden its field of application. For example, adding additional pumps and an automated valve system would allow alternating water sources from different observation wells to pass into the membrane inlet. Thus, the GE-MIMS can be adapted for the study of concentration changes of dissolved gases in different wells autonomously. However, for each additional observation well, the temporal resolution of each time series is reduced by 15 min.

Furthermore, the range of gas species which can be analyzed be the GE-MIMS can be expanded. Methane concentrations measurements (see Suggestion C), are a promising field for MIMS. Therefore, a calibration protocol for methane and non atmospheric gases in general, should be developed.
Furthermore, because of ion interference, it is not possible to measure Ne concentrations with the current GE-MIMS method. However, Ne has almost only atmospheric components (in contrast to He) and a low solubility. Thus, Ne is therefore far better suited to quantify excess air than He (Kipfer et al., 2002). The problem of Ne concentrations measurements should therefore be solved in the near future.

Suggestion E: MIMS and other aqueous environments
Membrane inlet mass spectrometers (MIMS), including the GE-MIMS, are successfully used for the on-site quantification of dissolved gases (and volatile species) in surface water (Tortell, 2005; Schlüter and Gentz, 2008; Gueguen and Tortell, 2008; Camilli and Duryea, 2009; Etzkorn et al., 2009) and in groundwater (Eschenbach and Well, 2011; Visser et al., 2011). Also, in other aqueous environments, like lake sediments or peat cores, "classical" MIMS have shown potential to perform spatially high resolution measurements (see e.g. Lloyd et al., 1996). However, due to the diffusive nature of such environments the flux of gases through the membrane is highly dependent on the local conditions, (e.g. porosity) leading to measurement bias. Hence, to perform quantitative and reliable measurements in such environments an innovative MIMS which circumvents these problems should be developed.

Bibliography

Aeschbach-Hertig, W., Peeters, F., Beyerle, U. and Kipfer, R. (1999). Interpretation of dissolved atmospheric noble gases in natural waters. *Water Resour. Res.* **35**, 2779–2792.

Aeschbach-Hertig, W., Peeters, F., Beyerle, U. and Kipfer, R. (2000). Palaeotemperature reconstruction from noble gases in ground water taking into account equilibration with entrapped air. *Nature* **405**, 1040–1044.

Allen, J. (1947). An improved electron multiplier particle counter. *Rev. Sci. Instrum.* **18**, 739–749.

Anderson, M. (2005). Heat as a ground water tracer. *Ground Water* **43**, 951–968.

BAFU (2010). Hydrologischer Atlas der Schweiz. *Bundes Amt für Umwelt* **HADES**, http://www.hydrologie.unibe.ch/hades/index.html.

BAFU (2011). Hydrologische Grundlagen und Daten: Thur-Andelfingen. *Bundes Amt für Umwelt* **2044**, http://www.hydrodaten.admin.ch/de/2044.html.

Baker, M., Valett, H. and Dahm, C. (2000). Organic carbon supply and metabolism in a shallow groundwater ecosystem. *Ecology* **81**, 3133–3148.

Ballentine, C. J. and Hall, C. M. (1999). Determining paleotemperature and other variables by using an error-weighted, nonlinear inversion of noble gas concentrations in water. *Geochim. Cosmochim. Acta* **63**, 2315–2336.

Bell, R., Short, R., van Amerom, F. and Byrne, R. (2007). Calibration of an in situ membrane inlet mass spectrometer for measurements of dissolved gases and volatile organics in seawater. *Environ. Sci. Technol.* **41**, 8123–8128.

Beste, K., Hellige, G., Hensel, I., Schenk, H. and Bretschneider, H. (1975). Blood-gas analysis with a mass spectrometer membrane inlet system. *Lung* **151**, 294–295.

Beyerle, U., Aeschbach-Hertig, W., Hofer, M., Imboden, D. M., Baur, H. and Kipfer, R. (1999). Infiltration of river water to a shallow aquifer investigated with $^{3}H/^{3}He$, noble gases and CFCs. *J. Hydrol.* **220**, 169–185.

Beyerle, U., Aeschbach-Hertig, W., Imboden, D., Baur, H., Graf, T. and Kipfer, R. (2000). A mass spectrometric system for the analysis of noble gases and tritium from water samples. *Environ. Sci. Technol.* **34**, 2042–2050.

Beyerle, U., Rüedi, J., Leuenberger, M., Aeschbach-Hertig, W., Peeters, F., Kipfer, R. and Dodo, A. (2003). Evidence for periods of wetter and cooler climate in the Sahel between 6 and 40 kyr bp derived from groundwater. *Geophys. Res. Lett.* **30**, 1173.

Binderheim-Banakay, E. S., Palmer, M. A. and Allan, J. D. (2000). NADUF-Messresultate 1977 - 1998. *Federal Office for the Environment (FOEN) Bern, 241*.

Boulton, A., Findlay, S., Marmonier, P., Stanley, E. H. and Valett, H. M. (1998). The functional significance of the hyporheic zone in streams and rivers. *Annu. Rev. Ecol. Syst.* **29**, 59–81.

Broecker, W. and Peng, T.-H. (1974). Gas exchange rates between air and sea. *Tellus* **27**, 21–35.

Brown, K. and Tautfest, G. (1956). Faraday-cup monitors for high-energy electron beams. *Rev. Sci. Instrum.* **27**, 696–702.

Brunke, M. and Gonser, T. (1997). The ecological significance of exchange processes between rivers and groundwater. *Freshwater Biol.* **37**, 1–33.

Camilli, R. and Duryea, A. (2009). Characterizing spatial and temporal variability of dissolved gases in aquatic environments with in situ mass spectrometry. *Environ. Sci. Technol.* **43**, 5014–5021.

Carignan, R. (1998). Automated determination of carbon dioxide, oxygen, and nitrogen partial pressures in surface waters. *Limnol. Oceanogr.* **43**, 969–975.

Chu, C., Lo, Y. and Sung, T. (2011). Review on recent developments of fluorescent oxygen and carbon dioxide optical fiber sensors. *Photonic. Sens.* **1**, 234–250.

Cirpka, O., Fienen, M., Hofer, M., Hoehn, E., Tessarini, A., Kipfer, R. and Kitanidis, P. K. (2007). Analyzing bank filtration by deconvoluting time series of electric conductivity. *Ground Water* **45**, 318–328.

Cirpka, O. and Kitanidis, P. (2001). Transport of volatile compounds in porous media in the presence of a trapped gas phase. *J. Conta. Hydro.* **49**, 263–285.

Datry, T., Malard, F. and Gibert, J. (2004). Dynamics of solutes and dissolved oxygen in shallow urban groundwater below a stormwater infiltration basin. *Sci. Total Environ.* **329**, 215–229.

Davey, N. G., Krogh, E. T. and Gill, C. G. (2011). Membrane-introduction mass spectrometry (MIMS). *Trends Anal. Chem.* **30**, 1477–1485.

de Hoffmann, E. and Stroobant, V. (2007). Mass spectrometry: principles and applications. *Wiley*.

Deffeyes, K. S. (1965). Carbonate equilibria: A graphic and algebraic approach. *Limnol. Oceanogr.* **10**, 412–426.

Defra (2002). The government's strategic review of diffuse water pollution from agriculture in England and Wales. *Department for Environment, Food and Rural Affairs (Defra)*.

Demarty, M., Bastien, J. and Tremblay, A. (2011). Annual follow-up of gross diffusive carbon dioxide and methane emissions from a boreal reservoir and two nearby lakes in Quebec, Canada. *Biogeosciences* **8**, 41–53.

Epstein, P. S. and Plesset, M. S. (1950). On the stability of gas bubbles in liquid-gas solutions. *J. Chem. Phys.* **18**, 1505–1509.

Eschenbach, W. and Well, R. (2011). Online measurement of denitrification rates in aquifer samples by an approach coupling an automated sampling and calibration unit to a membrane inlet mass spectrometry system. *Rapid. Commun. Mass. Spectrom.* **25**, 1993–2006.

Etzkorn, J. M., Davey, N. G., Thompson, A. J., Creba, A. S., LeBlanc, C. W., Simpson, C. D., Krogh, E. T. and Gill, C. G. (2009). The use of MIMS-MS-MS in field locations as an on-line quantitative environmental monitoring technique for trace contaminants in air and water. *J. Chromatogr. Sci.* **47**, 57–66.

Fry, V., Istok, J., Semprini, L. and O'Reilly, K. (1995). Retardation of dissolved oxygen due to a trapped gas phase in porous media. *Ground Water* **33**, 391–398.

Greskowiak, J., Prommer, H., Massmann, G. and Nuetzmann, G. (2006). Modeling seasonal redox dynamics and the corresponding fate of the pharmaceutical residue phenazone during artificial recharge of groundwater. *Environ. Sci. Technol.* **40**, 6615–6621.

Gueguen, C. and Tortell, P. D. (2008). High-resolution measurement of southern ocean CO_2 and O_2/Ar by membrane inlet mass spectrometry. *Mar. Chem.* **108**, 184–194.

Hall, C., Castro, M., Lohmann, K. and Ma, L. (2005). Noble gases and stable isotopes in a shallow aquifer in southern Michigan: Implications for noble gas paleotemperature reconstructions for cool climates. *Geophys. Res. Lett.* **32**, L18404.

Harland, B., Nicholson, P. and Gillings, E. (1987). Determination of volatile organic compounds in aqueous systems by membrane inlet mass spectrometry. *Water Res.* **21**, 107–113.

Hartmann, D. and Michel, P. (1992). Grundwasserschutz in der Schweiz. *GWA. Gas, Wasser, Abwasser* **72**, 167–173.

Hayashi, M. and Rosenberry, D. O. (2002). Effects of ground water exchange on the hydrology and ecology of surface water. *Ground Water* **40**, 309–316.

Hayashi, M., Vogt, T., Mächler, L. and Schirmer, M. (2012). Diurnal fluctuations of electrical conductivity in a pre-alpine river: Effects of photosynthesis and groundwater exchange. *J. Hydrol* **450-451**, 93 – 104.

Heaton, T. H. E. and Vogel, J. C. (1981). "Excess air" in groundwater. *J. Hydrol.* **50**, 201–216.

Holmen, K. and Liss, P. (1984). Models for air water gas transfer: an experimental investigation. *Tellus B* **36**, 92–100.

Holocher, J., Peeters, F., Aeschbach-Hertig, W., Kinzelbach, W. and Kipfer, R. (2003). Kinetic model of gas bubble dissolution in groundwater and its implications for the dissolved gas composition. *Environ. Sci. Technol.* **37**, 1337–1343.

Husmann, S. (1971). A new method for taking interstitial water out of submerged layers of sand and gravel. *Arch. Hydrobiol.* **68**, 519–527.

Huxol, S., Brennwald, M. S., Hoehn, E. and Kipfer, R. (2012). On the fate of ^{220}Rn in soil material in dependence of water content: Implications from field and laboratory experiments. *Chem. Geol.* **298-299**, 116–122.

Hynes, H. B. N. (2001). The ecology of running waters. *Univ. of Toronto Pr*.

Ingram, R. G. S., Hiscock, K. M. and Dennis, P. F. (2007). Noble gas excess air applied to distinguish groundwater recharge conditions. *Environ. Sci. Technol.* **41**, 1949–1955.

Jähne, B., Heinz, G. and Dietrich, W. (1987). Measurement of the diffusion coefficients of sparingly soluble gases in water. *J. Geophys. Res.* **92**, 10,767–10,776.

Johnson, R., Cooks, R., Allen, T., Cisper, M. and Hemberger, P. (2000). Membrane introduction mass spectrometry: Trends and applications. *Mass Spectrom. Rev.* **19**, 1–37.

Kaenel, B., Buehrer, H. and Uehlinger, U. (2000). Effects of aquatic plant management on stream metabolism and oxygen balance in streams. *Freshwater Biol.* **45**, 85–95.

Kana, T., Darkangelo, C., Hunt, M., Oldham, J., Bennett, G. and Cornwell, J. (1994). Membrane inlet mass spectrometer for rapid high-precision determination of N_2, O_2 and Ar in environmental water samples. *Anal. Chem.* **66**, 4166–4170.

Ketola, R., Kotiaho, T., Cisper, M. and Allen, T. (2002). Environmental applications of membrane introduction mass spectrometry. *J. Mass. Spectrom.* **37**, 457–476.

Kipfer, R., Aeschbach-Hertig, W., Peeters, F. and Stute, M. (2002). Noble gases in lakes and ground waters. *Rev. Mineral. Geochem.* **47**, 615–700.

Kirchner, J., Feng, X. and Neal, C. (2000). Fractal stream chemistry and its implications for contaminant transport in catchments. *Nature* **403**, 524–527.

Kirschbaum, M. (1995). The temperature-dependence of soil organic-matter decomposition, and the effect of global warming on soil organic-C storage. *Soil. Biol. Biochem.* **27**, 753–760.

Klump, S., Cirpka, O., Surbeck, H. and Kipfer, R. (2008). Experimental and numerical studies on excess-air formation in quasi-saturated porous media. *Water Resour. Res.* **44**, W05402.

Klump, S., Tomonaga, Y., Kienzler, P., Kinzelbach, W., Baumann, T., Imboden, D. and Kipfer, R. (2007). Field experiments yield new insights into gas exchange and excess air formation in natural porous media. *Geochim. Cosmochim. Acta* **71**, 1385–1397.

Korom, S. (1992). Natural denitrification in the saturated zone: A review. *Water Resour. Res.* **28**, 1657–1668.

Kotiaho, T. (1998). On-site environmental and in situ process analysis by mass spectrometry. *J. Mass Spectrom.* **31**, 1–15.

Kotiaho, T. and Lauritsen, F. (2002). Membrane inlet mass spectrometry. *Compr. Anal. Chem.* **16**, 531–557.

Leybold (1987). Grundlagen der Vakuumtechnik, Berechnungen und Tabellen **09**, Kat. Nr. 1 99 89.

Lippmann, J., Stute, M., Torgersen, T., Moser, D., Hall, J., Lin, L., Borcsik, M., Bellamy, R. and Onstott, T. (2003). Dating ultra-deep mine waters with noble gases and Cl-36, Witwatersrand Basin, South Africa. *Geochim. Cosmochim. Acta* **67**, 4597–4619.

Livingstone, D. M. (1991). The diel oxygen cycle in three subalpine swiss streams. *Arch. Hydrobiol.* **120**, 457–479.

Lloyd, D., Ellis, J. E., Hillman, K. and Williams, A. G. (1992). Membrane inlet mass spectrometry: probing the rumen ecosystem. *J. Appl. Bacteriol.* **73**, 155–163.

Lloyd, D. and Scott, R. (1983). Direct measurement of dissolved gases in microbiological systems using membrane inlet mass spectrometry. *J. Microbiol. Methods* **1**, 313–328.

Lloyd, D., Thomas, K., Cowie, G., Tammam, J. and Williams, A. (2002). Direct interface of chemistry to microbiological systems: membrane inlet mass spectrometry. *J. Microbial. Methods* **48**, 289–302.

Lloyd, D., Thomas, K., Price, D., O'Neil, B., Oliver, K. and Williams, T. (1996). A membrane-inlet mass spectrometer miniprobe for the direct simultaneous measurement of multiple gas species with spatial resolution of 1 mm. *J. Microbiol. Methods* **25**, 145–151.

Mächler, L., Brennwald, M. and Kipfer, R. (2012). Membrane inlet mass spectrometer for the quasi-continuous on-site analysis of dissolved gases in groundwater. *Environ. Sci. Technol.* **46**, 8288–8296.

Malard, F. and Hervant, F. (1999). Oxygen supply and the adaptations of animals in groundwater. *Freshwater Biol.* **41**, 1–30.

Mamyrin, B. and Tolstikhin, I. N. (1983). Helium isotopes in nature. *Elsevier Scientific Publishing Company, Amsterdam, The Netherlands* .

Manning, A., Solomon, D. and Sheldon, A. (2003). Applications of a total dissolved gas pressure probe in ground water studies. *Ground Water* **41**, 440–448.

Massmann, G. and Sueltenfuss, J. (2008). Identification of processes affecting excess air formation during natural bank filtration and managed aquifer recharge. *J. Hydrol.* **359**, 235–246.

Molina-Giraldo, N., Bayer, P., Blum, P. and Cirpka, O. (2011). Propagation of seasonal temperature signals into an aquifer upon bank infiltration. *Ground Water* **49**, 491–502.

Morrison, P. and Pine, J. (1955). Radiogenic origin of the helium isotopes in rock. *Ann. N. Y. Acad. Sci.* , 71–92.

O'Connell, A. M. (1990). Microbial decomposition (respiration) of litter in eucalypt forests of south-western Australia: An empirical model based on laboratory incubations. *Soil Biol. Biochem.* **22**, 154–160.

Peter, S., Koetzsch, S., Traber, J., Bernasconi, S. M., Wehrli, B. and Durisch-Kaiser, E. (2012a). Intensified organic carbon dynamics in the ground water of a restored riparian zone. *Freshwater Biol.* **57**, 1603–1616.

Peter, S., Mächler, L., Kipfer, R., Wehrli, B. and Durisch-Kaiser, E. (2012b). Assessment of biogeochemical processes in riparian groundwater under the influence of excess air formation. *in preparation* , 1–15.

Peter, S., Rechsteiner, R., Lehmann, M. F., Brankatschk, R., Vogt, T., Diem, S., Wehrli, B., Tockner, K. and Durisch-Kaiser, E. (2012c). Nitrate removal in a restored riparian groundwater system: functioning and importance of individual riparian zones. *Biogeosciences Discuss.* **9**, 6715–6750.

Poole, J., McNeill, G., Langman, S. and Dennis, F. (1997). Analysis of noble gases in water using a quadrupole mass spectrometer in static mode. *Appl. Geochem.* **12**, 707–714.

Poole, W. C. and Stewart, K. W. (1976). The vertical distribution of macrobenthos within the substratum of the Brazos River, Texas. *Hydrobiologia* **50**, 151–160.

Rivett, M., Buss, S., Morgan, P., Smith, J. and Bemment, C. (2008). Nitrate attenuation in groundwater: A review of biogeochemical controlling processes. *Water Res.* **42**, 4215–4232.

Rose, S. and Long, A. (1988). Monitoring dissolved oxygen in ground water: Some basic considerations. *Ground Water Monit. Rem.* **8**, 93–97.

Schlosser, P., Stute, M., Dörr, H., Sonntag, C. and Münnich, K. (1988). Tritium/^{3}He dating of shallow groundwater. *Earth Planet. Sci. Lett.* **89**, 353–362.

Schlüter, M. and Gentz, T. (2008). Application of membrane inlet mass spectrometry for online and in situ analysis of methane in aquatic environments. *J. Am. Soc. Mass. Spectrom.* **19**, 1395–1402.

Schmidt, A., Schlueter, M., Melles, M. and Schubert, M. (2008). Continuous and discrete on-site detection of radon-222 in ground- and surface waters by means of an extraction module. *Appl. Radiat. Isotopes* **66**, 1939–1944.

Schneider, P., Vogt, T., Schirmer, M., Doetsch, J., Linde, N., Pasquale, N., Perona, P. and Cirpka, O. (2011). Towards improved instrumentation for assessing river-groundwater interactions in a restored river corridor. *Hydrol. Earth Syst. Sci. Dis.* **8**, 2503–2553.

Schurr, J. and Ruchti, J. (1975). Kinetics of oxygen exchange, photosynthesis, and respiration in rivers determined from time-delayed correlations between sunlight and dissolved oxygen. *Aquat. Sci.* **37**, 144–174.

Schwarzenbach, R. P., Gschwend, P. M. and Imboden, D. M. (2003). Environmental organic chemistry. *John Wiley & Sons, Inc.* **ISBN 0-471-35750**.

Schweizer, S., Borsuk, M. E. and Reichert, P. (2007). Predicting the morphological and hydraulic consequences of river rehabilitation. *River Res. Applic.* **23**, 303–322.

Schwoerbel, J. (1961). Über die Lebensbedingungen und die Besiedlung des hyporheischen Lebensraumes. *Arch. Hydrobiol., Suppl.* **25**, 182–214.

Silliman, S., Ramirez, J. and McCabe, R. L. (1995). Quantifying downflow through creek sediments using temperature time series: one-dimensional solution incorporating measured surface temperature. *J. Hydrol.* **167**, 99–119.

Smith, G. D., Newhall, F., Robinson, L. H. and Swanson, D. (1964). Soil temperature regimes: Their characteristics and predictability. Technical Report SCS-TP-144, USDA, Soil Conservation Service.

Smith, S. and Kennedy, B. (1983). The solubility of noble gases in water and in NaCl brine. *Geochim. Cosmochim. Acta* **47**, 503–515.

SRS (2000). User's manual: Qms 100 series gas analyzer. *Stanford Research Systems*.

Stallman, R. (1965). Steady one-dimensional fluid flow in a semi-infinite porous medium with sinusoidal surface temperature. *J. Geophys. Res.* **70**, 2821–2827.

Streeter, H. and Phelps, E. B. (1925). A study of the pollution and natural purfication of the Ohio river. *Publ. Health Bull.* **146**.

Stumm, W. and Morgan, J. J. (1995). Aquatic chemistry: chemical equilibria and rates in natural waters. *Wiley*.

Stute, M., Schlosser, P., Clark, J. F. and Broecker, W. S. (1992). Paleotemperatures in the southwestern United States derived from noble gases in ground water. *Science* **256**, 1000–1003.

Sun, T., Hall, C. M., Castro, M. C., Lohmann, K. C. and Goblet, P. (2008). Excess air in the noble gas groundwater paleothermometer: A new model based on diffusion in the gas phase. *Geophys. Res. Lett.* **35**, L19401.

SVGW (2002). Infoblatt TWI 12. Zürich, Switzerland. *Schweizerischer Verein des Gas- und Wasserfachs*.

Thorp, J., Thoms, M. and Delong, M. (2006). The riverine ecosystem synthesis: biocomplexity in river networks across space and time. *River Res. Applic.* **22**, 123–147.

Tortell, P. (2005). Dissolved gas measurements in oceanic waters made by membrane inlet mass spectrometry. *Limnol. Oceanogr.-Meth.* **3**, 24–37.

Uehlinger, U. (2006). Annual cycle and inter-annual variability of gross primary production and ecosystem respiration in a floodprone river during a 15-year period. *Freshwater Biol.* **51**, 938–950.

Uehlinger, U. and Naegeli, M. W. (1998). Ecosystem metabolism, disturbance, and stability in a prealpine gravel bed river. *J. N. Am. Benthol. Soc.* **17**, 165–178.

Visser, A., Singleton, M. and Esser, B. (2011). Towards a mobile membrane inlet mass spectrometry (MIMS) system for the detection of atmospheric noble gases in groundwater. *Geophys. Res. Abstr.* **13, EGU2011-2007-1, EGU General Assembly 2011**, 1–1.

Vogel, J., Talma, A. and Heaton, T. H. E. (1981). Gaseous nitrogen as evidence for denitrification in groundwater. *J. Hydrol.* **50**.

Vogt, T., Hoehn, E., Schneider, P., Freund, A., Schirmer, M. and Cirpka, O. (2010a). Fluctuations of electrical conductivity as a natural tracer for bank filtration in a losing stream. *Adv. Water Resour.* **33**, 1296–1308.

Vogt, T., Schneider, P., Hahn-Woernle, L. and Cirpka, O. (2010b). Estimation of seepage rates in a losing stream by means of fiber-optic high-resolution vertical temperature profiling. *J. Hydrol.* **380**, 154–164.

Wakida, F. T. and Lerner, D. N. (2005). Non-agricultural sources of groundwater nitrate: a review and case study. *Water Res.* **39**, 3 – 16.

Weiss, R. (1970). The solubility of nitrogen, oxygen and argon in water and seawater. *Deep-Sea Res. Oceanogr. Abstr.* **17**, 721–735.

Weiss, R. (1971). Solubility of helium and neon in water and seawater. *J. Chem. Eng. Data* **16**, 235–241.

Weiss, R. and Kyser, T. (1978). Solubility of krypton in water and seawater. *J. Chem. Eng. Data* **23**, 69–72.

Weiss, R. F. (1968). Piggyback sampler for dissolved gas studies on sealed water samples. *Deep-Sea Res.* **15**, 695–699.

Weiss, R. F. (1974). Carbon dioxide in water and seawater: the solubility of a non-ideal gas. *Mar. Chem.* **2**, 203–215.

Whitman, R. and Clark, W. (1982). Availability of dissolved oxygen in interstitial waters of a sandy creek. *Hydrobiologia* **92**, 651–658.

Williams, D. and Hynes, H. B. N. (1974). The occurrence of benthos deep in the substratum of a stream. *Freshwater Biol.* **4**, 233–256.

Williams, M. and Oostrom, M. (2000). Oxygenation of anoxic water in a fluctuating water table system: An experimental and numerical study. *J. Hydrol.* **230**, 70–85.

Wilson, G. B. and McNeill, G. W. (1997). Noble gas recharge temperatures and the excess air component. *Appl. Geochem.* **12**, 747–762.

Wise, D. and Houghton, G. (1966). The diffusion coefficients of ten slightly soluble gases in water at 10-60°C. *Chem. Eng. Sci.* **21**, 999–1010.

Zartman, R. E., Reynolds, J. H. and Wasserburg, G. J. (1961). Helium, argon, and carbon in some natural gases. *J. Geophys. Res.* **66**, 277–306.

Appendix

Variables

Variable	Unit(s)	Definition
$\mathbf{a}$	ms^{-2}	Acceleration (vector) of a particle
A	$\mathrm{cm}^3_{\mathrm{STP}}\mathrm{g}^{-1}$	Total amount of air bubbles per water mass initially entrapped in groundwater
α_i	$\mathrm{cm}^3\mathrm{s}^{-1}$	Coefficient describing Q_w dependency of F_i^f
A_t	$\mathrm{cm}^3_{\mathrm{STP}}\mathrm{g}^{-1}$	Total Concentration of the remaining gas in the bubbles
$\mathbf{B}$	Vm^{-1}	Magnetic field
β	1	Gas transfer model parameter
C_i	$\mathrm{cm}^3_{\mathrm{STP}}\mathrm{g}^{-1}$	Concentration of a gas i in water
C_i^0	$\mathrm{cm}^3_{\mathrm{STP}}\mathrm{g}^{-1}$	Initial concentration of gas i in water before excess air formation
Γ_i	1	Coefficient describing F_i^f for $Q_\mathrm{w} \to \infty$
C_i^{ASW}	$\mathrm{cm}^3_{\mathrm{STP}}\mathrm{g}^{-1}$	Concentration of a gas i in air saturated water (ASW)
C_i^f	$\mathrm{cm}^3_{\mathrm{STP}}\mathrm{g}^{-1}$	Concentration of a gas i in water after excess air formation
C_{wa}^i	$\mathrm{cm}^3_{\mathrm{STP}}\mathrm{g}^{-1}$	Concentration of a gas i in water just entering the membrane inlet
$\overline{C}_{\mathrm{wa}}^i$	$\mathrm{cm}^3_{\mathrm{STP}}\mathrm{g}^{-1}$	Mean concentration of gas i of the water flowing through the membrane inlet
D_i	$\mathrm{m}^2\mathrm{s}^{-1}$	Molecular diffusion coefficient of gas i in water
D_m^i	$\mathrm{m}^2\mathrm{s}^{-1}$	Diffusion coefficient of gas i in a membrane
ΔC_i	$\mathrm{cm}^3_{\mathrm{STP}}\mathrm{g}^{-1}$	Concentration difference of gas i between the water entering and leaving the membrane inlet
$\Delta C_{\max}$	$\mathrm{cm}^3_{\mathrm{STP}}\mathrm{g}^{-1}$	Maximal concentration change between two measurements that can be resolved
ΔC_{wa}^i	$\mathrm{cm}^3_{\mathrm{STP}}\mathrm{g}^{-1}$	Concentration loss of gas i during through flow of the membrane inlet
$\mathbf{E}$	Vm^{-1}	Electric field
F_{CE}	1	Fractionation coefficient of the CE-model
F_{PR}	1	Fractionation coefficient of the PR-model
F_i^f	1	GE-MIMS nondimensional deviation function of gas i
h	m	(mean) Depth of a water body (e.g. river)
H_i	$\mathrm{cm}^3_{\mathrm{STP}}\mathrm{g}^{-1}$/atm	Henry's partitioning coefficient of a gas i

continued on next page

Variable	Unit(s)	Definition
l_m	m	Membrane thickness
J^i_{Me}	$\mathrm{cm}^3_{\mathrm{STP}}\mathrm{s}^{-1}$	Total flux of a gas i leaving the water through the membrane into the extraction chamber of the GE-MIMS
J^i_{MS}	$\mathrm{cm}^3_{\mathrm{STP}}\mathrm{s}^{-1}$	Total flux pumped out of the extraction chamber through the capillary into the MS
J^i_{ss}	$\mathrm{cm}^3_{\mathrm{STP}}\mathrm{s}^{-1}$	Total flux of a gas i in steady state through the membrane
J^i_{wa}	$\mathrm{cm}^3_{\mathrm{STP}}\mathrm{s}^{-1}$	Flux of gas i removed from the water flow (Q_{w})
k_r	h^{-1}	River exchange rate
k_i	ms^{-1}	Transfer coefficient of gas i through a stagnant water film
m	kg	Mass
M_i	gmol^{-1}	Standert atomic mass of element i
Ω_{PR}	$\mathrm{cm}^2\mathrm{s}^{-1}$	Geometry and time scaling parameter of the PR-model
P_{atm}	Pa (atm)	Atmospheric Pressure
P_{hyd}	Pa (atm)	Hydrostatic pressure
p_i	Pa (atm)	Partial pressure of a gas i
p_i^{atm}	Pa (atm)	Atmospheric partial pressure of a gas i in air
p_i^{EC}	Pa (atm)	Partial pressure of a gas i in the EC
p_i^{equ}	Pa (atm)	Partial pressure of a gas i in solubility equilibrium with an arbitrary dissolved gas concentration
Q	C	Electronic charge
Q_{w}	Lmin^{-1}	Water flow rate of the membrane inlet
r	m	(bubble) Radius
R_i^{cap}	$\mathrm{cm}^3_{\mathrm{STP}}\mathrm{g}^{-1}\mathrm{s}^{-1}$/atm	Flow-resistance of gas i in the capillary
S_{w}	mg/Kg	Salinity of the water
S_m	m^2	Membrane surface area
t	s	Time
T_0	K (°C)	Mean water temperature of a river
T_{ASW}	K (°C)	Temperature of a basin with ASW (before heating)
T_w	K (°C)	Temperature of water
T_{var}	K (°C)	Amplitude of a diel temperature variation in a river
$t_{1/2}$	s	Half life to reach steady state after the EC has been connected to the MS
v	ms^{-1}	Seepage velocity
v_f	ms^{-1}	Gas exchange velocity
$\mathbf{v_p}$	ms^{-1}	Velocity of a particle (vector)
z_i	1	Atmospheric air volume fraction of the gas i